

As Cold as a Black Hole: Extended Photon Spheres

Marcos Riojas

Center for the Fundamental Laws of Nature, Harvard University, Cambridge, MA, USA

E-mail: marcos_riojas@fas.harvard.edu

ABSTRACT: It is widely believed that self-gravitating radiation cannot reach thermal equilibrium with a black hole in asymptotically flat spacetime. The following observation is used to describe an exception to this rule. The photon sphere controls central aspects of the Israel junction conditions (IJC), the Tolman-Oppenheimer-Volkoff (TOV) equation, and finite-radius black hole thermodynamics. Through these results, we will describe how to compute coarse-grained entropies without using the Euclidean path integral. For instance, we find the IJCs and TOV equation are precisely equivalent at zero radial pressure. At fixed mass, adding shells in regions of positive specific heat *lowers* the asymptotic Hawking temperature, and the inverse specific heat at the photon sphere is proportional to $-\Lambda$.

The exception described here results from companion work with M.J. Strassler, where we found that a “hilligar black hole” (HBH) mimics an ordinary Schwarzschild black hole of mass M , sharing its Hawking temperature, photon ring, and, in equilibrium, its coarse-grained entropy $S = 4\pi M^2$. Here, we show these features are not tuned; they follow uniquely from joint mechanical and thermodynamic constraints. A necessary and sufficient condition for thermodynamic mimicry is found that is satisfied by a one parameter family of self-similar systems, all of which, excepting the HBH, require massless walls at the edges of their extended photon spheres. This family includes “stiffest stars” and “frozen stars”.

Contents

1	Introduction	2
1.1	Hillinger Black Holes	4
2	Review: The Stability Obstruction in Asymptotically Flat Spacetime	5
2.1	York Cavity Thermodynamics	6
2.2	Mechanical Stability of Shells Around Black Holes	7
2.3	Thermodynamics of Self-Gravitating Radiation	9
3	Time-Dependent Israel Junction Conditions	11
3.1	Static Shells around Black Holes	12
3.2	Static Z_2 Shells are Pure Tension and Sit at the Photon Sphere	13
4	Stability of Shells Around Black Holes	14
4.1	An Extended Formalism for Shell Stability	14
4.2	Thermal Stability in anti-de Sitter Space	17
4.3	Joint Stability of Shells around AdS Black Holes	19
4.4	The Specific Heat at the Photon Sphere is Inversely Proportional to $-\Lambda$	21
5	Self-Gravitating Radiation and the Photon Sphere	23
5.1	The Anisotropic Tolman-Oppenheimer-Volkoff (TOV) Equation	24
5.2	Shells of Anisotropic Self-Gravitating Radiation	25
5.2.1	TOV = IJC at Zero Radial Pressure	26
5.2.2	The Buchdahl Bound	30
5.2.3	Entropy Density at the Fixed Point	31
5.3	From Joint Stability to the Hillinger Black Hole	32
5.3.1	The Coldest Stable Nested Shell Configuration: the HBH	33
5.4	Shells Cool Black Holes \iff Specific Heat is Positive	36
5.5	Entropy of Systems in Equilibrium with Black Holes	37
5.5.1	Thermodynamics from IJC: Shells are Heat	37
5.5.2	Computing Coarse-Grained Entropies from IJC	39
5.5.3	Beyond Nested Shells: Boxes as Cold as a Black Hole	42
6	Discussion	45
A	Ultra-Compact Objects, Stability, and Optical Mimicry	46
B	The Euclidean Action and Thermodynamics	52
C	Braneworld Cosmology	57

1 Introduction

Black holes are thermodynamic systems [1–5] because asymptotic time stops violently at the horizon, but for macroscopic black holes this halting is gentle in Planck units. Astrophysical black holes are among the coldest objects in the universe, much colder than the cosmic microwave background, and their Bekenstein-Hawking entropy $S = A/(4\hbar G)$ dwarfs that of ordinary matter of the same mass. That raises the question we investigate in this note: can a black hole be surrounded by matter in stable thermal and mechanical equilibrium, and if so, what configuration could possibly match its temperature and entropy?

A sharp obstruction has been known since the 1980s. Firstly, black holes in asymptotically flat spacetime cannot reach stable thermal equilibrium with infinity because their asymptotic specific heat is negative [6]. In fact, asymptotically flat spacetime at finite temperature admits a Euclidean Schwarzschild saddle with a negative mode [7]. Addressing this, York [8] showed black holes in a finite cavity at fixed temperature have two branches of solutions. If the photon sphere is outside the cavity, the specific heat is positive and the system is stable. These branches merge at the minimum temperature because the cavity wall coincides with the photon sphere; see Fig. 3. Simply put, the first constraint is thermal: a stable cavity must be supported within the photon sphere of the black hole.

Mechanical stability is a separate matter. The Israel junction conditions [9] determine the location of a shell outside a black hole [10]. Their stability under radial perturbations was worked out by Brady, Louko, and Poisson (BLP) [11]. They found that unless we allow for superluminal sound waves, the equation of state must satisfy $\sigma \geq 2p$, where σ is the surface energy density and p is the surface pressure. In brief, the second constraint is that massive shells must sit outside the photon sphere; see Fig. 5. In conclusion then [11], joint thermodynamic and mechanical stability appears impossible; Israel noted, in their footnote, that a spherical box extending above and below the photon sphere could work.

The following thought experiment suggests a resolution. Consider an observer hovering just outside the photon sphere of a black hole; there the black hole appears as an infinite plane (Fig. 1). Moving outward slightly, the horizon looms as an enormous sphere with positive Gaussian curvature. However, after an infinitesimally thin and mechanically stable layer of radiation with $\sigma \simeq 2p$ is added just outside the photon sphere, its backreaction displaces the photon sphere slightly outward, with the horizon again appearing as an infinite plane. This is in essence a *hillingar*¹ mirage, seen in arctic conditions where light bends toward and travels along the frigid ocean’s surface, extending the visible horizon outward.

There is no obvious reason why this should work. Nonetheless, we will show it does; iterating this procedure produces a *hillingar* black hole (HBH), whose special properties were identified and studied with M.J. Strassler [12, 13]. This stability is marginal; its interpretation as a thermodynamic equilibrium state is discussed further below. The radiation is *anisotropic*, fully transverse to the horizon with zero radial pressure, and its *extended* photon sphere is an “ocean” precisely as cold as the black hole. See Fig 2.

¹Hillingar is an Old Norse term describing the upheaving of images above the horizon by an arctic mirage. When light rays curve at the same rate as Earth’s surface, the ocean’s surface appears flat and the visible horizon is extended outward. The “ocean” of the HBH is an exact gravitational analogue.

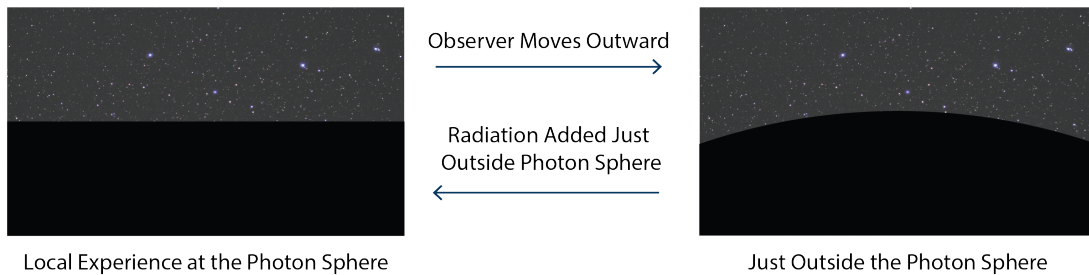


Figure 1. A procedure for constructing candidate equilibrium configurations. Massless particles orbit the black hole at the photon sphere [16], so the shadow of the horizon appears as an infinite plane. The obstruction described in the introduction, which suggests that stable thermal and mechanical equilibrium are fundamentally incompatible, is evaded by placing successive infinitesimal layers of self-gravitating radiation with $\sigma \simeq 2p$ just outside the photon sphere.

The HBH is not only an exception to the constraints. It also has the same temperature, coarse-grained entropy, and optical signature as a Schwarzschild black hole, as originally shown in [12, 13]; here we obtain this result using alternative methods. We will see why this occurs more generally. Note that its status as a black hole mimic [14, 15], including its Schwarzschild temperature, shadow, and – assuming thermal equilibrium is possible – coarse grained entropy, are not tuned; they are consequences of the constraints. Indeed, the HBH is the continuum realization of the stability-selected point in Fig. 11.

An outline of this note follows. The obstruction of [8, 11] is reviewed in Sec. 2, as well as Sorkin, Wald, and Zhang’s (SWZ) [17] analysis of the Tolman-Oppenheimer-Volkoff (TOV) [18, 19] equation and the thermodynamics of self-gravitating radiation. The time-dependent Israel junction conditions (IJC) for spherically symmetric spacetimes are derived in Sec. 3; the photon sphere is closely linked to the dynamics of Israel layers, with consequences for (e.g.) Randall-Sundrum (RS) branes [20, 21]. BLP’s [11] analysis is extended to general spherically symmetric spacetimes in Sec. 4, before specializing to anti-de Sitter spacetime. In Sec. 4.4 we show the general result that the inverse specific heat at the photon sphere in d dimensions is proportional to $-\Lambda_{\text{CC}}$, with consequences for what follows.

In Sec. 5 we extend the analysis of SWZ to anisotropic matter and show that in the limit of vanishing radial pressure, solutions to the TOV equation [18, 19, 22] organize into discrete Israel layers.² For traceless matter with $\sigma = 2p$ these layers are infinitesimal and continuous, forming an extended photon sphere at the point where the regions of mechanical and thermodynamical stability overlap in [11]. We show in Sec. 5.4 that, at fixed total mass, adding a shell around a black hole decreases the asymptotic temperature of the system if and only if the specific heat at the shell’s location is *positive*.

Black hole thermodynamics are obtained directly from the Israel junction conditions in Sec. 5.5. In this method, which does not need the Euclidean path integral, the temperature

²Results for the entropy of self-gravitating radiation were obtained using different methods by Kim and Lee [23], see [13] for additional discussion. They deduced the scaling behavior for the entropy density of anisotropic matter with constant coefficients $w_i \equiv p_i/\rho$ using an entropy maximization method.

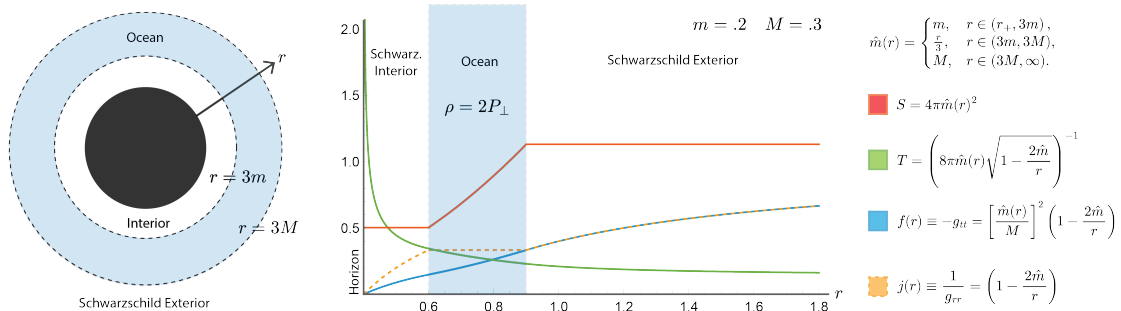


Figure 2. Hilling black holes are surrounded by an *aligned* extended photon sphere: an “ocean” of orbiting massless particles [12]. The continuous mass function $\hat{m}(r)$ is piecewise defined, taking the value m within the Schwarzschild interior, M within the Schwarzschild exterior, and $\hat{m} = r/3$ within the ocean. Here $\sigma = 2p$, in accordance with the thought experiment in Fig. 1.

of the system is tracked while building it up layer-by-layer. Under the strong assumption that this radiation can be maintained in thermal equilibrium with the black hole, we show (independently of the original argument in [13]) that $S = 4\pi M^2$ for the HBH. While the thermal equilibrium assumption is strong, it is not arbitrary: if an ocean forms dynamically as a black hole evaporates, Appendix B and Eq. (5.81) show that T_∞ remains fixed, as required for thermal equilibrium. This is a special property of the HBH.

In Sec. 5.5.3 we generalize these arguments to show that extended photon spheres form when a certain condition (Eq. (A.7)) holds. This relation takes the same form as the constraint in Eq. (5.108) that permits thermodynamic mimicry. Consequently, a one-parameter family of self-similar gases with this property have the temperature and coarse-grained entropy of a black hole. The frozen star [24–26], the stiffest star [27], and the HBH are members of this family; if the dominant energy condition (DEC) is satisfied, then thermodynamic mimicry occurs only for the HBH. The HBH is also an optical mimic [12].

We also find the curious result that if thermal equilibrium is maintained, then in anti-de Sitter space large black holes can become colder and increase their entropy by forming stable shells. This observation was originally made for the HBH in [13]; here we give a slightly more general perspective. This work is concluded with a brief discussion.³

1.1 Hilling Black Holes

The HBH was investigated in [12, 13], where its classical and thermodynamic properties were studied. In 3 + 1 dimensional asymptotically flat spacetime, the HBH has the metric:

$$ds^2 = -f(r)dt^2 + j(r)^{-1}dr^2 + r^2d\theta^2 + r^2\sin^2(\theta)d\phi^2 \quad (1.1)$$

$$j(r) = 1 - \frac{2\hat{m}(r)}{r}, \quad f(r) = \left[\frac{\hat{m}(r)}{M} \right]^2 j(r). \quad (1.2)$$

³While contemporary artificial intelligence tools were used for literature review, they are not responsible for the ideas and results in this paper.

The mass function $\hat{m}(r)$, the mass interior to a sphere of areal radius r , takes the form:

$$\hat{m}(r) = \begin{cases} m, & r \in (r_+, 3m), \\ \frac{r}{3}, & r \in (3m, 3M), \\ M, & r \in (3M, \infty). \end{cases} \quad (1.3)$$

As shown in Fig. 2, $\hat{m}(r) = r/3$ out to the black hole's photon sphere at $r = 3m$; it grows linearly in the ocean $r \in (3m, 3M)$ until reaching the critical photon orbit of the combined system at $r = 3M$.

The ocean has energy density ρ and transverse pressure P_\perp , where:

$$\rho = 2P_\perp = \frac{\hat{m}'(r)}{4\pi r^2} = \frac{1}{12\pi G r^2}. \quad (1.4)$$

For a single layer in the ocean, the energy density $\sigma = \rho/A$ and surface pressure $p = P_\perp/A$ satisfy $\sigma = 2p$, which saturates the $\sigma \geq 2p$ bound in [11]. Similar HBH solutions exist in all space-time dimensions, with any cosmological constant Λ , for $d \geq 4$ [12].

Following [12, 13], we shall refer to a continuous region where $rf'/2f = 1$ as an *extended photon sphere*. We will show that throughout any such region, the condition (A.7) holds. The case of primary interest here, the HBH ocean, is *aligned* in the following sense: at each radius within the ocean, the layers join smoothly at $r = 3\hat{m}$, and at its edges the ocean joins to the photon sphere of a Schwarzschild geometry without an IJC. Alignment occurs for the HBH because $\sigma = 2p$ throughout the ocean; equivalently, $rf'/2f = 1$ at each edge.

Although the HBH metric is simple, it seems to have appeared minimally in the literature. The HBH may be viewed as a luminal Einstein cluster around a Schwarzschild black hole. Einstein clusters were recently generalized to include horizons in [28]; see also [29]. After a literature search, we determined that the HBH appears at least as a special case of Model 1 in [30], where Einstein clusters around black holes were considered as dark matter candidates. Maeda, Cardoso, and Wang noted [30] the marginal stability of Model 1 in the limit $\alpha \rightarrow 1/3$, which places the ISCO radius at the photon sphere.

2 Review: The Stability Obstruction in Asymptotically Flat Spacetime

A thermal bath surrounding a Schwarzschild black hole, in asymptotically flat spacetime, faces mechanical and thermodynamic constraints. These appear to be mutually exclusive. This section reviews three classic results that together sharpen this obstruction.

In Sec. 2.1 we review York's saddle-point evaluation of the gravitational path integral in a finite spherical cavity. His analysis shows thermodynamically stable shells are inside the photon sphere. In Sec. 2.2 we review the stability analysis of Brady, Louko, and Poisson (BLP). Their analysis shows mechanically stable shells sit outside the photon sphere. Then, in Sec. 2.3, we review Sorkin, Wald, and Zhang (SWZ), who carefully considered entropy maximization for isotropic radiation. As a consequence, self-gravitating isotropic radiation in equilibrium cannot reach the photon sphere: $\mu_{\max} \equiv M/R \approx .246 < 1/3$.

In Sec. 5, we will see that the backreaction of *anisotropic* radiation creates an extended photon sphere. This region satisfies both stability criteria, while the HBH [12, 13] mimics the optics and thermodynamics of an ordinary Schwarzschild black hole of mass M .

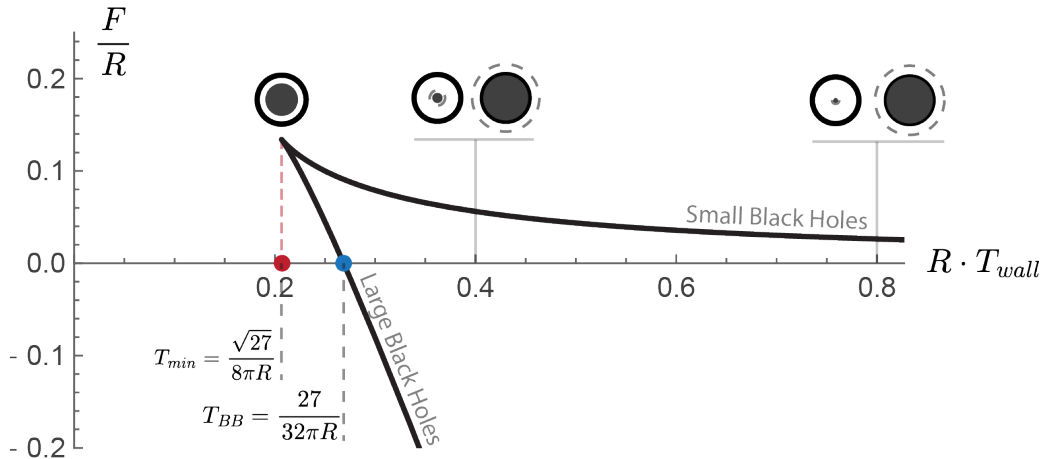


Figure 3. We illustrate York [8] using the modern swallow-tail diagram. The cavity wall is a solid black line; the photon sphere is a dashed line. There are two branches of black holes at fixed T_{wall} . Large black holes are thermodynamically stable and dominate the canonical ensemble above T_{BB} at $R = 9M/4$. At the minimum temperature $T_{min} = \frac{\sqrt{27}}{8\pi R}$, the branches merge at the photon sphere.

2.1 York Cavity Thermodynamics

York’s classic analysis of Schwarzschild thermodynamics in a finite cavity [8] uses the Euclidean saddle-point method of Hawking and Gibbons [31], but at finite distance; the fixed boundary data are the local (Tolman [32]) temperature T and area of the cavity wall.

If a Schwarzschild black hole of mass M sits at the center of the cavity, then the wall temperature is the Hawking temperature redshifted to the wall:

$$T(r) \equiv T = (8\pi M)^{-1} \left(1 - \frac{2M}{r}\right)^{-1/2}. \quad (2.1)$$

For fixed (r, T) , Eq.(2.1) is generically double-valued in M . Real positive solutions exist only above a minimum wall temperature:

$$T \geq \frac{\sqrt{27}}{8\pi r}. \quad (2.2)$$

These two branches merge at the minimum temperature, which coincides with the local Tolman temperature at the photon sphere. The large black hole’s photon sphere lies outside the cavity wall, while the small black hole’s photon sphere lies inside. This is similar to the familiar situation in AdS, where large black holes with positive specific heat have $r_h > L_{AdS}$, and small black holes with negative specific heat have $r_h < L_{AdS}$. See Fig. 3.

The Euclidean action includes the Einstein-Hilbert and Gibbons-Hawking-York terms:

$$I[g] = -\frac{1}{16\pi G_N} \left(\int_M d^4x \sqrt{|g|} R + 2 \int_{\partial M} d^3x \sqrt{|h|} K \right). \quad (2.3)$$

With the subtraction prescription, the on-shell action takes the compact form:

$$I = 12\pi M^2 - 8\pi M r + \beta r. \quad (2.4)$$

The Brown-York energy [8, 33] and coarse-grained entropy follow from the standard prescription:

$$E = \left(\frac{\partial I}{\partial \beta}\right)_A = r - r \left(1 - \frac{2M}{r}\right)^{1/2} \quad S = \beta \left(\frac{\partial I}{\partial \beta}\right)_A - I = 4\pi M^2. \quad (2.5)$$

Here $E \neq M$ at finite distance, because the difference in the S^2 for Schwarzschild and Minkowski gives $M = E - \frac{1}{2} \frac{E^2}{r}$. The specific heat changes sign at the photon sphere:

$$C_R \equiv T \left(\frac{\partial S}{\partial T}\right)_A = \left(\frac{\partial E}{\partial T}\right)_A = 8\pi M^2 \left[1 - \frac{2M}{r}\right] \left[\frac{3M}{r} - 1\right]^{-1}. \quad (2.6)$$

In Sec. 4.4 we show the specific heat at the photon sphere is inversely proportional to the cosmological constant for general spacetime dimensions; the particular definition of E does not change this behavior.⁴

The large black hole branch has positive specific heat and dominates the canonical ensemble above the Buchdahl temperature $T_{\text{BB}} = \frac{27}{32\pi R}$, where $R = 9M/4$. The free energy $F = E - TS$ changes sign at the same point:

$$2 \leq rM^{-1} < 2.25 \Leftrightarrow F < 0. \quad (2.7)$$

York's results [8] are similar to those of Hawking and Page in AdS [34], which were later interpreted in AdS/CFT by Witten [35, 36].

2.2 Mechanical Stability of Shells Around Black Holes

The Israel junction conditions for a static thin shell surrounding a Schwarzschild black hole were first worked out by Frauendiener, Hoenselaers, and Konrad [10], who determined the surface energy density σ and pressure p required to support a shell at areal radius R between Schwarzschild geometries of mass m (interior) and M (exterior).⁵ See Fig. 4. Defining $\alpha_{\pm} \equiv \sqrt{f_{\pm}(R)}$ with $f_{\pm} = 1 - 2M_{\pm}/R$, they found:

$$\sigma = \frac{1}{4\pi R} (\alpha_m - \alpha_M), \quad p = \frac{1}{8\pi R^2} \left(\frac{R - M}{\alpha_M} - \frac{R - m}{\alpha_m} \right). \quad (2.8)$$

They determined a minimum shell radius $R_{\text{min}} = 25M/12$ by saturating DEC ($p = \sigma$) for $m = 0$. They noted this was more compact than the Buchdahl radius $9M/4$ for a fluid ball.⁶

The connection between the photon sphere and the mechanical stability of thin shells around black holes was soon found by Brady, Louko, and Poisson (BLP) [11]. The IJC for a radially moving shell satisfies a one-dimensional effective equation of motion:

$$\beta_- - \beta_+ = 4\pi r \sigma, \quad \beta_{\pm} = \left(\dot{r}^2 + 1 - 2m_{\pm}/r\right)^{1/2}, \quad (2.9)$$

⁴Energy fluctuations would be naively expected to diverge at the photon sphere [8], but we show at third order in $F(E)$ that this effect is suppressed because the small and large black hole branches merge; see Appendix B for a calculation where the entropy also picks up a logarithmic correction.

⁵They were largely interested in constraining energy extraction from black holes. The related problem of lowering a DEC saturating rope toward the horizon had been previously studied [37] in this context. For a modern perspective on black hole mining, see [38]. Mining is one element of AMPS [39].

⁶The other branch of DEC saturation, $p = -\sigma$, puts the shell at the photon sphere (Sec. 3).

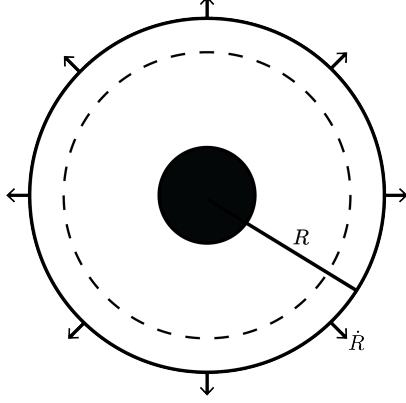


Figure 4. A thin shell around a black hole at radius R , with $\dot{R} \neq 0$. The stress tensor on the shell is $T_b^a = (-\sigma, p, \dots p)$. Shells placed inside the photon sphere in 3 + 1 dimensional asymptotically flat space, depicted as a dotted line at $R = 3M$, are mechanically unstable [11]; see Fig. 5.

where $\beta_{\pm} = (\dot{r}^2 + 1 - 2m_{\pm}/r)^{1/2}$ and $\dot{r} = dr/d\tau$. Together with the conservation equation, $\frac{d}{d\tau}(\sigma r^2) + p \frac{d}{d\tau}(r^2) = 0$, the static equilibrium conditions are:

$$\alpha_- - \alpha_+ = 4\pi r_0 \sigma_0, \quad \frac{m_+}{\alpha_+} - \frac{m_-}{\alpha_-} = 4\pi r_0^2 (\sigma_0 + 2p_0), \quad (2.10)$$

where $\alpha_{\pm} = (1 - 2m_{\pm}/r_0)^{1/2}$.

To determine stability against radial perturbations, they linearized the equation of state around equilibrium as $p = \lambda(\sigma - \tilde{\sigma})$, where $\lambda \equiv c_s^2$ is the squared speed of sound. Integrating the conservation equation and using the equilibrium conditions to eliminate $\tilde{\sigma}$ gives σ as a function of $z \equiv r/r_0$:

$$(1 + \lambda)\sigma/\sigma_0 = F/4z^2, \quad (2.11)$$

$$F(z) = \left(4\lambda + 1 - \frac{1}{\alpha_+ \alpha_-}\right) z^2 + \left(3 + \frac{1}{\alpha_+ \alpha_-}\right) z^{-2\lambda}. \quad (2.12)$$

Squaring the equation of motion twice yields an effective potential problem $r_0^2 \dot{z}^2 + V(z) = 0$, with $V(1) = V'(1) = 0$ by construction. Stability requires $V''(1) > 0$, which they showed is equivalent to the positivity of:

$$G(\lambda, \alpha_+, \alpha_-) \equiv 3(4\lambda + 1)\alpha_+^3 \alpha_-^3 + 4\lambda \alpha_+^2 \alpha_-^2 - (\alpha_+^2 + \alpha_-^2 + \alpha_+ \alpha_-). \quad (2.13)$$

They illustrated this result as a stability triangle in the (α_-, α_+) plane; the largest stable region is obtained with a luminal speed of sound, $\lambda = 1$. See Fig. 5. In the light-shell limit, $\alpha_+ = \alpha_- = \bar{\alpha}$, the stability boundary is at:

$$\bar{\alpha}(\lambda) = \left(\frac{\sqrt{4\lambda^2 + 36\lambda + 9} - 2\lambda}{3(4\lambda + 1)} \right)^{1/2}. \quad (2.14)$$

For $\lambda = 1$ this gives $\bar{\alpha} = 1/\sqrt{3}$, i.e. $r_0 = 3m_-$, the photon sphere. Mechanically stable shells satisfy $\sigma \geq 2p$, with the curve where $\sigma = 2p$ intersecting $\lambda = 1$ at the point where

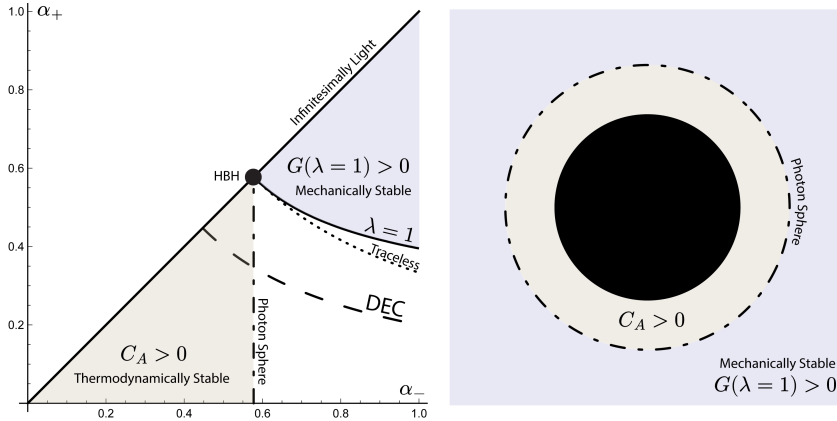


Figure 5. As shown by BLP [11], in asymptotically flat spacetime around a Schwarzschild black hole, the region of mechanical stability does not overlap with the thermodynamically stable region obtained by York [8]. These regions lie on opposite sides of the photon sphere, where they meet for massless $\sigma = 2p$ shells. This analysis is extended to AdS in Fig. 7.

the shell becomes massless. They concluded that for massive shells, joint stability was obstructed, because York’s result [8] requires $r \leq 3M$.

The flat-space stability triangle reviewed here corresponds to the limit $x \equiv r_0/L \rightarrow 0$ of the AdS analysis in Sec. 4, where we find that a finite window of joint mechanical and thermodynamic stability becomes available. For Schwarzschild, $f'(r) = 2m/r^2$ allows the equilibrium conditions to be expressed purely in terms of $\alpha_+\alpha_-$; the stability analysis is instead rephrased in terms of p_0/σ_0 in Sec. 4, linking it more closely to the IJC in Sec. 3.

2.3 Thermodynamics of Self-Gravitating Radiation

The thermodynamics of self-gravitating radiation within a spherical cavity was studied by Sorkin, Wald, and Zhang (SWZ) [17]. They showed that the problem of finding static equilibrium configurations can be recast as a variational principle for the total entropy.

They considered isotropic radiation of fixed total mass $M = m(R)$, with an equation of state $P = \rho/3$, and entropy density $s = a\rho^{3/4}$. This was placed in a box of radius R . They showed that by extremizing the total entropy functional:

$$I = \int_0^R \left(\frac{1}{r^2} \frac{dm}{dr} \right)^{3/4} \left(1 - \frac{2m(r)}{r} \right)^{-1/2} r^2 dr \quad \delta m(r)|_{0,R} = 0, \quad (2.15)$$

the Tolman-Oppenheimer-Volkoff (TOV) equation can then be obtained. In brief, they concluded that entropy extrema coincide with static equilibrium configurations.

They exploited scale invariance, introducing the dimensionless variables:

$$\mu \equiv \frac{m(r)}{r}, \quad q \equiv \frac{dm}{dr} = 4\pi r^2 \rho, \quad z \equiv \ln r. \quad (2.16)$$

This reduced the TOV equation to an autonomous system:

$$\frac{d\mu}{dz} = q - \mu, \quad \frac{dq}{dz} = \frac{2q \left(1 - 4\mu - \frac{2}{3}q \right)}{1 - 2\mu}. \quad (2.17)$$

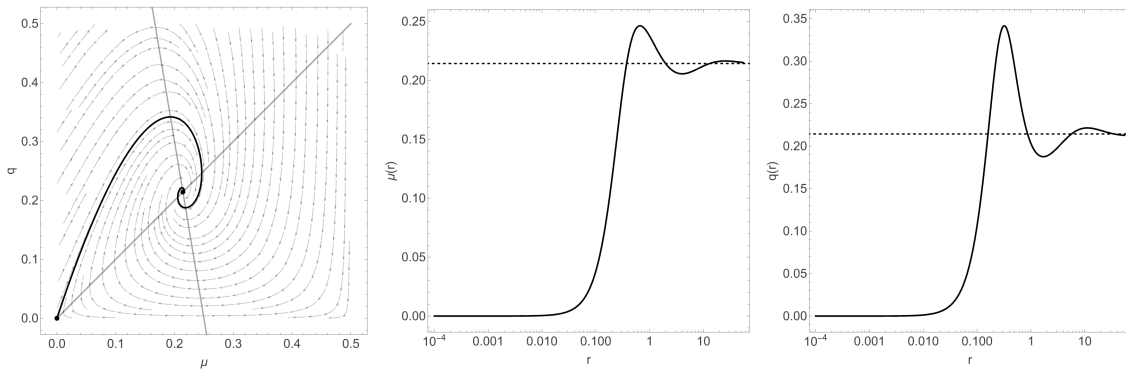


Figure 6. The solution to the Tolman-Oppenheimer-Volkoff (TOV) equation [17] for isotropic gas in thermal equilibrium. Here $q \equiv 4\pi r^2 \rho(r)$ and $\mu \equiv m(r)/r$. The vertical and horizontal nullclines are shown, crossing at the fixed point. The curve C spirals into the fixed point at $(\mu_*, q_*) = (\frac{3}{14}, \frac{3}{14})$; this approach is oscillatory, with μ and q executing damped oscillations around $\frac{3}{14}$ as $r \rightarrow \infty$.

Solution curves in the (μ, q) plane (see Fig. 6) can be understood using nullclines. The nullcline q_V , on which $d\mu/dz = 0$, is the line $q = \mu$; curves cross it vertically. The nullcline q_H , on which $dq/dz = 0$, is the line $4\mu + \frac{2}{3}q = 1$; curves cross it horizontally. These nullclines intersect at the fixed point $(\mu_*, q_*) = (\frac{3}{14}, \frac{3}{14})$.

The physically relevant solution C is regular at the origin with slope $q/\mu \rightarrow 3$ and spirals into the fixed point. The eigenvalues of the linearized system near the fixed point are $-\frac{3}{4} \pm i\sqrt{47}/4$, so the approach is oscillatory, with μ and q executing damped oscillations around $\frac{3}{14}$ as $r \rightarrow \infty$.

Each point on the curve is an equilibrium state at fixed box radius R , due to the scale invariance of this problem: $r \rightarrow \lambda r$, $m \rightarrow \lambda m$, $\rho \rightarrow \lambda^{-2}\rho$. Choosing where terminate the curve at $r = R$ gives a one-parameter family of equilibria labeled by M/R . These are stable up to the first turning point in μ , where $\mu_{max} \approx .246$, by the Poincaré turning point criterion [40–42]. The isotropic gas cannot reach the photon sphere because $\mu_{max} < \frac{1}{3}$. They noted that the entropy of these isotropic solutions scales as $S \sim M^{3/2}$.

They knew that at fixed mass, Eq. (2.15) diverges at the local Schwarzschild radius due to the redshift factor $\epsilon = (1 - 2m/r)^{-1/2}$. The thermal radiation has finite wavelength $\lambda \sim \rho^{-1/4}$ with proper distance from the horizon $D(r) > \lambda(r)$. Near the horizon, $D(r) \sim r^{1/2}\epsilon^{1/2}$, giving the inequality $\epsilon^{-1/2} \lesssim r^{1/2}\rho^{1/4}$. Inserting this into Eq. (2.15) gives $S \lesssim MR$, and so $S \sim M^2$ for $R \sim 2M$. We note this seems to be closely related to frozen stars [25, 26], which have the same energy density scaling.⁷

Now let us summarize. Consider a thermal bath with an inner surface at R_0 around a black hole. York’s calculation shows positive specific heat requires $R_0 \leq 3M$; however, the mechanical stability analysis by BLP for shells requires $R_0 \geq 3M$. We conclude that a

⁷The maximally entropic energy density profile obtained by SWZ is related to the proposal of Brustein, Medved, and Simhon [25, 26], who called these configurations “frozen stars”, see also [17]. The G_{rr} component of Einstein’s equations Eq. (5.6), for $\hat{m} = r/2$, gives $P_r = -\rho$. The TOV equation in Eq. (5.8) gives $P_{\perp} = 0$. Then Einstein’s equations require $\rho(r) = (4\pi r^2)^{-1}(d\hat{m}/dr)$; since $\hat{m} = r/2$, we have $\rho = 1/8\pi r^2$.

single shell will not suffice. In addition, isotropic radiation cannot reach the photon sphere because $\mu_{max} \leq 1/3$. The missing ingredient is anisotropy, as we will see in Sec. 5.

3 Time-Dependent Israel Junction Conditions

The well-known Israel junction conditions in D bulk dimensions are [9],

$$[K_{ab}] = -\kappa_D^2 \left(T_{ab} - \frac{1}{d-1} \gamma_{ab} T \right), \quad \kappa_D^2 = 8\pi G_D, \quad (3.1)$$

where γ_{ab} is the induced metric on the shell, $d = D - 1$ is the shell worldvolume dimension, and $T \equiv \gamma^{ab} T_{ab}$. The Israel layers it describes are best viewed as thin transition regions.

Here we extend an approach developed by Per Kraus [43] to more general spherically symmetric spacetimes. Let the shell have worldvolume dimension $d = n + 1$; take:

$$T^a{}_b = \text{diag}(-\sigma, p, p, \dots, p), \quad (3.2)$$

with n copies of p . The trace is $T = -\sigma + np$. The two independent jump conditions are:

$$\frac{[K^\tau{}_\tau]}{8\pi G_D} = \left(\frac{n-1}{n} \sigma + p \right) \quad \frac{[K^\theta{}_\theta]}{8\pi G_D} = - \left(\frac{\sigma}{n} \right). \quad (3.3)$$

Here $K^\theta{}_\theta = K^\phi{}_\phi$, and so on, for the angular directions. Note $[K]$ vanishes when the stress-energy tensor on the Israel layer is traceless:

$$[K] = [K^a{}_a] = \frac{8\pi G_D}{n} (np - \sigma) = \frac{8\pi G_D}{n} T^a{}_a. \quad (3.4)$$

The ratio Eq. (3.3) yields a compact expression for the Israel junction condition:

$$\frac{p}{\sigma} = -\frac{n-1}{n} - \frac{1}{n} \frac{[K^\tau{}_\tau]}{[K^\theta{}_\theta]}. \quad (3.5)$$

Now we determine the motion of these thin Israel layers in a time-independent bulk spacetime. Consider the following spherically symmetric, time-independent bulk ansatz:

$$ds^2 = -f(r) dt^2 + \frac{1}{j(r)} dr^2 + r^2 d\Sigma_n^2. \quad (3.6)$$

Parameterize the shell, with proper time τ , as $X^\mu = (t(\tau), R(\tau), \theta(\tau), \phi(\tau), \dots)$. Holding the angles fixed, the tangent vector $e^\mu_\tau \equiv \frac{\partial X^\mu}{\partial \tau} \equiv u^\mu$ is:

$$u^\mu = (\dot{t}, \dot{R}, 0, \dots, 0), \quad u^\mu u_\mu = -1. \quad (3.7)$$

From Eq. (3.6)-(3.7),

$$\dot{t}^2 = \frac{j(R) + \dot{R}^2}{f(R)j(R)}. \quad (3.8)$$

Let n^μ be the unit normal, with $n^\mu n_\mu = +1$ and $n_\mu u^\mu = 0$. This gives:

$$n^r = \epsilon \sqrt{j(R) + \dot{R}^2}, \quad \epsilon = \pm 1. \quad (3.9)$$

The extrinsic curvature is defined as $K_{ab} = e_a^\mu e_b^\nu \nabla_\mu n_\nu$. The angular components are:

$$K^\theta_\theta = \epsilon \frac{\sqrt{j(R) + \dot{R}^2}}{R}. \quad (3.10)$$

For the $\tau\tau$ component it is convenient to write:

$$K_{\tau\tau} = -n_\mu a^\mu, \quad a^\mu = u^\nu \nabla_\nu u^\mu = \frac{du^\mu}{d\tau} + \Gamma_{\alpha\beta}^\mu u^\alpha u^\beta. \quad (3.11)$$

Direct calculation gives:

$$K^\tau_\tau = \frac{\epsilon \left[\ddot{R} + \frac{f'(R)}{2f(R)} (j(R) + \dot{R}^2) - \frac{j'(R)}{2j(R)} \dot{R}^2 \right]}{\sqrt{j(R) + \dot{R}^2}}. \quad (3.12)$$

See Fig. 4 for an illustration of this configuration, for the special case where R is the radial direction to a spherical shell placed around a black hole.

3.1 Static Shells around Black Holes

To examine the stability of these shells we consider the static case, where $\dot{R} = \ddot{R} = 0$. Let $f = j$ on each side of the shell, which holds when the *bulk* stress-energy tensor vanishes. Then Eq. (3.10) and Eq. (3.12) reduce to:

$$K^\theta_\theta = \epsilon \frac{\sqrt{f(R)}}{R}, \quad K^\tau_\tau = \epsilon \frac{f'(R)}{2\sqrt{f(R)}}. \quad (3.13)$$

Here we consider shells with $\epsilon_+ = +1$ and $\epsilon_- = +1$:

$$[K^\tau_\tau] = \frac{f'_+(R)}{2\sqrt{f_+(R)}} - \frac{f'_-(R)}{2\sqrt{f_-(R)}}, \quad (3.14)$$

$$[K^\theta_\theta] = \frac{\sqrt{f_+(R)} - \sqrt{f_-(R)}}{R}. \quad (3.15)$$

Suppose each side is Schwarzschild–Tangherlini:

$$f(r) = 1 - \frac{\mu}{r^{n-1}}, \quad f'(r) = \frac{(n-1)\mu}{r^n}. \quad (3.16)$$

It is convenient to define:

$$\alpha_\pm \equiv \sqrt{f_\pm(R)}. \quad (3.17)$$

Then Eqs.(3.14)-(3.17) yield:

$$\frac{[K^\tau_\tau]}{[K^\theta_\theta]} = -\frac{n-1}{2} \left(1 + \frac{1}{\alpha_+ \alpha_-} \right), \quad (3.18)$$

and therefore, via Eq. (3.5):

$$\frac{p}{\sigma} = \frac{n-1}{2n} \left(\frac{1}{\alpha_+ \alpha_-} - 1 \right). \quad (3.19)$$

For the traceless case $T = 0$, appropriate for massless radiation, one has $\sigma = np$, so:

$$\alpha_+ \alpha_- = \frac{n-1}{n+1}. \quad (3.20)$$

For example, for $n = 2$ we have $\alpha_+ \alpha_- = 1/3$.

In particular, Eq. (3.17) can be used to obtain a recursion relation for layered shells. Writing $\alpha_{\pm}^2 = 1 - \mu_{\pm}/R^{n-1}$ and solving Eq. (3.20) for R^{n-1} gives:

$$R^{n-1} = \frac{(n+1) \left((n+1)\bar{\mu} \pm \sqrt{(n-1)^2 \bar{\mu}^2 + n(\delta\mu)^2} \right)}{4n}, \quad (3.21)$$

where we defined the ‘‘average’’ $\bar{\mu} \equiv \frac{\mu_+ + \mu_-}{2}$ and the ‘‘difference’’ $\delta\mu \equiv \mu_+ - \mu_-$.

If $\mu_+ = \mu_- \equiv \mu$ then Eq. (3.21) reduces to

$$R^{n-1} = \frac{n+1}{2} \mu \equiv R_{ps}^{n-1}, \quad (3.22)$$

which is the standard photon-sphere radius R_{ps} in $D = n + 2$ dimensions. For $n = 2$ we have $R = 3M$. Then in the infinitesimally light shell limit, static nested shells are located at the photon sphere.

For example, for $n = 2$ (4D) with $\mu_- = 2m$ and $\mu_+ = 2M$, Eq. (3.21) becomes:

$$\begin{aligned} R &= \frac{3}{8} \left(3m + 3M \pm \sqrt{9m^2 - 14mM + 9M^2} \right) \\ &= \frac{9}{4}\bar{m} + \frac{3}{4}\bar{m} \sqrt{1 + 2 \left(\frac{\delta m}{\bar{m}} \right)^2}, \end{aligned} \quad (3.23)$$

where $\delta m \equiv M - m$ and $\bar{m} \equiv \frac{M+m}{2}$. One layer can be self-supporting; this recovers the Buchdahl bound, since $m = 0$ gives $R = \frac{9}{4}M$. In Sec. 5.2, we will see that anisotropic gases satisfy these nesting relations at zero radial pressure.

3.2 Static Z_2 Shells are Pure Tension and Sit at the Photon Sphere

Here we show that Z_2 symmetric static branes⁸ are pure tension and are located at the photon sphere of the geometry. The Israel junction conditions for Z_2 symmetry have $\epsilon_+ = +1$ and $\epsilon_- = -1$, which gives:

$$[K^\theta_\theta] = \frac{2\sqrt{j(R) + \dot{R}^2}}{R} \quad (3.24)$$

$$[K^\tau_\tau] = \frac{2 \left[\ddot{R} + \frac{f'(R)}{2f(R)} \left(j(R) + \dot{R}^2 \right) - \frac{j'(R)}{2j(R)} \dot{R}^2 \right]}{\sqrt{j(R) + \dot{R}^2}} \quad (3.25)$$

Then Eq. (3.9) and Eq. (3.11) give:

$$\frac{[K^\tau_\tau]}{[K^\theta_\theta]} = \frac{K^\tau_\tau}{K^\theta_\theta} = \frac{\epsilon a^r/n^r}{\epsilon n^r/R} = \frac{a^r R}{j(R) + \dot{R}^2}, \quad (3.26)$$

⁸In the Randall-Sundrum [20, 21] and Karch-Randall models [44], one often takes a Z_2 reflection symmetry across the brane (an orbifold identification).

where $(n^r)^2$ eliminated $\epsilon = \pm 1$. The jump condition in Eq. (3.5) becomes:

$$\frac{p}{\sigma} = -\frac{n-1}{n} - \frac{1}{n} \frac{a^r R}{j(R) + \dot{R}^2}. \quad (3.27)$$

For a pure tension brane, $a^r = \frac{j(R) + \dot{R}^2}{R}$, and Eq. (3.11) gives:

$$\ddot{R} + \frac{f'(R)}{2f(R)} (j(R) + \dot{R}^2) - \frac{j'(R)}{2j(R)} \dot{R}^2 = \frac{j(R) + \dot{R}^2}{R}. \quad (3.28)$$

Now supposing the brane is static, we have:

$$\frac{Rf'(R)}{2f(R)} = 1 \implies R = R_{ps}. \quad (3.29)$$

The converse is similar; if the brane is static, inverting the above algebraic relations shows $p = -\sigma$, so the brane is pure tension. This is consistent with well-known results concerning Randall-Sundrum branes; see Appendix C for a non-trivial consistency check.

4 Stability of Shells Around Black Holes

Here we generalize the analysis of Brady, Louko, and Poisson [11], reviewed in Sec. 2.2, to general spherically symmetric spacetimes. In Sec. 4.2 and Sec. 4.3, the flat-space stability obstruction of Sec. 2 is generalized to AdS. In that case, joint stability is less difficult.

The specific heat at the photon sphere of a d -dimensional black hole is shown to be inversely proportional to the cosmological constant in Sec. 4.4. This is independent of how the energy is defined, provided it is monotonic in the mass enclosed within a finite region.

4.1 An Extended Formalism for Shell Stability

The Bianchi identity gives $\nabla^\mu T_{\mu\nu} = 0$, which leads to the usual expression for energy-momentum conservation on the thin Israel layer:

$$\dot{\sigma} + 2\frac{\dot{r}}{r}(\sigma + p) = 0. \quad (4.1)$$

This can be rewritten using the chain-rule, since $\sigma(R) = \sigma(R(\tau))$ implies $\dot{\sigma} = (d\sigma/dR)\dot{R}$:

$$\left(\frac{d\sigma}{dR}\right)\dot{R} + 2\frac{\dot{R}}{R}(\sigma + p) = 0. \quad (4.2)$$

Here we fix $\dot{\theta} = \dot{\phi} = 0$, and shall assume the equation of state for the brane is not pure tension *after* the perturbation: $(\sigma(R(\tau)) \neq -p(R(\tau)))$. It follows from this assumption that $\dot{\sigma} \neq 0$; from Eq. (4.2), this is needed for sound waves to propagate in the material. For static branes ($\dot{R} = 0$) we have:

$$\left.\frac{d\sigma}{dR}\right|_{R_0} = -\frac{2(\sigma_0 + p_0)}{R_0}. \quad (4.3)$$

The Israel junction conditions in Eq. (3.1), Eq. (3.14), and Eq. (3.15) require that:

$$\sqrt{\dot{R}^2 + f_-(R)} - \sqrt{\dot{R}^2 + f_+(R)} = \frac{\kappa^2}{2}\sigma(R)R. \quad (4.4)$$

This gives $\dot{R}^2 + V(R) = 0$, where:

$$V(R) = f_-(R) - \frac{(f_+(R) - f_-(R) - S^2)^2}{4S^2}, \quad (4.5)$$

and $S(R) \equiv \frac{\kappa^2}{2}\sigma(R)R$. Then a shell at R_0 is mechanically stable if:

$$V(R_0) = V'(R_0) = 0 \quad V''(R_0) > 0. \quad (4.6)$$

To determine a condition for stability we need $\sigma(r)$, which we obtain from a Taylor expansion around σ_0 . From the conservation equation Eq. (4.3) and the linearized equation of state $p = \lambda(\sigma - \bar{\sigma})$:

$$\frac{d\sigma}{dr} + \frac{2(1+\lambda)}{r}\sigma = \frac{2\lambda}{r}\bar{\sigma}. \quad (4.7)$$

Here $\lambda \equiv c_s^2$ is the square of the speed of sound for waves propagating on the shell. The boundary condition is $\sigma(r_0) = \sigma_0$. This gives:

$$(1+\lambda)\frac{\sigma}{\sigma_0} = \lambda\frac{\bar{\sigma}}{\sigma_0} + \left(1+\lambda - \lambda\frac{\bar{\sigma}}{\sigma_0}\right)\left(\frac{r}{r_0}\right)^{-2(1+\lambda)}. \quad (4.8)$$

To eliminate $\bar{\sigma}$, note that in equilibrium, the IJCs in asymptotically flat space give:

$$\frac{p}{\sigma} = \frac{n-1}{2n}\left(\frac{1}{\alpha_+\alpha_-} - 1\right). \quad (4.9)$$

For $n = 2$:

$$\frac{p_0}{\sigma_0} = \frac{1 - \alpha_+\alpha_-}{4\alpha_+\alpha_-}. \quad (4.10)$$

Then if the equation of state is expanded around the equilibrium solution:

$$\frac{\bar{\sigma}}{\sigma_0} = 1 - \frac{1}{\lambda}\frac{p_0}{\sigma_0} = \frac{4\lambda + 1 - \frac{1}{\alpha_+\alpha_-}}{4\lambda}. \quad (4.11)$$

Then we can define $z = r/r_0$ and get:

$$(1+\lambda)\frac{\sigma}{\sigma_0} = \frac{1}{4}\left(4\lambda + 1 - \frac{1}{\alpha_+\alpha_-}\right) + \frac{1}{4}\left(3 + \frac{1}{\alpha_+\alpha_-}\right)z^{-2(1+\lambda)}. \quad (4.12)$$

Define:

$$F(z) \equiv \left(4\lambda + 1 - \frac{1}{\alpha_+\alpha_-}\right)z^2 + \left(3 + \frac{1}{\alpha_+\alpha_-}\right)z^{-2\lambda} \quad (4.13)$$

Then:

$$(1+\lambda)\frac{\sigma}{\sigma_0} = \frac{F(z)}{4z^2} \quad (4.14)$$

Rephrasing the IJC using $z = r/r_0$ and $\dot{z} = \dot{r}/r_0$, with $V(z) \equiv V(r_0z)$:

$$r_0^2\dot{z}^2 + V(z) = 0. \quad (4.15)$$

Let us extend this result to the general case. We saw before that:

$$\frac{p}{\sigma} = -\frac{n-1}{n} - \frac{1}{n} \frac{[K_\tau^\tau]}{[K_\theta^\theta]} \quad (4.16)$$

The jumps are:

$$[K_\tau^\tau] = \frac{f'_+(R)}{2\sqrt{f_+(R)}} - \frac{f'_-(R)}{2\sqrt{f_-(R)}}, \quad [K_\theta^\theta] = \frac{\sqrt{f_+(R)} - \sqrt{f_-(R)}}{R}. \quad (4.17)$$

Specializing to $n = 2$ (4D) gives:

$$\frac{p(r_0)}{\sigma(r_0)} = -\frac{1}{2} - \frac{1}{2} \frac{\frac{f'_+(r_0)}{2\sqrt{f_+(r_0)}} - \frac{f'_-(r_0)}{2\sqrt{f_-(r_0)}}}{\frac{\sqrt{f_+(r_0)} - \sqrt{f_-(r_0)}}{r_0}} \quad (4.18)$$

The structural difference, in comparison to the analysis of BLP [11], is that $f'(r_0)$ simplifies nicely in asymptotically flat space, but not in AdS. It is still true that:

$$\frac{\bar{\sigma}}{\sigma_0} = 1 - \frac{1}{\lambda} \frac{p_0}{\sigma_0}. \quad (4.19)$$

Then the conservation law gives:

$$(1 + \lambda) \frac{\sigma(z)}{\sigma_0} = \left(\lambda - \frac{p_0}{\sigma_0} \right) + \left(1 + \frac{p_0}{\sigma_0} \right) z^{-2(1+\lambda)}. \quad (4.20)$$

This suggests that we define:

$$(1 + \lambda) \frac{\sigma}{\sigma_0} \equiv \frac{F(z)}{4z^2} \implies F(z) \equiv 4 \left(\lambda - \frac{p_0}{\sigma_0} \right) z^2 + 4 \left(1 + \frac{p_0}{\sigma_0} \right) z^{-2\lambda}. \quad (4.21)$$

To obtain $S(R)$ we use Eq. (4.4) for $\dot{R} = 0$ at $z \equiv r/r_0$ at $z = 1$:

$$S_0 \equiv S(1) = \sqrt{f_-(r_0)} - \sqrt{f_+(r_0)}, \quad S(z) = S_0 \frac{F(z)}{4(1+\lambda)z}. \quad (4.22)$$

$$V(z) = f_-(r_0 z) - \frac{(f_+(r_0 z) - f_-(r_0 z) - S(z)^2)^2}{4S(z)^2}. \quad (4.23)$$

To determine stability at $z = 1$ (where, by construction, $V(z) = V'(z) = 0$) we need to check if $V(z)$ is concave up or concave down. Note that $S(z)$ depends on $F(z)$, which in turn depends on Eq. (4.18).

If a pure tension brane satisfies the very rigid constraint that it remains pure tension after the perturbation, a straightforward calculation at the photon sphere yields:

$$V''(r_0) = r_0^2 h''(r_0), \quad h(r_0) \equiv \frac{f(r_0)}{r_0^2}. \quad (4.24)$$

At the photon sphere of a black hole, $h(R_0)$ is a local maximum of the effective potential. When an extended photon sphere exists, $h'' = 0$ [12]. For a more general result see App. A.⁹

Pure tension branes with rigid equations of state, e.g. unstabilized Randall-Sundrum branes, are unstable. The brane is stabilized by its response to a perturbation; when the brane is pushed inward, the stiffness of the brane provides a restoring force that keeps it there, causing sound waves to propagate in the material.

4.2 Thermal Stability in anti-de Sitter Space

The regions of mechanical and thermodynamic stability do not coincide in flat space; they only intersect at $r_0 = 3M$. However, we find that in AdS the regions overlap. To avoid ambiguity in this section, we write C_{r_0} instead of C_R , which is the standard notation.

To repeat the York computation for the specific heat C_{r_0} in AdS, we write:

$$T(r_0) = T_H(m, L) \sqrt{\frac{f_{\text{AdS}}(r_0)}{f(r_0)}}. \quad (4.26)$$

Here $f_{\text{AdS}} = 1 + \frac{r_0^2}{L^2}$ and $f = 1 + \frac{r_0^2}{L^2} - \frac{2m}{r_0}$. For convenience we define:

$$g(r_0) \equiv \sqrt{\frac{f_{\text{AdS}}(r_0)}{f(r_0)}}, \quad \Rightarrow \quad T(r_0) = T_H g(r_0). \quad (4.27)$$

The specific heat within a cavity at some r_0 is:

$$C_{r_0} \equiv \left(\frac{dE}{dT} \right)_{r_0} = \frac{(dE/dm)_{r_0}}{(dT/dm)_{r_0}}. \quad (4.28)$$

Following York [8], the thermodynamic energy is:

$$E(r_0) = r_0 f_{\text{AdS}}(r_0) \left(1 - \sqrt{\frac{f(r_0)}{f_{\text{AdS}}(r_0)}} \right). \quad (4.29)$$

A straightforward computation gives $(dE/dm)_{r_0} = g(r_0)$. This useful simplification gives an expression for C_{r_0} where g cancels:

$$\frac{dT}{dm} = g \frac{dT_H}{dm} + T_H \frac{dg}{dm} = g(r_0) \left(\frac{dT_H}{dm} + \frac{T_H}{r_0 f(r_0)} \right) \Rightarrow C_{r_0}^{-1} = \frac{dT_H}{dm} + \frac{T_H}{r_0 f(r_0)}. \quad (4.30)$$

⁹Traceless light shells, at the photon sphere, may be viewed as orbiting massless particles. Defining $f_-(R) \equiv f(R)$ for notational simplicity, write $f_+(R) = f(R) + \delta f(R)$ and take the light-shell limit of Eq. (4.5). Noting $|\delta f| = 2|\delta m|/R$, a short calculation yields:

$$\left(\frac{\dot{R}}{R} \right)^2 = \frac{1}{b(R)^2} - \frac{f(R)}{R^2}, \quad \frac{1}{b(R)^2} = \left(\frac{2|\delta m|}{\kappa^2 \sigma(R) R^3} \right)^2. \quad (4.25)$$

Energy conservation for the shell in Eq. (4.1), for an equation of state $p \equiv w\sigma$, gives $\sigma(R) \propto R^{-2(1+w)}$. For $w = 1/2$ (traceless) shells $\sigma(R)R^3 \propto (\sigma A)R = ER$ is conserved. Indeed, evaluating Eq. (4.5) at $r_0 = 3m$ and inserting it into Eq. (4.46) gives $\sigma_0 = 2p_0$. Taking $Rd\phi = d\tau$ gives the null geodesic equation.

A more general discussion can be found in Sec. 4.4, where we note the definition of $E(r_0)$ is unimportant for this analysis. The specific heat changes sign at the pole:

$$r_0 f(r_0) = -\frac{T_H}{dT_H/dm} \implies r_0 + \frac{r_0^3}{L^2} - 2m = -\frac{T_H(m, L)}{dT_H/dm}. \quad (4.31)$$

For instance, for AdS Schwarzschild black holes:

$$m = \frac{r_+}{2} \left(1 + \frac{r_+^2}{L^2} \right), \quad T_H = \frac{f(r_+)}{4\pi} = \frac{1}{4\pi r_+} \left(1 + \frac{3r_+^2}{L^2} \right). \quad (4.32)$$

This gives, for the first term in $C_{r_0}^{-1}$:

$$\frac{dT_H}{dm} = \frac{dT_H/dr_+}{dm/dr_+} = \frac{\left(\frac{3}{L^2} - \frac{1}{r_+^2} \right)}{2\pi \left(1 + \frac{3r_+^2}{L^2} \right)}. \quad (4.33)$$

The first term in $C_{r_0}^{-1}$ reflects the well-known spinodal transition, where the specific heat diverges at $r_+ = \frac{L}{\sqrt{3}}$. The finite distance computation gave the additional second term, which shifts the location of the pole in C_{r_0} .

This can be understood as follows. The specific heat changes sign only on the small black hole branch, where $\frac{dT_H}{dm} < 0$. In particular:

$$r_0 f(r_0) = r_0 + \frac{r_0^3}{L^2} - 2m, \quad \frac{d}{dr_0} (r_0 f(r_0)) = 1 + \frac{3r_0^2}{L^2} > 0. \quad (4.34)$$

The LHS is strictly increasing in r_0 , so there can be at most one radius r_0^* where the specific heat changes sign for fixed (m, L) .¹⁰

It is simple to understand this in slightly more detail. In flat space the specific heat changes sign at $r_0 = 3m$, which can be seen by asymptotically expanding at large L :

$$r_+(m) = 2m - \frac{8m^3}{L^2} + \frac{96m^5}{L^4} + O\left(\frac{1}{L^6}\right). \quad (4.36)$$

Inserting this into the Hawking temperature $T_H(r_+) = \frac{1}{4\pi r_+} \left(1 + \frac{3r_+^2}{L^2} \right)$ and once again expanding at large L yields:

$$T_H(m) = \frac{1}{8\pi m} + \frac{2m}{L^2\pi} - \frac{10m^3}{L^4\pi} + O\left(\frac{1}{L^6}\right) \quad (4.37)$$

Now we solve asymptotically at large L for the location of the pole in Eq. (4.31), which corresponds to the small black hole branch. This gives:

$$-\frac{T_H(m, L)}{dT_H/dm} = m + \frac{32m^3}{L^2} + \frac{192m^5}{L^4} + O\left(\frac{1}{L^6}\right). \quad (4.38)$$

¹⁰This mirrors the mechanical stability analysis in the next section, because the $A(x) = (1 + 3x^2)^2$ terms in $V''(1)$ are sensitive to:

$$\frac{p_0}{\sigma_0} = -\frac{1}{4} + \frac{1 + 3x^2}{4\alpha_+ \alpha_-}, \quad x = \frac{r_0}{L}. \quad (4.35)$$

That is, the r^2/L^2 term enhances the shell's restoring force and enlarges the mechanically stable region.

Finally, solving for the location of the pole and expanding again in large L gives:

$$r_0|_{C_{r_0}^{-1}=0} = 3m + \frac{5m^3}{L^2} + \frac{57m^5}{L^4} + O\left(\frac{1}{L^6}\right). \quad (4.39)$$

In conclusion then, in A(dS) the thermodynamically stable region sits outside (inside) the photon sphere. This procedure can be easily carried out to all orders.

To summarize, the specific heat C_{r_0} changes sign at r_0 *outside* the photon sphere on the small black hole branch. As we approach the spinodal point, at $r_+ \rightarrow \frac{L}{\sqrt{3}}$, the location where the specific heat changes sign runs off to asymptotic infinity. Indeed, for large black holes the specific heat is positive for all locations of the cavity wall r_0 .

More generally, the specific heat at the photon sphere is inversely proportional to the cosmological constant in all dimensions; see Sec. 4.4.

4.3 Joint Stability of Shells around AdS Black Holes

The mechanical stability of an infinitesimally light, traceless shell around a black hole in asymptotically flat spacetime is *marginal* at $r = 3M$ when the squared speed of sound is luminal: $\lambda = 1$. See Sec. 2.2.

Applying the formalism developed here, in AdS we find these shells are conditionally stable between $\lambda \in (\frac{1}{2}, 1)$. To show this we need $V''(z) > 0$ at $z = 1$, in the limit where $m \rightarrow M$. We shall assume the AdS radius L is the same on both sides of the shell.

The stability triangle depends on the AdS radius L . To make the comparison, it is convenient to define $x \equiv \frac{r_0}{L}$ which gives:

$$\frac{m}{r_0} = \frac{1 + x^2 - \alpha_-^2}{2} \quad \frac{M}{r_0} = \frac{1 + x^2 - \alpha_+^2}{2}. \quad (4.40)$$

Since α_{\pm} are not bounded above by 1, to fit the entire stability triangle inside $(0, 1) \times (0, 1)$ we rescale:¹¹

$$\alpha_{\pm} \equiv \tilde{\alpha}_{\pm} \sqrt{1 + x^2}. \quad (4.41)$$

This gives a complicated expression:

$$V''(1) = -\frac{\tilde{\alpha}_- \tilde{\alpha}_+ A(x) + \tilde{\alpha}_+^2 A(x) - 3\tilde{\alpha}_-^3 \tilde{\alpha}_+^3 B(x)(1 + 4\lambda) - \tilde{\alpha}_-^2 C(\tilde{\alpha}_+, x, \lambda)}{2\tilde{\alpha}_-^2 \tilde{\alpha}_+^2 (1 + x^2)} \quad (4.42)$$

$$A(x) \equiv (1 + 3x^2)^2, \quad B(x) \equiv (1 + x^2)^2 \quad (4.43)$$

$$C(\tilde{\alpha}_+, x, \lambda) \equiv -1 + 4\tilde{\alpha}_+^2 \lambda + 3x^4 (-3 + 4\tilde{\alpha}_+^2 (1 + \lambda)) + 2x^2 (-3 + \tilde{\alpha}_+^2 (6 + 8\lambda)). \quad (4.44)$$

In the limit where $x \rightarrow 0$, taking $\tilde{\alpha}_+ = \tilde{\alpha}_- = \tilde{\alpha}$ and solving for $V''(1) = 0$, we recover the flat space answer of Poisson et al. [11]:

$$\tilde{\alpha}(\lambda) = \left(\frac{\sqrt{4\lambda^2 + 36\lambda + 9} - 2\lambda}{3(4\lambda + 1)} \right)^{1/2} + O(x^2). \quad (4.45)$$

¹¹Curiously, this rescaling is the same factor that is needed to obtain the correct boundary temperature.

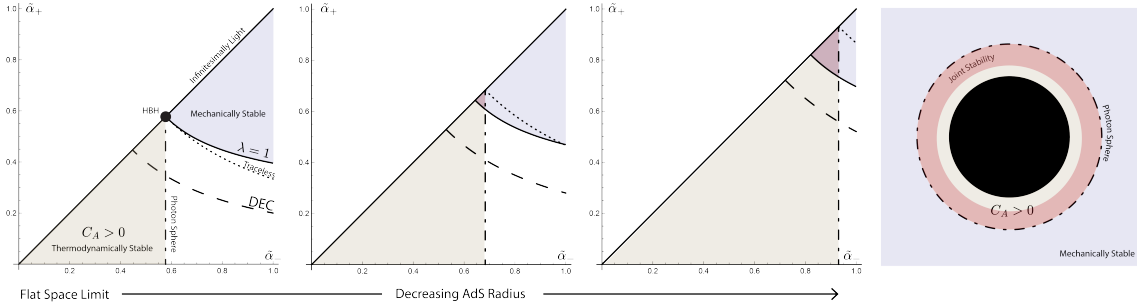


Figure 7. Overlapping regions of mechanical and thermodynamic stability for shells around small black holes satisfying $m \ll L_{AdS}$ are shown. The thermodynamically stable region grows with r_+ . The flat-space limit recovers Fig. 5. Shells are *stable* at the photon sphere, where these regions now overlap. The mechanically stable region approaches the horizon in the limit $L_{AdS} \rightarrow 0$. In the planar black hole limit, the region of joint stability fills the entire spacetime outside of the horizon.

To generalize BLP’s analysis [11] we need one more insight. It follows from the IJCs, see Eq. (4.18), that:

$$\frac{p_0}{\sigma_0} = -\frac{1}{4} + \frac{1+3x^2}{4\alpha_+\alpha_-} = -\frac{1}{4} + \frac{(1+3x^2)}{4(1+x^2)\tilde{\alpha}_+\tilde{\alpha}_-}. \quad (4.46)$$

These suffice to repeat the stability analysis of BLP in AdS. See Fig. 7. As in flat space, DEC is satisfied by a large margin. The $\sigma_0 = 2p_0$ curve intersects the photon sphere in the infinitesimally light shell limit.

An infinitesimally thin shell at the photon sphere is mechanically stable in AdS. The condition that $V''(1) > 0$, in the light shell limit, reads:

$$\lambda > \frac{L^2 + 27m^2/2}{L^2 + 27m^2}. \quad (4.47)$$

This ranges between $\frac{1}{2}$ (small L) and 1 (large L). For $\lambda = 1$ the shell is mechanically stable for all finite L in the light-shell limit because $V''(1) = \frac{54m^2}{L^2}$.

As the AdS curvature increases ($L_{AdS} \rightarrow 0$), the mechanically stable region approaches the horizon monotonically. To see this, choose $\lambda = 1$, $\tilde{\alpha}_+ = \tilde{\alpha}_- = \tilde{\alpha}$, and solve Eq. (4.42) for $\tilde{\alpha}^2$. Taking the limit of the resulting expression as $x \rightarrow \infty$ gives $\tilde{\alpha}^2 = \frac{1}{15} (3\sqrt{61} - 12)$. Since $\tilde{\alpha} \equiv kx$ in this limit, $k \rightarrow 0$, so the region of mechanical stability extends arbitrarily close to the horizon as the black hole becomes large compared to the AdS scale.

The region of overlapping mechanical and thermodynamic stability fills all of spacetime for an infinitely large black hole; it overlaps only at the photon sphere for an infinitesimally small one. Curiously, unlike in flat space, sound waves may causally propagate on a shell inside the photon sphere, even though massless particles would fall into the black hole.¹²

¹²For large AdS curvature (small L) the sound waves propagate at the sound speed of a (2+1)-dimensional CFT. In higher dimensions the pattern $\lambda \equiv c_s^2 = 1/(d-1)$ appears to hold at small L .

4.4 The Specific Heat at the Photon Sphere is Inversely Proportional to $-\Lambda$

Here we show the following general result, which holds in all dimensions where photon spheres exist ($n \geq 2$). The inverse specific heat $C_{r_0}^{-1}$ at the photon sphere of a black hole is proportional to (minus) the cosmological constant Λ .

This fact is independent of the definition of E , provided E is monotonic in μ , because:

$$C_{r_0}^{-1} = \frac{dT}{dE} \Big|_{r_0} = \frac{dT/d\mu}{dE/d\mu} \Big|_{r_0} \propto \frac{dT}{d\mu} \Big|_{r_0}. \quad (4.48)$$

To determine where $\frac{dT}{d\mu} \Big|_{r_0}$ changes sign, write the local temperature in terms of the surface gravity $\kappa \equiv \frac{f'(r_+)}{2}$ and calculate:

$$T(r_0) = \frac{\kappa}{2\pi\sqrt{f(r_0)}} \implies \frac{d \ln T}{d\mu} \Big|_{r_0} = \frac{d \ln \kappa}{d\mu} - \frac{1}{2} \frac{1}{f(r_0)} \frac{\partial f(r_0)}{\partial \mu} \Big|_{r_0}. \quad (4.49)$$

For general Schwarzschild-Tangherlini black holes where $f(r) = 1 + \epsilon \frac{r^2}{L^2} - \frac{\mu}{r^{n-1}}$, the r and μ derivatives are related by $r\partial_r f = -(n-1)\mu\partial_\mu f + 2\epsilon \frac{r^2}{L^2}$. At the photon sphere, this gives:

$$\frac{d \ln T}{d\mu} \Big|_{r_{\text{ps}}} = \frac{d \ln \kappa}{d\mu} + \frac{1}{(n+1)\mu f(r_{\text{ps}})}. \quad (4.50)$$

Note that $\mu = r_h^{n-1} \left(1 + \epsilon \frac{r_h^2}{L^2}\right)$, where $r_{\text{ps}}^{n-1} = \frac{n+1}{2}\mu$. This gives:

$$\kappa = \frac{1}{2r_h} \left[(n-1) + \epsilon(n+1) \frac{r_h^2}{L^2} \right] \quad f_{\text{ps}} = f(r_{\text{ps}}) = \frac{n-1}{n+1} + \epsilon \frac{r_{\text{ps}}^2}{L^2}. \quad (4.51)$$

For later use, it is convenient to define the ratio:

$$\left(\frac{r_{\text{ps}}}{r_h}\right)^{n-1} = \frac{n+1}{2} \left(1 + \epsilon \frac{r_h^2}{L^2}\right) \equiv Q. \quad (4.52)$$

Then we obtain:

$$\mu \frac{d \log T}{d\mu} \Big|_{r_{\text{ps}}} = \frac{\left(1 + \epsilon \frac{r_h^2}{L^2}\right) \left[\epsilon(n+1) \frac{r_h^2}{L^2} - (n-1)\right]}{\left[(n-1) + \epsilon(n+1) \frac{r_h^2}{L^2}\right]^2} + \frac{1}{(n-1) + \epsilon(n+1) \frac{r_{\text{ps}}^2}{L^2}}. \quad (4.53)$$

In asymptotically flat spacetime, $\epsilon = 0$ and these terms cancel exactly. We now consider AdS ($\epsilon = 1$) and dS ($\epsilon = 1 - 1$) in turn, pausing to consider how certain features are reflected in their mirror arguments.

In AdS ($\epsilon = 1$) the first term in Eq. (4.53) changes sign at the spinodal point, where $\frac{r_h^2}{L^2} = \frac{n-1}{n+1}$ and the two black hole branches merge. Both terms are manifestly positive on the large black hole branch. On the small black hole branch, we need to show that:

$$\left(\frac{(n-1) + (n+1) \frac{r_h^2}{L^2}}{(n-1) + (n+1) \frac{r_{\text{ps}}^2}{L^2}}\right) > \left(1 + \frac{r_h^2}{L^2}\right) \frac{(n-1) - (n+1) \frac{r_h^2}{L^2}}{(n-1) + (n+1) \frac{r_h^2}{L^2}}. \quad (4.54)$$

For this purpose it is convenient to rewrite our expressions in terms of Q using Eq. (4.52):

$$\mu \frac{d \log T}{d \mu} \Big|_{r_{\text{ps}}} = \frac{Q(Q-n)}{(n+1)(Q-1)^2} + \frac{1}{(n-1) + (2Q-n-1)Q^{2/(n-1)}}. \quad (4.55)$$

In this language the spinodal transition in AdS occurs at $Q = n$. Both terms are manifestly positive on the large black hole branch. On the small black hole branch, we need:

$$n > Q > \frac{n+1}{2}, \quad (2Q-n-1) \left[nQ - 1 - (n-Q)Q^{\frac{n+1}{n-1}} \right] > 0. \quad (4.56)$$

The first factor in Eq. (4.56) is positive because $Q > (n+1)/2$ on the small black hole branch. The second factor is also positive; to see this, call the second term $H(Q)$:

$$H(Q) \equiv nQ - 1 - (n-Q)Q^{\frac{n+1}{n-1}}, \quad H\left(\frac{n+1}{2}\right) > 0 \quad \text{for } n \geq 2. \quad (4.57)$$

To establish proportionality later, we will use the fact that $H(Q)$ is positive in each case. In passing we note that $H(Q)$ is positive on the small black hole branch, since:

$$H'(Q) = n + Q^{\frac{2}{n-1}} \left(\frac{2n(Q - \frac{n+1}{2})}{n-1} \right) > 0. \quad (4.58)$$

In dS ($\epsilon = -1$) the black hole horizon coincides with the cosmological horizon in the Nariai limit, which occurs when $\frac{r_h^2}{L^2} = \frac{n-1}{n+1}$ and $Q = 1$. The relation has mirror interpretations in AdS and dS. In AdS this is the spinodal point, while in dS it is the Nariai limit. We are not aware of this parallel being emphasized before in this form.¹³

In dS the AdS argument is essentially mirrored with signs reversed. Black holes below the Nariai limit satisfy $1 < Q < \frac{n+1}{2}$; by similar reasoning we need to show:

$$\frac{(n-1) - (n+1)\frac{r_h^2}{L^2}}{(n-1) - (n+1)\frac{r_{\text{ps}}^2}{L^2}} < \left(1 - \frac{r_h^2}{L^2} \right) \frac{(n-1) + (n+1)\frac{r_h^2}{L^2}}{(n-1) - (n+1)\frac{r_h^2}{L^2}}. \quad (4.59)$$

In other words:

$$1 < Q < \frac{n+1}{2}, \quad (2Q-n-1) \left[nQ - 1 - (n-Q)Q^{\frac{n+1}{n-1}} \right] < 0. \quad (4.60)$$

The first factor is manifestly negative in dS because $1 < Q < (n+1)/2$. The second factor is the same $H(Q)$ used in the AdS case.

We now show that $H'(Q)$ has a single root at $Q = 1$; we will see that $H(Q) > 0$. When photon spheres exist, $n \geq 2$, and so $Q > 1$ in both AdS and dS.

It is helpful to write $H'(Q)$ as:

$$H'(Q) = n \left[1 - \frac{(n+1-2Q)Q^{2/(n-1)}}{n-1} \right] \equiv n \left[1 - \frac{G(Q)}{n-1} \right]. \quad (4.61)$$

¹³Curiously, if the analytic continuation of the AdS Hawking-Page transition in Eq. (4.53) at $r_h = L$ occurred on a physical branch, it would give $Q = 0$.

Note that $G(1) = n - 1$. Additionally:

$$G'(Q) = \frac{2(n+1)}{n-1} Q^{2/(n-1)-1} (1-Q) < 0. \quad (4.62)$$

Then for $Q > 1$ we have $G(Q) < n - 1$ and $H'(Q) > 0$. It follows that $H(Q) > 0$ because $H(1) = 0$. We conclude that $H(Q) > 0$ in both AdS and dS; $Q = \frac{n+1}{2}$ is precisely the flat space limit where $C_R^{-1} = 0$.

Meanwhile, it follows from Eq. (4.50) and Eq. (4.52) that:

$$(n-1) + (2Q - n - 1)Q^{2/(n-1)} = (n+1)f(r_{\text{ps}}). \quad (4.63)$$

It follows from Eq. (4.52) that $2Q - n - 1 = -\frac{2\Lambda r_h^2}{n}$. Then Eq. (4.55) can be written as:

$$\mu \left. \frac{\partial \log T}{\partial \mu} \right|_{r_{\text{ps}}} = \frac{(2Q - n - 1)H(Q)}{(n+1)(Q-1)^2(n+1)f(r_{\text{ps}})} \propto -\Lambda. \quad (4.64)$$

Then the inverse specific heat $C_{r_0}^{-1}$ at the photon sphere is proportional to $-\Lambda$, as claimed.¹⁴

5 Self-Gravitating Radiation and the Photon Sphere

Here we present our main arguments. One key objective is to extend SWZ [17], reviewed in Sec. 2.3, to anisotropic matter. First we derive the anisotropic TOV equation, clarifying the role of the photon sphere, in Sec. 5.1. In Sec. 5.2 we show that Israel layers form in the limit where the radial pressure goes to zero. We then reflect on their thermodynamics using entropy maximization in Sec. 5.2.3. See Kim and Lee [23] for previous work, which found scaling relations using a temperature independent entropy maximization method.

In Sec. 5.3, we find an exception to the joint stability obstruction reviewed in Sec. 2: the HBH [12, 13]. At zero radial pressure, the self-similar fixed point in SWZ's analysis (Fig. 6) becomes the line of fixed points in Fig. 11. The solution curve (C in Fig. 6) crosses these fixed points in locations which we show are equivalent to the Israel junction conditions. If this line is crossed once, it gives an extended photon sphere, in this case made of thin traceless shells, realizing the thought experiment in Fig. 1. The HBH sits at the single point where the mechanical and thermodynamic stability regions meet in Fig. 5.

In Sec. 5.3.1, we show the HBH is the coldest stable nested shell configuration around a black hole; the Hawking temperature is unchanged at fixed total mass. In Sec. 5.4, we show the following general result: at fixed total mass, adding a shell around a black hole decreases the asymptotic temperature iff the local specific heat at the shell is *positive*. This gives a simple interpretation of the result in Sec. 5.3.1: shells at the photon sphere leave the asymptotic temperature unchanged, because $\Lambda = 0$ there (see Sec. 4.4), making the resulting configuration (e.g. the HBH) precisely as cold as a black hole of mass M .

In Sec. 5.5.2, an alternative approach to black hole thermodynamics is developed; instead of the Euclidean path integral, it makes direct use of shells and anisotropic thermodynamic relations. Using this method, we show that an HBH in thermal equilibrium

¹⁴The inverse specific heat vanishes at the photon sphere in asymptotically flat spacetime [8, 45].

has the same coarse-grained entropy and the same temperature as a black hole of mass M . As such, these independent methods verify the key results in [12, 13], where we used the Euclidean path integral and entropy maximization methods.

In the final section, we consider when Einstein’s equations allow extended photon spheres in Sec. 5.5.3, and find thermodynamic mimicry takes the same form. It then follows that a self-similar family of solutions, including “frozen stars” [24–26] and “stiffest stars” [27] can satisfy $S = 4\pi M^2$ under certain conditions. Thermodynamic mimicry holds for these solutions when they have massless walls, which generically violate DEC. Walls can break optical mimicry, and more reasonable massive walls break thermodynamic mimicry.

In contrast, the HBH does not need walls to hold its orbiting massless particles. This luminal “Einstein cluster” [28, 30, 46–49] satisfies the usual energy conditions.

5.1 The Anisotropic Tolman-Oppenheimer-Volkoff (TOV) Equation

Here we review the well-known anisotropic Tolman-Oppenheimer-Volkoff equation, from a perspective that makes the structure related to the photon sphere manifest.

Take a static and spherically symmetric metric ansatz:

$$ds^2 = -f(r)dt^2 + \frac{1}{j(r)}dr^2 + r^2d\Omega^2, \quad (5.1)$$

as well as a spherically symmetric, anisotropic stress-energy tensor:

$$T_\nu^\mu = \text{diag}(-\rho, P_r, P_\perp, P_\perp) \quad G_\nu^\mu + \Lambda\delta_\nu^\mu = 8\pi GT_\nu^\mu. \quad (5.2)$$

The (rr) and (tt) components of Einstein’s equation are:

$$\frac{f'(r)j(r)}{rf(r)} + \frac{j(r)}{r^2} - \frac{1}{r^2} = 8\pi P_r - \Lambda, \quad (5.3)$$

$$-\frac{j'(r)}{r} + \frac{1-j(r)}{r^2} = \frac{1}{r^2} \frac{d}{dr} [r(1-j(r))] = 8\pi\rho + \Lambda. \quad (5.4)$$

The (tt) component Eq. (5.4) can be integrated directly:

$$j(r) = 1 - \frac{2\hat{m}(r)}{r} - \frac{\Lambda r^2}{3} \quad \hat{m}'(r) = 4\pi r^2 \rho(r). \quad (5.5)$$

Combined with the (rr) component Eq. (5.3), this yields:

$$\frac{rf'(r)}{2f(r)} = \frac{\hat{m}(r) + 4\pi r^3 P_r - \frac{1}{3}\Lambda r^3}{r - 2\hat{m}(r) - \frac{1}{3}\Lambda r^3}. \quad (5.6)$$

The Bianchi identity $\nabla^\mu T_{\mu\nu} = 0$ gives the condition of hydrostatic equilibrium:

$$P_r'(r) = -\frac{f'(r)(P_r(r) + \rho(r))}{2f(r)} - \frac{2(P_r(r) - P_\perp(r))}{r}. \quad (5.7)$$

Using Eq. (5.6) and Eq. (5.7), the anisotropic TOV equation takes the form:

$$P_r'(r) = -(P_r(r) + \rho(r)) \frac{\hat{m}(r) + r^3 \left(4\pi P_r(r) - \frac{1}{3}\Lambda\right)}{r(r - 2\hat{m}(r) - \frac{1}{3}\Lambda r^3)} - \frac{2(P_r(r) - P_\perp(r))}{r}. \quad (5.8)$$

It is worth noting that the photon sphere condition $rf'/2f = 1$ appears in these equations. The fact that Eq. (5.8) becomes simple when $P_r' = P_r = 0$ will be useful for our purposes.

5.2 Shells of Anisotropic Self-Gravitating Radiation

Sorkin, Wald, and Zhang (SWZ) argued [17] that the TOV equation follows from an entropy maximization principle, by varying the action:

$$I = \int_0^{r_0} \left(\frac{1}{r^2} \frac{dm}{dr} \right)^{3/4} \left[1 - \frac{2m(r)}{r} \right]^{-1/2} r^2 dr. \quad (5.9)$$

This can be straightforwardly generalized to anisotropic gases. The following argument, which is adapted from companion work [13], begins by writing:

$$I = \int s(\rho) \sqrt{h} d^3x = 4\pi \int s(\rho) \left(1 - \frac{2m(r)}{r} \right)^{-1/2} r^2 dr. \quad (5.10)$$

Varying the action and integrating by parts, with the usual assumption that $\delta m = 0$ at the edges of the interval, and defining the temperature $(\partial s / \partial \rho)|_r = 1/T$, a straightforward calculation gives:

$$\frac{T'}{T} = \frac{rm' - m - 4\pi r^3 (sT)}{r(r - 2m)}. \quad (5.11)$$

Assuming that the anisotropic TOV equation holds, it follows that:

$$sT = \rho + P_r. \quad (5.12)$$

Taking the radial derivative of $sT = P_r + \rho$, we find

$$\frac{dP_r}{dr} + \left[\frac{d\rho}{dr} - T \frac{ds}{dr} \right] = s \frac{dT}{dr}. \quad (5.13)$$

This resembles the condition for energy conservation:

$$\frac{dP_r}{dr} + \left[\frac{2(P_\perp - P_r)}{r} \right] = -\frac{f'(r)(P_r(r) + \rho(r))}{2f(r)} = s \frac{dT}{dr}. \quad (5.14)$$

Combining these two equations and using

$$\frac{ds}{dr} = \left(\frac{\partial s}{\partial \rho} \right)_r \frac{d\rho}{dr} + \left(\frac{\partial s}{\partial r} \right)_\rho = \frac{1}{T} \frac{d\rho}{dr} + \left(\frac{\partial s}{\partial r} \right)_\rho, \quad (5.15)$$

gives the following thermodynamic equation:

$$\frac{d\rho}{dr} - T \frac{ds}{dr} = -T \left(\frac{\partial s}{\partial r} \right)_\rho = \frac{2(P_\perp - P_r)}{r}. \quad (5.16)$$

Note this implies that s depends explicitly on r only in anisotropic gases. Also, since $(\partial \rho / \partial s)_r = 1/T$, we obtain the differential relation:

$$d\rho = T ds + (P_\perp - P_r) d \log A, \quad A \equiv 4\pi r^2. \quad (5.17)$$

These relations hold for spherically symmetric $P_r(r)$ and $P_\perp(r)$. The relations found by Kim and Lee [23] in the special case $P_r = w_r \rho$, $P_\perp = w_\perp \rho$ where w_r, w_\perp are constants, can be recovered from this approach. For additional discussion, see companion work [13].

5.2.1 TOV = IJC at Zero Radial Pressure

The anisotropic TOV equation reduces to the Israel junction conditions in the zero radial pressure limit.¹⁵ We apply the SWZ analysis of the TOV equation to anisotropic radiation.

We take a static, spherically symmetric metric:

$$ds^2 = -f(r)dt^2 + \frac{dr^2}{1 - 2m(r)/r} + r^2 d\Omega^2 \quad (5.18)$$

As in SWZ [17], we take the definitions:

$$\mu(r) \equiv \frac{m(r)}{r}, \quad q(r) \equiv 4\pi r^2 \rho(r), \quad z = \ln r. \quad (5.19)$$

Here $m(r)$ satisfies:

$$\frac{dm}{dr} = 4\pi r^2 \rho = q(r) \implies \frac{d\mu}{dz} = q - \mu. \quad (5.20)$$

For anisotropic null gas, this reads:

$$P_r = w_r \rho, \quad P_\perp = w_\perp \rho, \quad w_r + 2w_\perp = 1. \quad (5.21)$$

In these variables, the TOV equation in Eq. (5.8) becomes:

$$q'(z) = \frac{-(1 + w_r)q^2 + q\left(\frac{2w_\perp}{w_r} - \frac{1+4w_\perp+w_r}{w_r}\mu\right)}{1 - 2\mu}. \quad (5.22)$$

This reduces to the problem studied by SWZ when the gas is isotropic, i.e. $w_r = w_\perp = 1/3$. For the null gas this simplifies to:

$$q'(z) = -\frac{q[\mu(3 - w_r) + w_r(1 + w_r)q + (w_r - 1)]}{w_r(1 - 2\mu)} \quad (5.23)$$

To understand the behavior of these solutions it is useful to consider the curves where $q(\mu)$ becomes vertical and horizontal. These are the vertical and horizontal nullclines for the system. When $q'(z) = 0$ the trajectory $q(\mu)$ is horizontal; when $q(\mu) = \mu$ we have $\mu'(z) = 0$ and the curve is vertical. Calling these curves q_V and q_H :

$$q_H(\mu) \equiv \frac{2w_\perp - (1 + 4w_\perp + w_r)\mu}{(1 + w_r)w_r} \quad q_V(\mu) \equiv \mu. \quad (5.24)$$

These solutions $q(\mu)$ spiral around the fixed point, which occurs where they cross at:

$$(\mu_*, q_*) \equiv \left(\frac{2w_\perp}{(1 + w_r)^2 + 4w_\perp}, \frac{2w_\perp}{(1 + w_r)^2 + 4w_\perp} \right). \quad (5.25)$$

At large r , the mass function becomes linear, with $m(r) \sim \left(\frac{2w_\perp}{(1+w_r)^2+4w_\perp}\right)r$, as the curve in the (μ, q) plane approaches the fixed point at (μ_*, q_*) .

As the radial pressure is decreased, solutions spiral increasingly rapidly around the fixed point, as shown in Fig. 8 and Fig. 9. Indeed, in the limit where $w_r \rightarrow 0$, the horizontal nullcline q_H becomes vertical and centered on:

$$\mu = \frac{2w_\perp}{1 + 4w_\perp}. \quad (5.26)$$

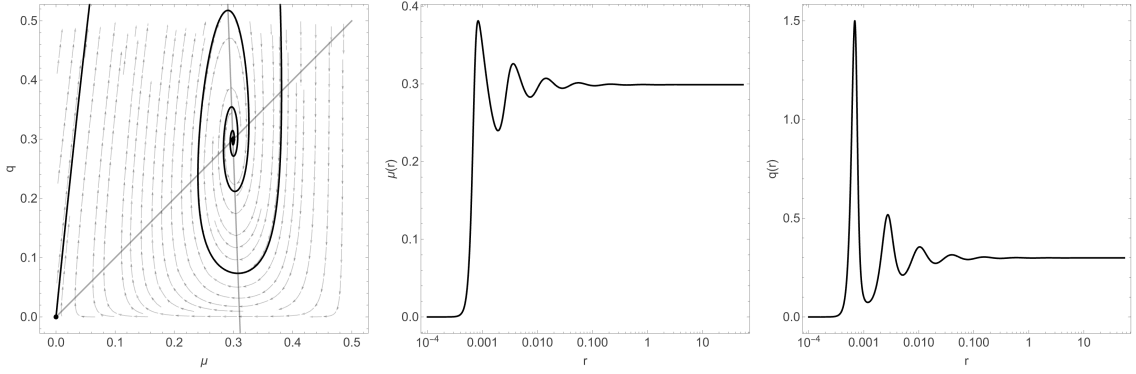


Figure 8. Self-gravitating gas solutions spiral around the fixed point as $w_r \rightarrow 0$. These are unstable beyond the first turning point in $\mu(r)$ [17, 41]. The existence of an infinite number of discrete non-singular layers in this limit has been noted by Andréasson [50].

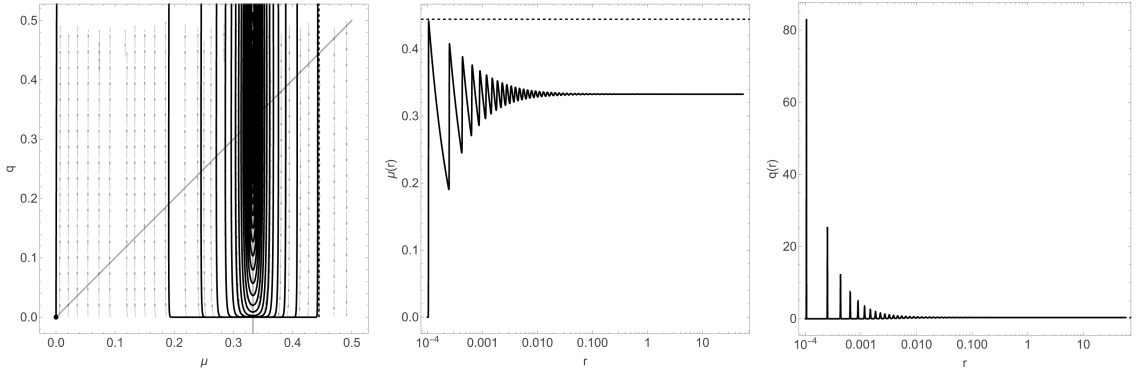


Figure 9. The self-gravitating anisotropic radiation spontaneously forms thin Israel layers as $w_r \rightarrow 0$. The streamlines that become vertical in this limit spiral around $\mu = 1/3$. The parameter $\mu \equiv \frac{M}{R}$ saturates the Buchdahl bound, pictured as a dotted line, in the first layer. The isolated fixed point at $(\mu, q) = (\frac{1}{3}, \frac{1}{3})$ becomes a line of fixed points at $w_r = 0$, see Fig. 10.

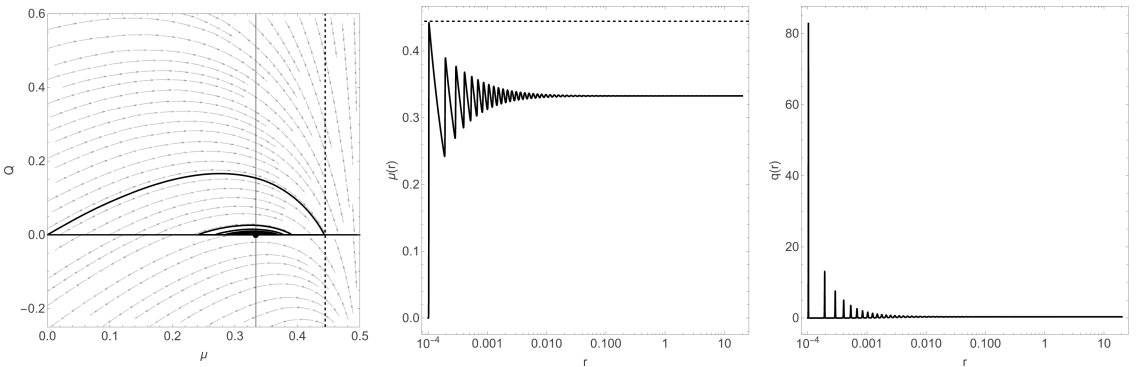


Figure 10. The solution in (Q, μ) coordinates. In the $\epsilon \rightarrow 0$ limit the isolated fixed point becomes a line of fixed points. The endpoints where the curve intersects the line of fixed points recover the Israel junction conditions. Consistent with mechanical stability, shells appear where $\mu \leq 1/3$; $\mu \equiv M/R$ then jumps temporarily to $\mu \geq 1/3$, giving alternating stable and unstable light rings.

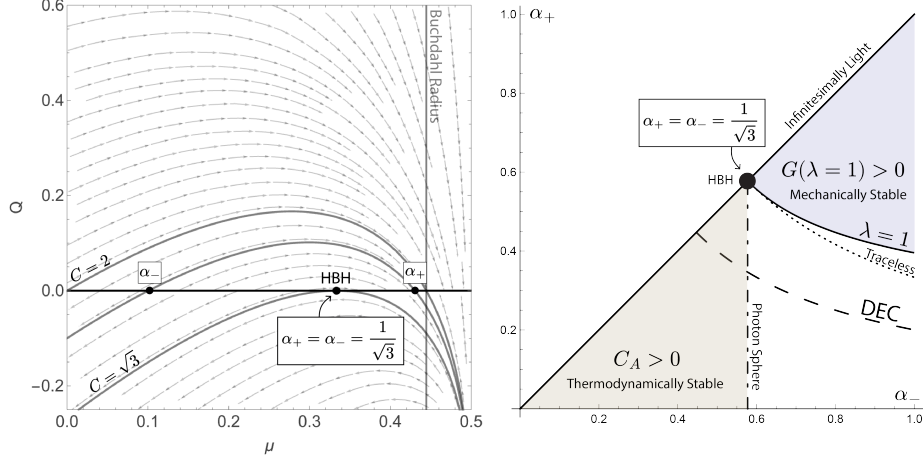


Figure 11. The Israel junction conditions are solved using TOV in the $w_r \rightarrow 0$ limit (left). $Q(\mu)$ crosses the line of fixed points, yielding $\alpha_{\pm} = \sqrt{1 - 2\mu}$. For $w_{\perp} = \frac{1}{2}$, equivalently $\sigma = 2p$, the HBH touches this line once for $\alpha_{\pm} = 1/\sqrt{3}$, matching BLP [11] (right). The Buchdahl bound satisfies $C = 2$. As discussed below, the diagrams for other w_{\perp} are analogous. Self-similar Einstein clusters satisfy $\alpha_+ = \alpha_-$. The HBH is a marginally stable, luminal Einstein cluster around a black hole.

To parse the degenerate limit $w_r \rightarrow 0$, it is convenient to introduce the variables:

$$\varepsilon \equiv w_r, \quad Q \equiv \varepsilon q, \quad \xi \equiv \frac{z}{\varepsilon}. \quad (5.27)$$

The limit where $\varepsilon \rightarrow 0$ gives:

$$\frac{d\mu}{d\xi} = Q, \quad \frac{dQ}{d\xi} = -\frac{Q(3\mu + Q - 1)}{1 - 2\mu}, \quad \frac{dQ}{d\mu} = \frac{(dQ/d\xi)}{(d\mu/d\xi)} = \frac{1 - 3\mu - Q}{1 - 2\mu}. \quad (5.28)$$

In these (Q, μ) coordinates, the degenerate behavior observed at small w_r becomes well-behaved; see Fig. 10. This is solved by the family of solutions:

$$Q(\mu) = 3\mu - 2 + C\sqrt{1 - 2\mu}. \quad (5.29)$$

To give one example, consider the case that saturates the Buchdahl bound. It is a traceless shell enclosing vacuum; with regularity at the origin $(\mu, q) = (0, 0)$, we find $C = 2$:

$$Q(\mu) = 3\mu - 2 + 2\sqrt{1 - 2\mu}. \quad (5.30)$$

The curve for that shell ends when $Q(\mu_*) = 0$, which occurs precisely at the Buchdahl radius $\mu = 4/9$. This traceless matter saturates the bound obtained by Andréasson [51].

For the other cases, we require that two layers are joined smoothly at the boundary between layers where $Q = 0$. The same constant C applies at both ends:

$$C = \frac{2 - 3\mu_-}{\sqrt{1 - 2\mu_-}} = \frac{2 - 3\mu_+}{\sqrt{1 - 2\mu_+}}. \quad (5.31)$$

¹⁵We expect it is more generally true that setting one pressure component to zero gives an IJC for shells oriented along that normal direction. This will be revisited in an upcoming article.

Suppose the total masses enclosed within neighboring layers are, respectively, $\mu_- = m/R$ and $\mu_+ = M/R$. Solving for R gives:

$$R = \frac{3}{8} \left(3m + 3M \pm \sqrt{9m^2 - 14mM + 9M^2} \right). \quad (5.32)$$

This matches our Israel junction condition for a shell around a black hole; note that for $m = 0$ we recover the Buchdahl radius $\mu = 4/9$.

We have just considered Eq. (5.23) for null gas. For more general, not necessarily null, gravitating radiation an identical procedure yields:

$$Q(\mu) = (1 + 4w_\perp) \mu - (1 + 2w_\perp) + C\sqrt{1 - 2\mu}. \quad (5.33)$$

For the first layer, $Q(0) = 0$ fixes $C = 1 + 2w_\perp$, so:

$$Q(\mu) = (1 + 4w_\perp) \mu + (1 + 2w_\perp) \left(\sqrt{1 - 2\mu} - 1 \right). \quad (5.34)$$

The first layer ends where $Q(\mu_*) = 0$, which occurs at the radius:

$$\mu_* = \frac{4w_\perp (1 + 2w_\perp)}{(1 + 4w_\perp)^2}. \quad (5.35)$$

The Buchdahl radius is recovered in the limit $w_\perp \rightarrow 1/2$. The first layer approaches its local horizon $\mu = 1/2$ in the limit where $w_\perp \rightarrow \infty$.

To determine the other layers, we need only require that two layers are joined smoothly where $Q = 0$. This gives the matching condition:

$$\frac{(1 + 2w_\perp) - (1 + 4w_\perp) \mu_-}{\sqrt{1 - 2\mu_-}} = \frac{(1 + 2w_\perp) - (1 + 4w_\perp) \mu_+}{\sqrt{1 - 2\mu_+}}. \quad (5.36)$$

The mass contained within these layers satisfies, respectively, $\mu_- = m/R$ and $\mu_+ = M/R$. This gives a nesting rule for successive layers:

$$R = \frac{(1 + 4w_\perp) \left((1 + 4w_\perp) (m + M) \pm \sqrt{(1 + 4w_\perp)^2 (M - m)^2 + 4mM} \right)}{8w_\perp (1 + 2w_\perp)}. \quad (5.37)$$

The IJCs in Sec. 3 are recovered directly in the $w_r \rightarrow 0$ limit, equivalently $Q = 0$. Returning to our earlier definition in Eq. (3.17), we have $\alpha \equiv \sqrt{1 - 2\mu}$. Then at the boundary layer, where $Q = 0$, Eq. (5.33) yields:

$$C(\alpha) = \frac{1 + (1 + 4w_\perp) \alpha^2}{2\alpha}. \quad (5.38)$$

Requiring smoothness at the boundary layers gives:

$$\frac{1 + (1 + 4w_\perp) \alpha_-^2}{2\alpha_-} = \frac{1 + (1 + 4w_\perp) \alpha_+^2}{2\alpha_+}. \quad (5.39)$$

Solving for w_\perp gives:

$$\frac{p}{\sigma} \equiv w_\perp = \frac{1}{4} \left(\frac{1}{\alpha_+ \alpha_-} - 1 \right), \quad (5.40)$$

a perfect match for the Israel junction condition in Eq. (3.19).

The physical meaning of C is as follows. For a given w_\perp , the two boundary values α_\pm are the two roots of Eq. (5.33):

$$\alpha_+\alpha_- = \frac{1}{1+4w_\perp}, \quad \alpha_+ + \alpha_- = \frac{2C}{1+4w_\perp}. \quad (5.41)$$

Using Eq. (3.17), $\alpha_\pm \equiv \sqrt{f_\pm(R)}$, so C is the average of the redshift factors on each side:

$$C = \frac{1}{2} \left(\frac{1}{\alpha_+} + \frac{1}{\alpha_-} \right). \quad (5.42)$$

If the region inside the Israel layer is empty, regularity at the origin gives the maximum value of C , which occurs at $\alpha = 1/\sqrt{1+4w_\perp}$:

$$1 \leq \sqrt{1+4w_\perp} \leq C \leq 1+2w_\perp \leq 2. \quad (5.43)$$

The roots α_\pm are the inner and outer edges of a vacuum region between matter layers. When $C = \sqrt{1+4w_\perp}$, the curve is tangent to the line of fixed points, making the layers continuous. For $w_\perp = 1/2$, Eq. (5.43) recovers the values of $\sqrt{3} \leq C \leq 2$ for the null case; $C = 2$ recovers the Buchdahl bound, while $C = \sqrt{3}$ places each layer at its local photon sphere; $w_\perp = 0$ gives $C = 1$. In particular, $w_\perp = 1/2$ gives an ultra-compact Einstein cluster, where massless radiation orbits at the speed of light within its local photon sphere. We will see in Sec. 5.3 that this is the HBH.

The IJC can be determined from Fig. 11 as follows. First choose some C and find where the solution for Q crosses the line of fixed points. Their intersections give values of μ that determine the IJC through $\alpha_\pm = \sqrt{1-2\mu}$. Alternatively, one can use Eq. (5.40).

In brief, this section has established three results in the zero radial pressure limit: (1) the IJC are given precisely by the points where the exact solutions to the TOV equation Eq. (5.33) cross the line of critical points in Fig. 11, (2) the photon sphere sits at $\alpha_\pm = 1/\sqrt{3}$, dividing stable and unstable fixed points; for the HBH, the $Q(\mu)$ curve is tangent to the critical line, and is the same point where mechanical and thermodynamical stability coincide in Fig. 5, and (3) the Buchdahl bound is the $C = 2$ endpoint of this same family of solutions. Similar comments apply to the self-similar family of solutions in Sec. 5.5.3.

5.2.2 The Buchdahl Bound

Here we comment briefly on the Buchdahl bound. This gives an alternative perspective on the related discussion that appears in the companion papers [12, 13].

The saturation occurs for the solution that is *luminal* at the fixed point in the continuum limit. To see this, let us consider the velocity of these orbits more generally. The local circular orbit velocity as measured by a static observer at radius r is given by:

$$\Omega^2 \equiv \left(\frac{d\phi}{dt} \right)^2 = \frac{f'(r)}{2r} \implies v_{\text{loc}}^2(r) = \frac{r^2 \Omega^2}{f(r)} = \frac{r f'(r)}{2f(r)} = \frac{m(r) + 4\pi r^3 P_r(r)}{r - 2m(r)}. \quad (5.44)$$

At the fixed point we have:

$$v_{\text{loc}}^2 = \frac{\nu(1+w_r)}{1-2\nu}. \quad (5.45)$$

For $w_r = 0$ and $w_\perp = 1/2$ as is appropriate for orbiting massless radiation, we have $\nu = 1/3$ and so the motion is luminal: $v_{\text{loc}} = 1$. At the fixed point, we have photons orbiting their local photon sphere. This condition will be of interest later in Sec. 5.5.3.

Away from the fixed point the motion on shells can be acausal, however this is not an issue for the HBH. Note that, in terms of the μ and Q variables:

$$v_{\text{loc}}^2(r) = \frac{\mu(r) + w_r q(r)}{1 - 2\mu(r)} = \frac{\mu + Q}{1 - 2\mu}. \quad (5.46)$$

For $Q = 0$ the orbits of the constituents of the shell are superluminal for $\mu > 1/3$. For the shell enclosing vacuum, where $Q(\mu) = 3\mu - 2 + 2\sqrt{1 - 2\mu}$, this becomes:

$$v_{\text{loc}}^2 = 2 \left(\frac{1}{\sqrt{1 - 2\mu}} - 1 \right). \quad (5.47)$$

For traceless radiation a single shell enclosing vacuum saturates the Buchdahl bound $\mu = 4/9$; $v_{\text{loc}} = 2$, which is superluminal. More generically, the velocity of the orbiting geodesics oscillates around a constant value,¹⁶ saturating in the limit. The fixed point for traceless radiation saturates at ($\nu = 1/3$, $w_r = 0$), which gives $v_{\text{loc}} = 1$. Indeed, we will see shortly that this gives the HBH: a marginally stable, luminal Einstein cluster.

5.2.3 Entropy Density at the Fixed Point

The solution at the fixed point where q_H and q_V intersect is self-similar. This motivates the thermodynamics of self-similar fluids in more detail. For these solutions we now repeat the discussion that appears in [13] concerning the scaling behavior $S \propto M^p$, for some power p .

In the previous section we saw that for anisotropic gas, $\rho = Ts - P_r$. For $P_r = w_r \rho$ and $P_\perp = w_\perp \rho$:

$$s(r) = \frac{\rho(r)(1 + w_r)}{T(r)}. \quad (5.48)$$

For the self-similar fixed-point solutions this gives:

$$\rho(r) = \frac{q(r)}{4\pi r^2} = \frac{\nu}{4\pi r^2}, \quad m(r) = \nu r, \quad \nu = \frac{2w_\perp}{1 + 4w_\perp}. \quad (5.49)$$

For $\Lambda = 0$, Einstein's equations Eq. (5.3) require:

$$\frac{r f'(r)}{2f(r)} = \frac{\hat{m}(r) + 4\pi r^3 P_r}{r - 2\hat{m}(r)} = \frac{\nu(1 + w_r)}{1 - 2\nu} \equiv \frac{\delta}{2}, \quad (5.50)$$

where we specialized to the fixed point¹⁷ in the last step. This gives the g_{tt} component $f(r)$, and the local temperature $T(r)$, up to a coefficient:

$$f(r) \propto r^\delta \implies T(r) = \frac{T_H}{\sqrt{f(r)}} \propto r^{-\delta/2}. \quad (5.51)$$

At the fixed point we have $g_{rr} = \frac{1}{1 - 2\nu}$, which is constant. This gives the power-law scaling:

¹⁶The velocity at the fixed point satisfies $v_{\text{loc}}^2 = \frac{r f'(r)}{2f(r)} = \frac{\hat{m}(r) + 4\pi r^3 P_r}{r - 2\hat{m}(r)} = \frac{\nu(1 + w_r)}{1 - 2\nu} \equiv \frac{\delta}{2}$, as shown in [12].

¹⁷For isotropic gases the fixed point gives the right scaling. From Eq. (5.8), $f(r) \propto \rho(r)^{-\frac{2w}{w+1}}$, giving the Stefan-Boltzmann law for isotropic radiation. In contrast, anisotropic radiation at the fixed point satisfies $r f'/2f = \text{const}$; both terms in Eq. (5.8) are proportional. This gives $T \propto f^{-1/2} \propto \rho^{\delta/4}$. For the stiffest isotropic stars consistent with causality [27], $w = 1$, which gives $s(r) \propto 1/r$, so $S \propto M^2$.

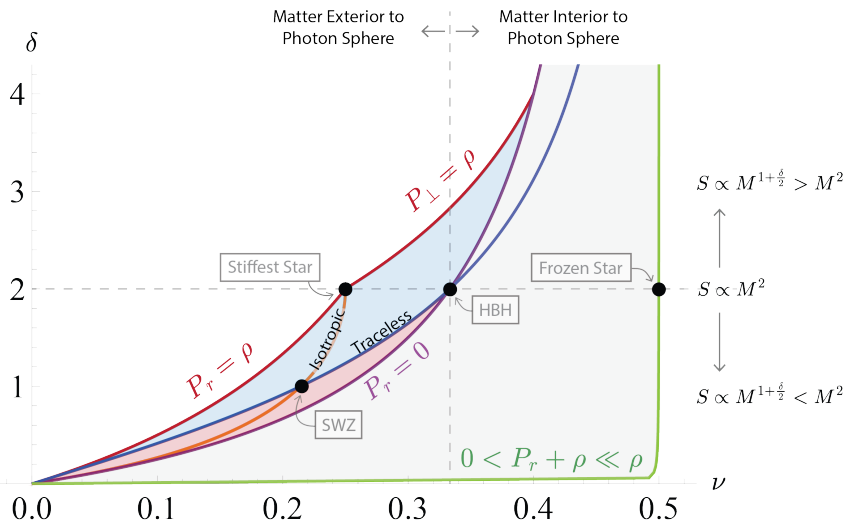


Figure 12. From [12, 13], the entropy density of self-similar solutions in the (δ, ν) plane. In [13] it was shown that the HBH satisfies $T = (8\pi M)^{-1}$ and $S = 4\pi M^2$. In Sec. 5.5.3, we show that for $\sigma = 0$ this can be conditionally extended to the entire $\delta = 2$ family, including ‘frozen stars’ [24–26] (see also [41]) and “stiffest stars” [27]. The conditions $\delta = 2$ and $\nu = 1/3$ occur together for the HBH, which is *aligned* as discussed in Sec. 1.1. In particular, since $\sigma = 2p$ as in the thought experiment (Fig. 1), no IJC is needed in Eq. (3.5). Other cases require an IJC and are *misaligned*.

$$s(r) \propto r^{\frac{\delta}{2}-2} \implies S \equiv \int \sqrt{g_{rr}}(4\pi r^2)s(r)dr \propto M^{1+\frac{\delta}{2}}. \quad (5.52)$$

For the entropy to grow as $S \propto M^2$, we need $\delta = 2$. This gives the photon sphere condition:

$$\frac{r f'(r)}{2f(r)} = 1, \quad \nu = \frac{1}{3} \implies \rho = \frac{1}{12\pi r^2}, \quad m(r) = \frac{r}{3}. \quad (5.53)$$

In the limit where $w_r \rightarrow 0$, where the radiation orbits the black hole and discrete Israel layers emerge, we obtain the solution discussed in the previous section where $\alpha_{\pm} = 1/\sqrt{3}$. The layers form a continuum that extends the photon sphere of the black hole outward.

Simply put, the anisotropic generalization of SWZ [17] has led immediately to a single solution that is marginally stable for both York [8] and BLP [11]. The HBH does not require walls, because $P_r = 0$; it has an extended photon sphere, because $\delta = 2$; its particles orbit within, because $T^{\mu}_{\mu} = -\sigma + 2p = 0$. It lies at the intersection of these three curves in the (δ, ν) plane; see Fig. 12, from [12, 13], where the entropy density of self-similar solutions is organized. Related solutions with $S \propto M^2$ have appeared in the literature, see [26, 27].

In Sec. 5.5.3, we show the $\delta = 2$ family of self-similar solutions satisfies $S = 4\pi M^2$ under stringent conditions. This thermodynamic mimicry holds only for massless walls, so every member of the $\delta = 2$ family other than the HBH (where $\sigma = 2p$) violates DEC.

5.3 From Joint Stability to the Hillinggar Black Hole

We have seen that the anisotropic TOV equation, in the zero radial pressure limit, organizes matter into discrete Israel layers. At the photon sphere these layers are infinitesimal and

continuous, saturating the BLP bound $\sigma = 2p$, placing it at the marginal boundary of thermodynamic and mechanical stability. No IJC is needed because $\sigma = 2p$ in Eq. (3.5). Each shell sits at its local photon sphere; the mass interior to this shell satisfies $\hat{m}(r) = r/3$.

From this starting point, these constraints lead to the solution obtained in [12] following identical reasoning. For the self-similar and transverse anisotropic null gas, the TOV equation becomes algebraic. Inserting $\hat{m}(r) = r/3$ into Eq. (5.5) and solving for Λ determines $j(r)$ in Eq. (5.1):

$$j(r) = \frac{1 - r^2\Lambda}{3} = \frac{1}{3} \mp \frac{r^2}{L^2}. \quad (5.54)$$

The photon sphere condition $rf'/2f = 1$ gives $f(r) \propto r^2$. Its coefficient can be determined from the Lyapunov exponent λ_M , which controls massless geodesics near the photon sphere:

$$\lambda_M^2 \equiv \left. \frac{f(r)}{r^2} \right|_{r=3M} = \left(\frac{1}{27M^2} - \frac{\Lambda}{3} \right). \quad (5.55)$$

It is the inverse timescale associated with the rate that particles spiral toward or away from the photon sphere [52]. To match to the exterior Schwarzschild metric we must choose:

$$f(r) = \lambda_M^2 r^2 = \left(\frac{1}{27M^2} - \frac{\Lambda}{3} \right) r^2. \quad (5.56)$$

Here M is the ADM mass. Then the metric Eq. (5.1) takes the form:

$$j(r) \equiv a^{-1} = 1 - \frac{\Lambda r^2}{3} - \frac{2\hat{m}(r)}{r}, \quad f(r) = \left[\frac{\lambda_M}{\hat{\lambda}(r)} \right]^2 j(r). \quad (5.57)$$

The Lyapunov exponent $\hat{\lambda}(r)$ and mass-function $m(r)$ are piecewise defined:

$$\hat{\lambda}^2(r) = \frac{1}{27\hat{m}(r)^2} - \frac{\Lambda}{3}, \quad \hat{m}(r) = \begin{cases} m, & r \in (r_+, 3m) \\ r/3, & r \in (3m, 3M) \\ M, & r \in (3M, \infty) \end{cases} \quad (5.58)$$

This has recovered the solution considered in [12, 13]: the HBH.

This system sits at the single location where thermodynamical and mechanical stability for thin shells overlap in Fig. 5, realizing the thought experiment illustrated in Fig. 1; see Fig. 2. Entropy maximization gives $\nu = 1/3$ (the photon sphere position) and $\delta = 2$ (the photon sphere condition); every radial shell within the ocean sits at the local photon sphere.

We emphasize that photon spheres are not merely properties of a background space-time, as in Schwarzschild at $r = 3M$. Through their collective behavior, massless particles naturally form continuous regions with marginally stable orbits.

5.3.1 The Coldest Stable Nested Shell Configuration: the HBH

Consider a black hole of horizon mass m_0 , surrounded by finitely many static spherical shells, with successive vacuum regions R_k with Schwarzschild masses m_k :

$$R_1 < \dots < R_N, \quad m_0 < m_1 < \dots < m_N = M. \quad (5.59)$$

Let us require that each of these shells is mechanically stable; then by Sec. 2.2:

$$R_k \geq 3m_{k-1} \quad (k = 1, \dots, N). \quad (5.60)$$

We show the temperature exceeds $T_\infty = \frac{1}{8\pi M}$ for all configurations with finitely many shells, extending the argument shown in Appendix C of [13], for traceless shells, to the general case. The exceptions are the trivial case with no shells, which is an ordinary Schwarzschild black hole of mass M , and a non-trivial case with infinitely many infinitesimally light traceless shells at the photon sphere, the HBH.

Let T_H denote the temperature of a Schwarzschild black hole at infinity of mass M . Let T_∞ be the resulting temperature of the combined configuration. The Schwarzschild temperature measured at infinity is:

$$T_\infty = \frac{1}{8\pi m_0} \prod_{k=1}^N \sqrt{\frac{1 - \frac{2m_k}{R_k}}{1 - \frac{2m_{k-1}}{R_k}}}. \quad (5.61)$$

As compared to the Hawking temperature of a black hole of mass M , the ratio is:

$$\frac{T_\infty}{1/(8\pi M)} = \frac{M}{m_0} \prod_{k=1}^N \sqrt{\frac{1 - \frac{2m_k}{R_k}}{1 - \frac{2m_{k-1}}{R_k}}} \equiv \prod_{k=1}^N \Phi_k(R_k), \quad (5.62)$$

$$\Phi_k(R) \equiv \frac{m_k}{m_{k-1}} \sqrt{\frac{1 - \frac{2m_k}{R}}{1 - \frac{2m_{k-1}}{R}}}. \quad (5.63)$$

For fixed $m_{k-1} < m_k$, $\Phi_k(R)$ is strictly increasing for $R > 2m_k$, because:

$$\frac{d}{dR} \ln \Phi_k = \frac{m_k - m_{k-1}}{(R - 2m_k)(R - 2m_{k-1})} > 0. \quad (5.64)$$

A short calculation shows the unique crossing point where $\Phi_k(R_k) = 1$ is:

$$R_k^* = \frac{2(m_k^2 + m_k m_{k-1} + m_{k-1}^2)}{m_k + m_{k-1}}, \quad 3m_{k-1} < R_k^* < 3m_k. \quad (5.65)$$

Now we show that $\Phi(R_k) > 1$ for stable nested shells. Because $\Phi(R)$ is a monotonically increasing function of R , this amounts to showing that $G(\lambda, k_+, k_-)$ is strictly negative when evaluated at the crossing point $R = R_k^*$, with $\lambda \equiv c_s^2$ the squared speed of sound:

$$G(\lambda, \alpha_+, \alpha_-) \equiv 3(4\lambda + 1)\alpha_+^3 \alpha_-^3 + 4\lambda \alpha_+^2 \alpha_-^2 - (\alpha_+^2 + \alpha_-^2 + \alpha_+ \alpha_-). \quad (5.66)$$

Here $\alpha_\pm \equiv \sqrt{1 - 2m_\pm/R}$, with $m_- = m_{k-1}$ and $m_+ = m_k$. For shells where sound wave propagation is causal, we need only consider $\lambda \leq 1$. The condition $\Phi_k(R_k^*) = 1$ reads $m_k^2 \alpha_+^2 = m_{k-1}^2 \alpha_-^2$, giving $k_+ = \eta k_-$, where for convenience we define:

$$\eta \equiv \frac{m_{k-1}}{m_k} \in (0, 1). \quad (5.67)$$

It is straightforward to show that inverting Eq. (5.65) for $\alpha_-^2(R_k^*)$ gives:

$$\alpha_-^2(R_k^*) = 1 - \frac{2m_{k-1}}{R_k^*} = \frac{m_k^2}{m_k^2 + m_k m_{k-1} + m_{k-1}^2} = \frac{1}{1 + \eta + \eta^2}. \quad (5.68)$$

Substituting $k_+ = \eta k_-$ and $k_- = \frac{1}{1+\eta+\eta^2}$ into $G(\lambda, k_+, k_-)$, one finds that $G(\lambda, k_+, k_-)$ is negative when the following polynomial is negative:

$$G < 0 \iff P(\eta, \lambda) \equiv 3(4\lambda + 1)\eta^3 + 4\lambda\eta^2(1 + \eta + \eta^2) - (1 + \eta + \eta^2)^3 < 0. \quad (5.69)$$

Causality requires $\lambda \leq 1$, which suggests separating this polynomial as:

$$P(\eta, \lambda) = P(\eta, 1) + (\lambda - 1) \cdot \left(4\eta^2(1 + 4\eta + \eta^2)\right). \quad (5.70)$$

$$P(\eta, 1) = -1 - 3\eta - 2\eta^2 + 12\eta^3 - 2\eta^4 - 3\eta^5 - \eta^6. \quad (5.71)$$

The second term in Eq. (5.70) is manifestly negative for causal shells, so it suffices to show the first term Eq. (5.71) is negative on $\eta \in (0, 1)$. That term takes the form of, essentially, the simplest possible negative palindromic polynomial that manifestly vanishes at $\eta = 1$.¹⁸

Then $\Phi(R_k) > 1$ for stable nested shells. Multiplying over all shells gives $T_\infty > \frac{1}{8\pi M}$. If there are no shells, we have simply a Schwarzschild black hole of mass M , with temperature $T_\infty = \frac{1}{8\pi M}$. There is also a non-trivial limit suggested by Eq. (5.65). Let these shell's masses become infinitesimal, as they approach the local photon sphere:

$$\delta m_k \equiv m_k - m_{k-1} \rightarrow 0, \quad R_k \rightarrow 3m_k. \quad (5.72)$$

In this limit each $\Phi_k \rightarrow 1$. More precisely, writing $m_k = (1 + \varepsilon_k) m_{k-1}$:

$$\Phi_k(3m_k) \equiv \frac{m_k}{m_{k-1}} \sqrt{\frac{1 - \frac{2m_k}{3m_k}}{1 - \frac{2m_{k-1}}{3m_k}}} = \frac{(1 + \varepsilon_k)^{3/2}}{\sqrt{1 + 3\varepsilon_k}} = 1 + \frac{3\varepsilon_k^2}{2} + O(\varepsilon_k^3). \quad (5.73)$$

In the continuum limit the product tends to 1, and the resulting configuration is the HBH:

$$\hat{m}(r) = \frac{r}{3}, \quad r \in (3m, 3M). \quad T_\infty = \frac{1}{8\pi M}. \quad (5.74)$$

Once again $\Phi(R)$ is monotonic, but now $\Phi(R_k) = 1$ can occur within a broad region where mechanical and thermal stability are satisfied; these stable shells can cool the combined system while holding M constant. If that radiation is in thermal equilibrium with the black hole, then the coarse-grained entropy increases.

¹⁸It is simple to numerically verify this claim. However a satisfying analytic argument exists as follows. The Abel-Ruffini theorem states that no solution in radicals exists for the roots of a polynomial of degree 5 or higher with arbitrary coefficients. However, *palindromic* polynomials of degree n have the following remarkable property: for even degree $2k$, divide by x^k and substitute $u = x + \frac{1}{x}$ to reduce their degree by half. In our case, this process (with $N \equiv \eta + \eta^{-1}$) gives a cubic polynomial that factors as $-(N-2)(N^2+5N+9)$. For $\eta \in (0, 1)$ we have $N > 2$, so $(N-2)$ is positive. Then $P(\eta, 1) < 0$ for $\eta \in (0, 1)$, and so $G < 0$ at R_k^* .

5.4 Shells Cool Black Holes \iff Specific Heat is Positive

Here we clarify the physical meaning of the divergent specific heat at the photon sphere of a black hole. The mechanism controlling the shell configuration is identical. Define:

$$T_\infty = T_H(m_0, L) \prod_{k=1}^N \sqrt{\frac{f_{m_k}(R_k)}{f_{m_{k-1}}(R_k)}}. \quad (5.75)$$

Here we are allowing for an AdS curvature L . The ratio of the temperature at infinity for the shell configuration, T_∞ , to the Hawking temperature of a black hole of mass M is:

$$\frac{T_\infty}{T_H(M)} = \prod_{k=1}^N \Phi_k(R_k), \quad \Phi(R) = \frac{T_H(m, L)}{T_H(m + \delta m, L)} \sqrt{\frac{f_{m+\delta m}(R)}{f_m(R)}}. \quad (5.76)$$

For one infinitesimal shell, varying the mass while holding R fixed gives:

$$\delta \ln \frac{T_\infty}{T_H(M, L)} = \delta \ln \Phi(R) = -\delta \ln T_H + \frac{1}{2} \delta \ln f_m(R). \quad (5.77)$$

The second term takes a simple form for black hole metrics:

$$\frac{1}{2} \delta \ln f_m(R) = \frac{1}{2} \frac{\partial_m f_m(R)}{f_m(R)} \delta m. \quad (5.78)$$

Then the variation of the redshift factor for the shells, Φ_k , gives:

$$\delta \ln \Phi(R) = -\left(\frac{d \ln T_H}{dm} + \frac{1}{R f_m(R)} \right) \delta m = -\frac{1}{T_H} \left(\frac{dT_H}{dm} + \frac{1}{R f_m(R)} \right) \delta m. \quad (5.79)$$

The specific heat at finite radius is given by Eq. (4.30):

$$C_R^{-1} = \frac{dT_H}{dm} + \frac{T_H}{R f(R)}. \quad (5.80)$$

Comparing to Eq. (5.79) gives one of the main results of this note, illustrated in Fig. 13:

$$\boxed{\delta \ln \frac{T_\infty}{T_H(M, L)} = -\frac{C_R^{-1}}{T_H} \delta m.} \quad (5.81)$$

Forming shells of thermal radiation around a black hole, with fixed total mass M , cools the system if and only if the specific heat at the location of the shell is *positive*.

To determine whether a black hole surrounded by nested shells is colder than the original configuration, we compute the ratio:

$$\frac{T_\infty}{T_H(M)} = \prod_{k=1}^N \Phi_k(R_k), \quad \Phi_k = \frac{T_H(m_{k-1})}{T_H(m_k)} \sqrt{\frac{f_{m_k}(R_k)}{f_{m_{k-1}}(R_k)}}. \quad (5.82)$$

It was just shown that:

$$\delta \ln \Phi = -\frac{C_R^{-1}}{T_H} \delta m, \quad C_R^{-1} = \frac{dT_H}{dm} + \frac{T_H}{R f(R)}. \quad (5.83)$$

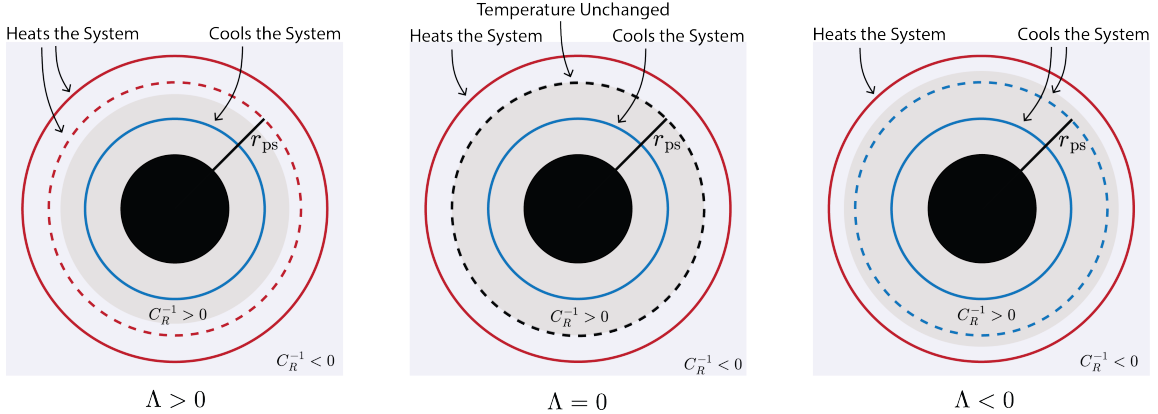


Figure 13. Locations of possible shells. The asymptotically measured Hawking temperature T_∞ , after building a shell around a black hole, changes with sign opposite to that of the locally measured specific heat (Eq. (5.81)). Shells placed where $C_R^{-1} < 0$ increase the asymptotically measured temperature (red), while shells placed where $C_R^{-1} > 0$ decrease it (blue). At the photon sphere, $C_{r_0}^{-1}(r_{\text{ps}}) \propto -\Lambda$ (Eq. (4.53)). As illustrated (center) for asymptotically flat spacetime, the temperature is unchanged when shells are added at the photon sphere at fixed total mass.

So $\Phi < 1$ if and only if $C_R^{-1} > 0$. Mechanically stable shells in asymptotically flat spacetime have $C_R^{-1} \leq 0$, with equality at the photon sphere; this is why the HBH is as cold as a black hole, which is the coldest such configuration.

However, in asymptotically AdS spacetime, $C_R^{-1} > 0$ at the photon sphere, so the evaporation process runs away. This gives a different perspective on [13, 53], where we pointed out that AdS black holes may be thermodynamically unstable in the microcanonical ensemble. From this perspective, they can increase their entropy by emitting radiation and cooling off. They thus increase their entropy in the *microcanonical* ensemble for the unintuitive reason that their *local* specific heat is positive in the *canonical* ensemble.

Taken at face value, canonical and microcanonical stability for black holes admitting such equilibrium shell configurations are in tension, indicating possible ensemble inequivalence in AdS/CFT. Note that we have implicitly made the very strong assumption that thermal equilibrium between the black hole and the surrounding matter is possible.

5.5 Entropy of Systems in Equilibrium with Black Holes

Here we introduce a practical method for computing coarse-grained entropies without using the Euclidean path integral, which we then greatly generalize in Sec. 5.5.3.

First we consider a simpler case at $P_r = 0$, where our procedure can be understood as follows. By adding shells and tracking the asymptotically measured temperature, the coarse-grained entropy of a system in thermal equilibrium with a black hole is calculated. Shells in equilibrium around black holes have been considered previously, see [45, 54–56].

5.5.1 Thermodynamics from IJC: Shells are Heat

Here we derive black hole thermodynamics directly from the IJC; the geometry is built layer by layer while tracking the asymptotic temperature. A summary is as follows.

The IJCs Eq. (2.10) determine the surface density σ of an infinitesimal thin shell at radius R between Schwarzschild geometries of mass m and $m + \delta m$. Expanding to first order in δm , we obtain the well-known Brown-York quasilocal energy [8]. The asymptotic temperature Eq. (5.87) follows from gravitational redshift. If local thermodynamic equilibrium holds, the gravitational first law $\delta S(\hat{m}) = \delta \hat{m}/T_\infty(\hat{m})$ Eq.(5.86) follows, in a local form depending on the mass $\hat{m}(r)$ enclosed within areal radius r .

We begin with the free energy $F \equiv E_{BY} - TS$ [8], where E_{BY} is the Brown-York energy satisfying $(\delta E_{BY})_r \equiv \delta M \left(1 - \frac{2M}{r}\right)^{-1/2}$. Expanding the Israel junction condition for infinitesimally thin static shells Eq. (2.10) in δM :

$$\sigma = \frac{1}{4\pi R} (\alpha_- - \alpha_+) \approx \frac{1}{4\pi R^2} \frac{\delta M}{\sqrt{1 - \frac{2M}{R}}} \implies (\delta E_{BY})_r \equiv \frac{\delta M}{\sqrt{1 - \frac{2M}{R}}} = A\sigma. \quad (5.84)$$

It follows from direct integration in δM that $E_{BY} = R \left(1 - \sqrt{1 - 2m_+/R}\right)$. York showed [8] that $dE_{BY} = T(r)dS - p_Y dA$, where the surface pressure is $p_Y = (8\pi R)^{-1} \left(\frac{1 - m_+/R}{\alpha_+} - 1\right)$. To recover his exact differential from our approach, we compute:

$$\left. \frac{\partial E_{BY}}{\partial R} \right|_{m_+} = \left(1 - \frac{1 - m_+/R}{\alpha_+}\right) dR = \frac{1}{8\pi R} \left(1 - \frac{1 - m_+/R}{\alpha_+}\right) dA. \quad (5.85)$$

Then $dE_{BY} = T(r)dS - p_Y dA$. We have derived York's local thermodynamics directly from the Israel junction conditions without making use of the Euclidean path integral.

The next step gives a physical picture. The TdS term in York's thermodynamics increases the mass of the system – which amounts to adding heat – by depositing a thin Israel layer at the boundary. The $p_Y dA$ term holds the mass fixed while varying the boundary area. Then holding the boundary area fixed, this increases the entropy:

$$\boxed{\delta S(\hat{m}) = \frac{\delta E_{BY}}{T(r)} = \frac{\delta \hat{m}/\sqrt{f}}{T_\infty/\sqrt{f}} = \frac{\delta \hat{m}}{T_\infty(\hat{m})}.} \quad (5.86)$$

This is the first law of gravitational thermodynamics, obtained through Israel junction conditions. Normalization is set by (e.g.) Bogoliubov coefficients, see Appendix B.

The coarse-grained entropy of infinitesimally light nested shells in thermal equilibrium with a black hole can be computed from Eq. (5.86). For one infinitesimal step at radius r :

$$T_\infty(\hat{m} + \delta \hat{m}) = T_H(m_0) \prod_k \sqrt{\frac{1 + \frac{R_k^2}{L^2} - \frac{2(\hat{m} + \delta \hat{m})}{R_k}}{1 + \frac{R_k^2}{L^2} - \frac{2\hat{m}}{R_k}}} \implies \boxed{d \ln T_\infty = -\frac{d\hat{m}}{r f(r)}}. \quad (5.87)$$

This can determine T_∞ from $\hat{m}(r)$. For instance, the HBH ($L \rightarrow \infty$) satisfies $\hat{m} = r/3$, for which the continuum product of shell factors gives:

$$d \ln T_\infty = -\frac{d\hat{m}}{\hat{m}} \implies T_\infty(M) = T_\infty(m) \frac{m}{M} = \frac{1}{8\pi M}. \quad (5.88)$$

These two expressions in Eq. (5.86) and Eq. (5.87) suffice to compute coarse-grained entropies of configurations of nested shells using simple elementary integrals. This method

seems to be new to the literature. It recovers results obtained from Euclidean path integral and entropy maximization methods in the companion papers [12, 13].

This method is generalized further in Sec. 5.5.3.

5.5.2 Computing Coarse-Grained Entropies from IJC

Here we compute coarse-grained entropies using the IJC, beginning with the HBH in asymptotically flat spacetime. Again, we stress that we shall assume thermal equilibrium for these (marginally) thermodynamically stable systems.

The coarse-grained entropy of the ocean – a cloud of massless (e.g.) photons orbiting and extending the photon sphere of the black hole – can be computed from Eq. (5.86) and Eq. (5.87). First Eq. (5.87) gives $T(\hat{m}) = (8\pi\hat{m})^{-1}$; then Eq. (5.86) gives:

$$S_{\text{ocean}} \equiv S(M) - S(m) = \int_m^M 8\pi\hat{m} d\hat{m} = 4\pi(M^2 - m^2). \quad (5.89)$$

After including the black hole with $S_{\text{bh}} = 4\pi m^2$, the total entropy of the HBH [12, 13] is:

$$S(M) = S_{\text{bh}}(m) + S_{\text{ocean}}(M, m) = 4\pi M^2. \quad (5.90)$$

Evaporation into an ocean is not entropically forbidden since the initial Schwarzschild black hole has the same coarse-grained entropy as an HBH. Throughout the evaporation process, for thermal equilibrium to be maintained the constant value of T_∞ given by Eq. (5.88) is required. This is a non-trivial *output* of the model; $C_R^{-1} = 0$ at the photon sphere, so the asymptotic temperature is fixed as the black hole evaporates; see Eq. (5.81).

This procedure works equally well for an ordinary Schwarzschild black hole; placing layers on the horizon of the hole builds up an entropy $S = 4\pi M^2$. To see this, suppose successive shells are placed at their own Schwarzschild radius $R = 2\hat{m}$. Recall that:

$$\sigma = \frac{\delta m}{4\pi R^2 \sqrt{1 - \frac{2\hat{m}}{r}}}, \quad T_{\text{loc}} = \frac{T_H}{\sqrt{1 - \frac{2\hat{m}}{r}}}. \quad (5.91)$$

These quantities diverge at the horizon, but the shell entropy δS is redshift independent:

$$\delta S = \frac{\delta E_{BY}}{T(r)} = \frac{\delta\hat{m}/\alpha_-}{T_\infty(\hat{m})/\alpha_-} = 8\pi\hat{m} \delta\hat{m} \implies S_{\text{bh}}(M) = 4\pi M^2. \quad (5.92)$$

This is consistent with the Bekenstein bound. The HBH case has been illustrated in Fig. 14.

The same formalism can be readily extended to more general configurations. Now we consider Einstein clusters formed by a continuum of nested shells, recovering the results first obtained in the companion papers [12, 13] using our independent method.

For an Einstein cluster around a black hole, the asymptotically measured Hawking temperature satisfies Eq. (5.87). For these solutions, Eqs. (5.49)-(5.50) give $\hat{m} = \nu r$ and $\delta = \frac{4w_\perp}{1+w_r} = 4w_\perp$, and then:

$$d \log T_\infty = -\frac{d\hat{m}}{r f(r)} = -\frac{\nu}{1-2\nu} \frac{d\hat{m}}{\hat{m}} = -\frac{\delta}{2} \frac{d\hat{m}}{\hat{m}} = -w_\perp d \log(A). \quad (5.93)$$

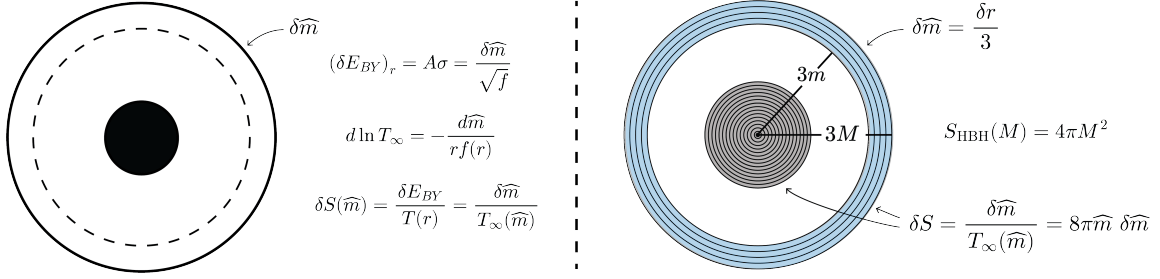


Figure 14. An illustration of the procedure where coarse-grained entropies are computed by building up the geometry layer by layer. Left: the addition of one light shell changes the Brown-York energy by $\delta\widehat{m}/\sqrt{f}$, and also changes the asymptotically measured Hawking temperature. This builds up some coarse-grained entropy $\delta S(\widehat{m}) = \delta\widehat{m}/T_\infty(\widehat{m})$. Right: The coarse-grained entropy of a black hole of mass m , and an ocean of mass $M - m$, is computed by building it up layer by layer.

In the last step we used $A = 4\pi r^2$. For Schwarzschild black holes of mass m this gives:

$$T_\infty(M) = \frac{1}{8\pi m} \left(\frac{m}{M}\right)^{\delta/2}. \quad (5.94)$$

If this cluster can be held in thermal equilibrium with the black hole, Eq. (5.86) shows:

$$S_O = \int_m^M \frac{d\widehat{m}}{T_\infty(\widehat{m})} = \int_m^M d\widehat{m} (8\pi m) \left(\frac{\widehat{m}}{m}\right)^{\delta/2} = \frac{16\pi}{2+\delta} \left(M^{1+\delta/2} m^{1-\delta/2} - m^2\right). \quad (5.95)$$

This was also obtained in Sec. 5.1 [13] by a different method. For $\delta = 2$ the total coarse-grained entropy of this system around a black hole is $S = 4\pi M^2$. As a consistency check, note that $\frac{\delta}{2} \equiv \frac{r f'(r)}{2f(r)} = 1$ is precisely the HBH, for which massless particles orbit within an extended photon sphere.

In anti-de Sitter spacetime we have seen that forming shells around black holes at fixed total mass cools the combined system. Unlike in asymptotically flat spacetime, Sec. 4 shows there exists an extended region where such shells are *stable* rather than marginally stable. At the local photon sphere, $f = \frac{1}{3} + \frac{9\widehat{m}^2}{L^2}$, which using Eq. (5.87) gives [13]:

$$d \ln T_\infty = -\frac{d\widehat{m}}{\widehat{m} \left(1 + \frac{27\widehat{m}^2}{L^2}\right)} \implies T_\infty(M) = T_\infty(m) \frac{m}{M} \sqrt{\frac{1 + \frac{27M^2}{L^2}}{1 + \frac{27m^2}{L^2}}}. \quad (5.96)$$

This system cools as shells are added, increasing the coarse-grained entropy. The minimum temperature is reached in the regime where only a small black hole remains; it is surrounded by an ocean of radiation with $M \gg m$. The Hawking temperature, before considering shells, is $T_H(m) = 1/8\pi m$; the asymptotically measured temperature is:

$$T_\infty(M) = \frac{1}{8\pi M} \sqrt{1 + \frac{27M^2}{L^2}} \implies \lim_{M \rightarrow \infty} T_\infty(M) = \frac{3\sqrt{3}}{8\pi L}. \quad (5.97)$$

This minimum temperature satisfies $T_{\min} \sim 1/L$. From Eq. (5.86), dS can be written as:

$$dS = \frac{dM}{T_\infty(M)} = \frac{8\pi M dM}{\sqrt{1 + \frac{27M^2}{L^2}}}. \quad (5.98)$$

This gives¹⁹ Hagedorn-like behavior, as shown in [13, 53]:

$$S(M) - S(0) = \frac{8\pi L^2}{27} \left(\sqrt{1 + \frac{27M^2}{L^2}} - 1 \right) \sim \frac{8\pi L}{3\sqrt{3}} M = \frac{M}{T_{min}} \sim ML. \quad (5.99)$$

Let us see what occurs for more general AdS black holes of mass m . From Eq. (5.96) evaluated at $T_\infty(\hat{m})$, the entropy from Eq. (5.86) is:

$$dS_{\text{shell}} = \frac{d\hat{m}}{T_\infty(\hat{m})} = \frac{1}{T_\infty(m)} \frac{\hat{m}}{m} \frac{\sqrt{1 + \frac{27m^2}{L^2}}}{\sqrt{1 + \frac{27\hat{m}^2}{L^2}}} d\hat{m}. \quad (5.100)$$

Including the black hole $S = \pi r_+^2$, this immediately reproduces the result of [13, 53], which was obtained using the Euclidean path integral and entropy maximization methods:

$$S = \pi r_+^2 + \frac{L^2}{27mT_\infty(m)} \sqrt{1 + \frac{27m^2}{L^2}} \left(\sqrt{1 + \frac{27M^2}{L^2}} - \sqrt{1 + \frac{27m^2}{L^2}} \right). \quad (5.101)$$

If thermalization is viewed as impossible, these solutions might be used to constrain stress-energy tensors in AdS/CFT [57], giving a perspective on how bulk matter content is related to the boundary theory.²⁰

If a stable shell can reach thermal equilibrium with the black hole, then canonical stability ($C_{r_0}^{-1} > 0$) is incompatible with microcanonical stability. As shown in Sec. 5.4, forming shells at fixed total mass decreases the temperature if and only if $C_{r_0}^{-1} > 0$. This increases the coarse-grained entropy of the system by forming an ocean:

$$S_{\text{ocean}} = \int_m^M \frac{d\hat{m}}{T_\infty(\hat{m})} > \int_m^M \frac{d\hat{m}}{T_H(\hat{m})} = \Delta S_{\text{bh}}. \quad (5.102)$$

In any case, if black holes can cool by forming shells while remaining in thermal equilibrium, Eq. (5.102) will drive a feedback loop; if unchecked at large M , this is consistent with (5.99).

Finally, it is interesting to consider the consequences of placing these shells where the specific heat changes sign, as we have done in asymptotically flat spacetime:

$$C_R^{-1} = \frac{dT_H}{dm} + \frac{T_H}{Rf(R)} = T_H \left(\frac{d \log T_H}{dm} + \frac{1}{Rf(R)} \right) = 0. \quad (5.103)$$

We have seen in Sec. 4 that shells at this location are mechanically stable. Under the strong assumption that the system can reach thermal equilibrium with the black hole, provided the matter is mechanically stable with non-negative specific heat, this gives:

$$d \ln T_\infty = -\frac{d\hat{m}}{Rf_{\hat{m}}(R)} = \frac{d \ln T_H}{d\hat{m}} d\hat{m} = d \ln T_H(\hat{m}), \quad (5.104)$$

¹⁹The Hagedorn-like behavior (identified first in [13, 53]) is obtained here using shells, giving another perspective. We thank Daniel Jafferis for extensive discussion on this issue.

²⁰Although the Hagedorn-like scaling $S \sim EL$ was found in [13] near a minimum temperature, the expected $S \sim E^{2/3}$ scaling [35, 36] at large E can be recovered by taking E large before sending the boundary cutoff to infinity [13]. We thank Daniel Jafferis for discussion on this point.

$$S_{\text{ocean}} = \int_m^M \frac{d\hat{m}}{T_\infty(\hat{m})} = \int_m^M \frac{d\hat{m}}{T_H(\hat{m})} = \int \frac{1}{\frac{1}{4\pi r_+} \left(1 + \frac{3r_+^2}{L^2}\right)} \left(\frac{1}{2} \left(1 + \frac{3r_+^2}{L^2}\right)\right) dr_+ = \pi r_+^2 \Big|_m^M. \quad (5.105)$$

This system has the same coarse-grained entropy as a black hole precisely because it is exactly as cold as one. In AdS this can be done only on the small black hole branch; on the large black hole branch, C_R^{-1} is strictly positive.

The result is quite general; if the inverse specific heat vanishes at the location where the shell is placed, then the entropy of the system follows directly from the first law of black hole thermodynamics. This observation is further generalized below.

5.5.3 Beyond Nested Shells: Boxes as Cold as a Black Hole

Now we consider configurations where more general self-gravitating gases are contained between two Israel layers, generalizing the discussion of Sec. 5.5.2.

Adding the (tt) and (rr) components of Einstein's equations, Eq. (5.3) and Eq. (5.4), the cosmological constant cancels:

$$\frac{j}{8\pi r} \left(\frac{f'}{f} - \frac{j'}{j} \right) = \rho + P_r. \quad (5.106)$$

The temperature at the horizon is well-known to be $T_\infty = \frac{1}{4\pi} \sqrt{f'(r_h) j'(r_h)}$. The asymptotically measured temperature therefore changes as:

$$d \log T_\infty = \frac{1}{2} \left[\frac{j'(r)}{j(r)} - \frac{f'(r)}{f(r)} \right] dr = -\frac{4\pi r (\rho + P_r)}{j(r)} dr. \quad (5.107)$$

This recovers Eq. (5.87) in the vacuum thin shell limit.

The configuration is precisely as cold as a black hole when the temperature matches point-wise Eq. (5.88); for $\Lambda=0$, Eq. (5.5) requires:

$$\frac{P_r}{\rho} = \frac{3j(r) - 1}{1 - j(r)} = \frac{r - 3\hat{m}(r)}{\hat{m}(r)}. \quad (5.108)$$

This is closely related to the condition required for an extended photon sphere to form, as explained in Appendix A. An extended photon sphere forms when Eq. (A.7) holds:

$$P_\perp(r) = \frac{1 - 2\hat{m}'(r)}{8\pi r^2}, \quad P_r = \frac{r - 3\hat{m}(r)}{4\pi r^3}, \quad \rho = \frac{\hat{m}'(r)}{4\pi r^2}, \quad \implies \frac{P_r}{\rho} = \frac{r - 3\hat{m}(r)}{r\hat{m}'(r)}. \quad (5.109)$$

Thus Hod's condition [58] for degenerate light rings, when applied over an extended region, takes precisely the same form as thermodynamic mimicry. For Eq. (5.108) to be maintained throughout an extended region, we are naturally led to specialize to self-similar gases, within which $\hat{m}(r) = \nu r$ and $r f' / 2f = 1$. The HBH [12, 13] is the simplest case.

To explore this in more detail, we determine coarse-grained entropies of these systems, starting with the walls enclosing the self-gravitating gas. Using the results of Sec. 5.5.2, the coarse-grained entropy of a thin shell at radius R , where $A = 4\pi R^2$ and $E = \sigma A$, reads:

$$dS = \frac{dE + p dA}{T(R)} = \frac{(\sigma + p)dA}{T(R)}. \quad (5.110)$$

The IJC for the shell, in Eq. (3.5), can be conveniently rewritten using Eq. (A.32):

$$8\pi(\sigma + p) = [K^\tau{}_\tau] - [K^\theta{}_\theta] = \frac{1}{R} \left[\sqrt{j} \left(\frac{rf'}{2f} - 1 \right) \right]_R. \quad (5.111)$$

The induced metric must match at the interface Eq. (B.4), so $f(r)$ is a continuous function, and can be moved inside the bracket.

The locally measured Tolman temperature satisfies $T(r) = T_\infty/\sqrt{f(r)}$. The coarse-grained entropy on the shell of area $A = 4\pi R^2$ is then:

$$S_{\text{shell}} = \frac{R}{2T_\infty} \left[\sqrt{fj} \left(\frac{rf'}{2f} - 1 \right) \right]_R. \quad (5.112)$$

So it is for walls. Now we consider the coarse-grained entropy between them. The proper volume element is $dV = 4\pi r^2 dr/\sqrt{j}$. Then Eq. (5.12) and Eq. (5.106) yield:

$$S_{\text{bulk}} = \frac{1}{T_\infty} \int dr 4\pi r^2 (\rho + P_r) \sqrt{\frac{f(r)}{j(r)}} = \frac{1}{2T_\infty} \int dr r \sqrt{fj} \left(\frac{f'}{f} - \frac{j'}{j} \right). \quad (5.113)$$

Assembling these results, and including the black hole, the full coarse-grained entropy is:

$$S = \frac{A_{\text{H}}}{4} + \sum_{\text{shells}} \frac{1}{2T_\infty} \left[r \sqrt{fj} \left(\frac{rf'}{2f} - 1 \right) \right]_{R_i} + \frac{1}{2T_\infty} \int_{\text{gas}} r \sqrt{fj} \left(\frac{f'}{f} - \frac{j'}{j} \right) dr. \quad (5.114)$$

To sum up, the area term for the horizon is added to the coarse-grained entropy of the (an)isotropic fluid and (when they are needed), the walls. No wall is needed at the photon sphere, where its respective term vanishes. The gas term vanishes in vacuum, where $f = j$.

The Euler relation²¹ in Eq. (5.114) is general, and one of the main results of this note. It permits direct evaluation of coarse-grained entropies without the Euclidean path integral. The discussion below Eq. (5.108) now motivates us to specialize to self-similar solutions. Einstein's equations require $8\pi r^2(\rho + P_\perp) = 1$, the condition responsible for the optical mimicry of the HBH.²² These satisfy Eq. (5.49) and Eq. (5.50), which gives Eq. (5.109):

$$\hat{m} = \nu r, \quad \rho = \frac{\nu}{4\pi r^2}, \quad P_r = \frac{1 - 3\nu}{4\pi r^2}, \quad P_\perp = \frac{1 - 2\nu}{8\pi r^2}. \quad (5.116)$$

Indeed, since $w_r \equiv P_r/\rho = (1 - 3\nu)/\nu$, the entire self-similar family satisfies the temperature mimicry condition Eq. (5.108).

²¹Following identical reasoning to that of the argument originally given in Section 4.2 of [13], this expression can be used to find an Euler relation for a *misaligned* self-similar gas with *massless walls*:

$$2T_\infty S = \frac{4 + w_r(2 - \delta)}{\delta + 2} \left[M - m \left(\frac{m}{M} \right)^{\delta/2} \right]. \quad (5.115)$$

Indeed, this is an Euler relation for the self-similar gas. For $\delta = 2$ and $m = 0$ we recover $2T_\infty S = M$, the same as that satisfied by a black hole. This is consistent with Eq. (5.118) and with the earlier result in [13].

²²The condition $8\pi r^2(\rho + P_\perp) = 1$ holds for this entire self-similar family of solutions, so they can have an odd number of light rings [58]. This is relevant to their stability, as discussed in App. A.

When the assumptions given above hold, if we further assume $\hat{m}(r)$ is *continuous*, then this family has the temperature and coarse-grained entropy of a black hole of mass M :

$$S = 4\pi m^2 + \int_m^M \frac{d\hat{m}}{T_\infty(\hat{m})} = 4\pi m^2 + 8\pi \int_m^M \hat{m} d\hat{m} = 4\pi M^2. \quad (5.117)$$

Combining Eq. (5.111), Eq. (5.114), and Eq. (5.116), we find the entropy is distributed between the self-similar gas and the (massless)²³ Israel layers as:

$$S = \frac{A_{\text{H}}}{4} - 4\pi m(3m - R_{\text{in}}) + 4\pi M(3M - R_{\text{out}}) + 4\pi(1 + w_r)(M^2 - m^2) = 4\pi M^2. \quad (5.118)$$

These are the coarse-grained entropies of, respectively, (1) the inner black hole horizon, (2) the inner Israel layer, (3) the outer Israel layer, and (4) the self-gravitating gas between the Israel layers, where $R_{\text{in}} = m/\nu$ and $R_{\text{out}} = M/\nu$.

This one parameter family of self-similar solutions with $T = (8\pi M)^{-1}$ and $S = 4\pi M^2$ includes the $\delta = 2$ line in Fig. 12. The assumption that $\hat{m}(r)$ is continuous imposes a constraint on the IJC; before turning to this caveat, we proceed to discuss how this coarse-grained entropy is distributed between the self-gravitating gases and the Israel layers.

The stiffest star [27] satisfies $\nu = 1/4$ and $w_r = 1$, so the self-similar gas has $S_{\text{gas}} = 8\pi(M^2 - m^2)$. The outer wall at $R_{\text{out}} = 4M$ has $S_{\text{out}} = -4\pi M^2$, and the inner wall at $R = 4m$ has $S_{\text{in}} = 4\pi m^2$. Now turning to the frozen star [24–26], it satisfies $\nu = 1/2$ and $w_r = -1$. In this case $sT = \rho + P_r = 0$ by Eq. (5.12). The self-similar gas carries no coarse-grained entropy. The walls sit at their local horizons $R_{\text{in}} = 2m$ and $R_{\text{out}} = 2M$; the inner wall cancels the horizon’s area term, while the outer wall carries $S_{\text{out}} = 4\pi M^2$.²⁴

The HBH is the only *aligned* member of this family, in the sense discussed in Sec. 1.1. The coarse-grained entropy of the ocean is $4\pi M^2$. There are no Israel layers at the inner and outer edges of the HBH because $\sigma = 2p$ (equivalently, $rf'/2f = 1$), which is consistent with their vanishing coarse-grained entropies in Eq. (5.114). For thermodynamic mimicry to hold for the other $\delta = 2$ members of this family, the IJCs in Eq. (3.5) require massless walls, but $\sigma = 0$ and $p = -RP_r/2\sqrt{j}$ severely violates the DEC: $\sigma \geq |p|$ unless $P_r = 0$.

Massive walls can be considered, where $\sigma \geq 0$ is a free parameter, but then thermodynamic mimicry breaks down because Eq. (5.81) vanishes only for infinitesimally light shells at the photon sphere, i.e. $\sigma = 2p$. This concurs with Fig. 5 in [11]. There does remain the possibility of massive walls that are not thin shells. However, if $T_\infty = (8\pi\hat{m})^{-1}$, then $T_\infty\hat{m}$ is constant, but at the interface of the Schwarzschild region we have, from Eq. (5.87):

$$d \log(T_\infty\hat{m}) = \frac{R - 3\hat{m}}{\hat{m}(R - 2\hat{m})} d\hat{m} \neq 0, \quad \text{unless } R = 3\hat{m}. \quad (5.119)$$

In conclusion, massive walls break thermodynamic mimicry unless $R = 3\hat{m}$, but massless walls with non-vanishing transverse pressure violate DEC. This is not an issue for the HBH. Its photon sphere is *aligned*; indeed, Eq. (5.119) vanishes for the HBH because $\hat{m} = r/3$.

²³These are massless because $\hat{m}(r)$ is assumed to be continuous. For clarity, $rf'/2f = 1$ in the gas (not necessarily the walls) for these self-similar solutions.

²⁴This is consistent with [26], which argued that the frozen star satisfies $T = (8\pi M)^{-1}$ and $S = 4\pi M^2$. Note the horizonless limit. The surface pressure $p \gg \sigma = 0$ matches the $p_\perp \gg \rho$ transition region of [26].

6 Discussion

The well-known obstruction [8, 11] to placing a black hole in stable thermal equilibrium with self-gravitating radiation has been revisited. The thought experiment of Fig. 1 builds up a *hillingar* black hole (HBH) [12, 13] by placing layers at $r = 3M$, maintaining the photon sphere geometry through backreaction. This sharp exception has been borne out.

The HBH has been uniquely selected by the joint stability problem [8, 11], and is an optical [12] and thermodynamic [13] mimic of an ordinary Schwarzschild black hole. It seems unlikely that these properties would arise together, through this mechanism, if the solution lacks a microscopic realization. A key question is whether a microscopic model can be constructed, or ruled out; ruling it out would more fully establish that self-gravitating matter cannot reach stable equilibrium with a black hole in asymptotically flat spacetime.

Throughout this analysis, see also companion work [12, 13], we have seen that optical and thermodynamic mimicry are closely related.²⁵ For instance, in Sec. 5.5.3 we found a one-parameter self-similar family of solutions mimics a Schwarzschild black hole thermodynamically. Each is an extended photon sphere, satisfying $8\pi r^2(\rho + P_\perp) = 1$, inside a spherical box around a black hole. The distributions of their coarse-grained entropies between the gas and walls vary throughout this family, which includes “frozen stars” [24–26] and “stiffest stars” [27]. The HBH, the exception to the obstruction [8, 11], also happens to be the only member of this family without walls. Indeed, it satisfies $\sigma = 2p$ (as in Fig. 1), and is *aligned* as discussed in Sec. 1.1 and Sec. 5.5.3. The HBH therefore satisfies thermodynamic mimicry without violating the dominant energy condition (DEC).

The HBH should be viewed as a toy model for a more realistic system, such as an equilibrium between Hawking quanta within the thermal atmosphere of a black hole and its photon sphere. Although the formal assumption of thermal equilibrium is strong, it is supported by the following non-trivial consistency check. Up to our assumptions, evaporating to form an ocean is entropically possible; consistently, an explicit Bogoliubov computation in Appendix B shows that the ocean redshifts the horizon so that $T_\infty = 1/8\pi M$, as required for thermal equilibrium, while Eq. (5.81) gives the same conclusion. In any case, wavelengths of modes within an ocean in equilibrium with the black hole will be of order M , which seems inconsistent with a naive picture of particles on orbits. Strong rotation, as in Kerr, also seems likely to destabilize the ocean. For additional discussion, see [12, 13].

Even if stability is ruled out, these results probe the structure of semi-classical quantum gravity. For instance, the Bekenstein bound holds even when anisotropic radiation reaches thermal equilibrium with a black hole. Pushing this probe further could produce useful results. Several formal results obtained here – such as the connection between the photon sphere and the IJC/TOV equations, the fact that $C_R^{-1}\Big|_{\text{ps}} \propto -\Lambda$, and the IJC approach to black hole thermodynamics in Sec. 5 – are independent of these subtleties.

These extended photon spheres can be constructed straightforwardly and generically. Through Einstein’s equations we may easily imagine a *hillingar* black hole, and consider its properties, but it remains to be seen if they also appear in nature.

²⁵This connection between optical and thermodynamic mimicry at $\Lambda = 0$ suggests a deeper principle.

Acknowledgments

I thank Matt Strassler for extensive collaboration on the companion papers [12, 13] and for many essential discussions that shaped this work.²⁶ I am grateful to Andreas Karch and Lisa Randall for their support, comments, and conversations as I explored these ideas, and to Daniel Jafferis for extensive discussions throughout this project. I also thank Akshay Ghalsasi, Rashmish Mishra, Sonia Paban, Matt Reece, Suvrat Raju, Andrew Strominger, and Hongji Wei for comments and conversations. Calculations used the Mathematica packages `diffgeo.m` (Headrick) [59] and `OGR` [60] (Shoshany). This work was supported by the **Gravity, Spacetime, and Particle Physics** (GRASP) Initiative at Harvard University.

A Ultra-Compact Objects, Stability, and Optical Mimicry

Ultra-compact objects (UCOs) are defined as self-gravitating systems with a light ring; substantial discussion on the stability of these objects exists in the literature [14, 15].

It has been conjectured, following a key observation concerning stability by Keir [61], that ultra-compact objects with light-rings are black holes [62]. Long-lived modes are generically expected to appear for horizonless systems with light-rings, which tend to appear in pairs [62–64]. It was shown [64] that light-rings appear in pairs for smooth, horizonless, stationary ultra-compact objects under certain stated assumptions. This instability may arise from low-frequency modes trapped between the outer and inner light-rings [63, 65]; there has been discussion of “echoes” in the literature, see for example [66].

It was pointed out by Hod [58] that an interesting horizonless exception exists to the argument of [64]. The exception applies to UCOs satisfying the relation:

$$8\pi r_{ps}^2 (\rho + P_{\perp}) = 1, \quad (\text{A.1})$$

where r_{ps} is the radius of the light-ring, ρ is the density of the matter fields, and P_{\perp} is the transverse pressure. Hod’s argument applies to constant density stars, which are horizonless objects; he gives an example where certain stars saturating $R = 3M$ possess a solitary light-ring in the exterior region with $r_{ps} = 3M$.

More generally, an extended photon sphere forms precisely when $8\pi r^2 (\rho + P_{\perp}) = 1$. This is related to the fact that the HBH has a single light ring at $r = 3M$. One finds $V_{\text{eff}}(r) = \ell^2 h(r) + \epsilon f(r)$ for null geodesics, see for example [12]. This gives:

$$V_{\text{eff}} = h(r)l^2, \quad V'_{\text{eff}} = h'(r)l^2, \quad V''_{\text{eff}} = h''(r)l^2, \quad (\text{A.2})$$

where $h(r) \equiv f(r)/r^2$. The stability of the light ring at the photon sphere $r = r_{ps}$ hinges on the sign of $V''_{\text{eff}}(r)$, which can be straightforwardly written as:

$$V''_{\text{eff}}|_{r_{ps}} = \frac{2l^2 f(r_{ps})}{r_{ps}^3} \frac{d}{dr} \left(\frac{r f'(r)}{2f(r)} \right), \quad (\text{A.3})$$

²⁶The metric was constructed in [12]; the present note shows it arises as the uniquely determined solution to the York/BLP joint stability problem in asymptotically flat spacetime [8, 11]. The thermodynamics were obtained using the Euclidean path integral and entropy maximization in [13]; Sec. 5.5 recovers these results independently using a method developed here. The $C_{ps}^{-1} \propto -\Lambda$ identity, IJC-from-phase-portrait correspondence, stability analysis, and approach to the thermodynamics are original to this note.

where we used the condition $rf'/2f = 1$ to simplify the expression at $r = r_{\text{ps}}$. Now we bring in the formalism developed in Sec 5.1; Eq. (5.6) shows that:

$$\frac{rf'(r)}{2f(r)} = \frac{\widehat{m} + 4\pi r^3 P_r - \frac{1}{3}\Lambda r^3}{r - 2\widehat{m} - \frac{1}{3}\Lambda r^3}. \quad (\text{A.4})$$

Since $rf'/2f = 1$ is satisfied at the light ring, Eq. (A.4) gives $\widehat{m} = \frac{1}{3}(r - 4\pi r^3 P_r)$. Meanwhile, in this case the condition of hydrostatic equilibrium in Eq. (5.7) requires:

$$P'_r(r) = -\frac{P_r + \rho}{r} - \frac{2(P_r - P_\perp)}{r}. \quad (\text{A.5})$$

Taking the derivative in Eq. (A.3), and using Eq. (A.4), Eq. (A.5), $\widehat{m} = \frac{1}{3}(r - 4\pi r^3 P_r)$, and $\widehat{m}'(r) = 4\pi r^2 \rho$ into the resulting expression, we find:

$$V''_{\text{eff}}|_{r_{\text{ps}}} = \frac{-6f(r)l^2}{r_{\text{ps}}^4} \left(\frac{1 - 8\pi r^2 (P_\perp + \rho)}{1 - r^2 \Lambda + 8\pi r^2 P_r} \right) = 0 \iff 8\pi r^2 (P_\perp + \rho) = 1. \quad (\text{A.6})$$

This is precisely Hod's [58] condition. Although the HBH is not horizonless, the entire self-similar family of 5.5.3, which includes the HBH, nonetheless satisfies this relation.

In fact there exists an infinite family of solutions satisfying this condition throughout an extended region, in addition to the HBH. Noting that $\rho(r) = \widehat{m}'(r)/4\pi r^2$, by enforcing the condition Eq. (A.5), an extended photon sphere exists precisely when²⁷:

$$\boxed{P_\perp(r) = \frac{1 - 2\widehat{m}'(r)}{8\pi r^2}, \quad P_r = \frac{r - 3\widehat{m}(r)}{4\pi r^3}, \quad \rho = \frac{\widehat{m}'(r)}{4\pi r^2}} \quad (\text{A.7})$$

This is closely related to thermodynamic mimicry, as mentioned in the main text. The self-similar family discussed there satisfies this relation.

Israel Layers Break Optical Mimicry

To supplement our discussion of optical mimicry, we show that the height of the peaks of the effective potential $V_{\text{eff}}(r) \equiv h(r)\ell^2$ is strictly decreasing for nested Israel layers.

Within the vacuum Schwarzschild regions, we have:

$$\frac{d \log h}{d \log r} = -2 \frac{r - 3\widehat{m} - 4\pi r^3 P_r}{r - 2\widehat{m} - \frac{1}{3}\Lambda r^3} = -2 \left(\frac{r - 3\widehat{m}}{rj(r)} \right). \quad (\text{A.8})$$

The denominator is positive outside the horizon, so $h'(r)$ changes sign at $r = 3\widehat{m}$. For static solutions Israel layers are placed *outside* the photon sphere of the Schwarzschild metric. Each vacuum annulus contributes at most one point where $h'(r) = 0$; these occur when an Israel layer causes μ to exceed $1/3$, as in Fig. 10.

Each such peak occurs at $r_k = 3m_k$, so for $h_k^{\text{peak}} = f(3m_k)/(3m_k)^2$:

$$\frac{h_k^{\text{peak}}}{h_{k-1}^{\text{peak}}} = \frac{\lambda_{m_k}^2}{\lambda_{m_{k-1}}^2} = \frac{\frac{1}{27m_k^2} - \frac{\Lambda}{3}}{\frac{1}{27m_{k-1}^2} - \frac{\Lambda}{3}} < 1. \quad (\text{A.9})$$

²⁷A much simpler derivation is given in Appendix C of [12].

Since $\Lambda = 1/27m_k^2$ is the Nariai limit, the peaks are strictly decreasing for physical solutions.

Geodesics that penetrate a photon sphere at $r = 3M$ can, in principle, return to asymptotic infinity if a higher peak in V_{eff} exists within $r < 3M$. For the HBH each shell sits at precisely $r = 3\hat{m}$. This makes V_{eff} a plateau; no walls are required at the edges, and so a geodesic penetrating $r = 3M$ cannot return.

Indications of Possible Mechanical Stability

To fully demonstrate the stability of the ocean, we would need to show that neither the Regge-Wheeler equation (for axial perturbations), nor the Zerilli equation (for polar perturbations), admit unstable QNMs with $\text{Im}(\omega) > 0$. Both equations satisfy:

$$\frac{d^2 Z}{dr_*^2} + [\omega^2 - V(r)] Z = 0. \quad (\text{A.10})$$

The tortoise coordinate r_* satisfies $dr_* = dr/\sqrt{fj}$. For the Schwarzschild metric it was shown by Chandrasekhar that the Regge-Wheeler and Zerilli equations have identical spectra [67]. The full extension of the Regge-Wheeler and Zerilli equations to non-vacuum spacetimes is an open problem in the literature; however, there is some agreement on the following Regge-Wheeler potential [68–71], which uses the inverse-Cowling approximation:

$$V_{RW}(r) = f(r) \left[\frac{\ell(\ell+1)}{r^2} - \frac{6\hat{m}(r)}{r^3} + 4\pi(\rho - P_r) \right]. \quad (\text{A.11})$$

An Israel layer at the edge of the ocean would complicate matters; fortunately, for the HBH there is no Israel layer at the edge of the ocean. Additionally, the Regge-Wheeler potential is constant throughout the ocean because $f(r) \propto r^2$ and $m(r) \propto r$, with $P_r = 0$:

$$V_0 \equiv V_{RW}|_{\text{ocean}} = \frac{3\ell(\ell+1) - 5}{81M^2}. \quad (\text{A.12})$$

Since $3\ell(\ell+1) - 5 \geq 1$ for all $\ell \geq 1$, we have $V_0 > 0$. In the ocean, $\sqrt{fj} = r/(9M)$; then $dr_* = \frac{9Mdr}{r}$, so the tortoise coordinate is $r_* = 9M \ln r + c_1$, with c_1 some constant. Then the tortoise coordinate is smooth and logarithmic within the ocean:

$$\Delta \equiv r_*|_{3M} - r_*|_{3m} = 9M \ln \left(\frac{M}{m} \right) > 0. \quad (\text{A.13})$$

Proposition 1. *Consider an “ocean” region containing gravitating matter, extending from $r_{\text{in}} < r < r_{\text{out}}$, with (1) no Israel layers at the interface. Suppose (2) the tortoise coordinate is smooth and logarithmic within that region, and (3) the RW potential is constant and non-negative within that region. Then subject to a WKB approximation at the edges of this region, the Regge-Wheeler equation has no unstable QNMs.*

By Assumption (1) there are no Israel layers, so the Regge-Wheeler equation applies. By Assumption (2), the tortoise coordinate is smooth and logarithmic within the “ocean”:

$$\frac{dr_*}{dr} = \frac{\alpha}{r} \implies \Delta \equiv r_*(r_{\text{out}}) - r_*(r_{\text{in}}) = \alpha \ln \frac{r_{\text{out}}}{r_{\text{in}}} > 0. \quad (\text{A.14})$$

By Assumption (3) the Regge-Wheeler potential is constant within this region, so $V_{RW} \equiv V_0$. Then the Regge-Wheeler equation is:

$$\frac{d^2 Z}{dr_*^2} + (\omega^2 - V_0) Z = 0. \quad (\text{A.15})$$

It is straightforward to show that solution to the Regge-Wheeler equation takes the form:

$$Z(r) = Cr^{ik} + Dr^{-ik}, \quad \Omega^2 \equiv \omega^2 - V_0, \quad k \equiv \alpha\Omega. \quad (\text{A.16})$$

Now we obtain a condition on the QNMs satisfying the Regge-Wheeler equation, subject to the conditions (1), (2), and (3). It follows by direct calculation that:

$$\frac{Z'}{Z} = \frac{ik}{r} \frac{1 - Rr^{-2ik}}{1 + Rr^{-2ik}}. \quad (\text{A.17})$$

Here we have used the definitions:

$$R \equiv \frac{D}{C}, \quad x \equiv \frac{\omega}{\Omega}, \quad \varphi \equiv \left(\frac{r_{\text{in}}}{r_{\text{out}}} \right)^{2ik} = e^{-2i\Omega\Delta}. \quad (\text{A.18})$$

In asymptotically flat spacetime QNMs are strictly ingoing at the horizon and strictly outgoing at asymptotic infinity. This leaves the question of what the boundary conditions should be for our problem unanswered. To test the waters of this problem, we take:²⁸

$$Z \sim e^{-i\omega r_*} \quad (r = r_{\text{in}}), \quad Z \sim e^{+i\omega r_*} \quad (r = r_{\text{out}}). \quad (\text{A.19})$$

The mode is strictly ingoing toward the horizon at the bottom of the ocean, and strictly outgoing toward asymptotic infinity at the top of the ocean. This then simplifies the problem. Since $\frac{dr_*}{dr} = \frac{1}{\sqrt{fj}}$ is continuous at both boundaries, $Z'/Z = \pm i\omega \frac{dr_*}{dr}$, which gives:

$$\left. \frac{Z'}{Z} \right|_{r=r_{\text{in}}} = -\frac{i\omega\alpha}{r_{\text{in}}}, \quad \left. \frac{Z'}{Z} \right|_{r=r_{\text{out}}} = \frac{i\omega\alpha}{r_{\text{out}}}. \quad (\text{A.20})$$

Combined with Eq. (A.17), this leads to two matching conditions for the QNMs:

$$Rr_{\text{in}}^{-2ik} = \frac{1+x}{1-x}, \quad Rr_{\text{out}}^{-2ik} = \frac{1-x}{1+x}. \quad (\text{A.21})$$

Subsequently eliminating R yields the condition:

$$\left(\frac{r_{\text{in}}}{r_{\text{out}}} \right)^{2ik} \frac{1+x}{1-x} = \frac{1-x}{1+x}. \quad (\text{A.22})$$

This QNM condition can be rewritten sharply in terms of the Möbius transformation $g(z)$:

$$\varphi = g(x)^2, \quad g(z) \equiv \frac{1-z}{1+z}. \quad (\text{A.23})$$

The properties of the Möbius transformation permit us to rule out unstable QNMs for Regge-Wheeler potentials of this form.

²⁸The objective here is only to present a plausibility argument. It is important to check if long-lived modes within the ocean could destabilize the structure, which can be an issue for horizonless UCOs; see [58, 61, 62, 64, 65], but note the HBH satisfies Hod's condition in [58]. Naively, it seems unlikely that the flat effective potential would effectively trap such modes. In any case, a more careful treatment is needed.

Lemma 1. For any $z \in \mathbb{C}$, $|g(z)| < 1$ if and only if $\text{Re}(z) > 0$. The proof follows from direct computation:

$$|g(z)|^2 = \frac{|1-z|^2}{|1+z|^2} = \frac{1-2\text{Re}(z)+|z|^2}{1+2\text{Re}(z)+|z|^2}. \quad (\text{A.24})$$

Theorem 1. No unstable QNMs exist with $\text{Im}(\omega) > 0$, because $\varphi = g(x)^2$ is not satisfied. Here we implicitly assume the WKB approximation used previously is justified.

Proof. It suffices to consider modes with $\text{Re}(\omega) \geq 0$ because Eq. (A.23) is invariant under $\omega \rightarrow -\omega^*$. Let $\omega = a + ib$ with $a \geq 0$ and $b > 0$. Write $\Omega = \sqrt{\omega^2 - V_0} = A + iB$ for either choice of square root branch; we show the contradiction holds for both cases.

Note that $|\varphi| = |e^{-2i\Omega\Delta}| = e^{2B\Delta}$, so $B > 0$ implies $|\varphi| > 1$ and $B < 0$ implies $|\varphi| < 1$.

Case $a > 0$. From $\Omega^2 = \omega^2 - V_0$ with V_0 real:

$$\text{Im}(\Omega^2) = 2AB = \text{Im}(\omega^2) = 2ab \implies AB = ab. \quad (\text{A.25})$$

Then we have $\text{Im}(\omega^2 - V_0) = 2ab > 0$. Both branches give $AB > 0$, hence A and B have the same sign. A short computation gives $\text{Re}(x) = \frac{b(a^2+B^2)}{B|\Omega|^2}$.

- If $B > 0$, then $|\varphi| > 1$. However, $\text{Re}(x) > 0$, so $|g(x)^2| < 1$. Contradiction.
- If $B < 0$, then $|\varphi| < 1$. However, $\text{Re}(x) < 0$, so $|g(x)^2| > 1$. Contradiction.

Case $a = 0$. Now we have $\omega = ib$ and $\omega^2 - V_0 < 0$. Write $\Omega = \pm i\kappa$ with $\kappa = \sqrt{b^2 + V_0} > 0$. Since $\varphi \equiv e^{-2i\Omega\Delta} = e^{\pm 2\kappa\Delta}$, it follows that $\varphi > 1$ when $\Omega = +i\kappa$ and $\varphi < 1$ when $\Omega = -i\kappa$. Note $x = \frac{\omega}{\Omega} = \frac{ib}{\pm i\kappa} = \pm \frac{b}{\kappa} \in \mathbb{R}$; $|x| = \frac{b}{\kappa} < 1$, with $g(x) = \frac{1-x}{1+x} > 0$. Since $g(0) = 1$ and $g'(x) < 0$, $\Omega = i\kappa$ implies $x > 0$ and $g(x)^2 < 1$; $\Omega = -i\kappa$ implies $x < 0$ and $g(x)^2 > 1$. Then φ and $g(x)^2$ are on opposite sides of 1, which contradicts $\varphi = g(x)^2$.

In each case the QNM condition $|\varphi| = |g(x)^2|$ cannot be satisfied for $\text{Im}(\omega) > 0$. \square

Proposition 2. *The only geometry where Assumptions (1), (2) and (3) apply is the HBH.*

To show this result we need only Einstein's equations and the Israel junction conditions. The Regge-Wheeler potential Eq. (A.11) in terms of $\widehat{m}'(r) = 4\pi r^2 \rho(r)$ reads:

$$V_{RW} = f(r) \left[\frac{\ell(\ell+1)}{r^2} - \frac{6\widehat{m}(r)}{r^3} + \frac{\widehat{m}'(r)}{r^2} - 4\pi P_r(r) \right]. \quad (\text{A.26})$$

We require that V_{RW} is constant in the ocean region; since the $l(l+1)$ term is the only one carrying l dependence, its coefficient must be constant:

$$\frac{f(r)}{r^2} = A, \quad \implies \quad f(r) = Ar^2. \quad (\text{A.27})$$

Equivalently, for the RW to be constant within this region, the region must be an extended photon sphere. Since $f(r) \propto r^2$, Einstein's equations Eq. (5.6) with $\Lambda = 0$ require:

$$1 = \frac{rf'}{2f} = \frac{\widehat{m}(r) + 4\pi r^3 P_r(r)}{r - 2\widehat{m}(r)} \implies 4\pi r^2 P_r = 1 - \frac{3\widehat{m}}{r}. \quad (\text{A.28})$$

Inserted into the Regge-Wheeler equation, this gives:

$$V_{RW} = A \left[\ell(\ell + 1) - 1 + \widehat{m}'(r) - \frac{3\widehat{m}(r)}{r} \right]. \quad (\text{A.29})$$

Then for V_{RW} to be constant, $\widehat{m}(r)$ takes the form:

$$\widehat{m}'(r) - \frac{3\widehat{m}(r)}{r} = \text{const.} \implies \widehat{m}(r) = Cr^3 + ar. \quad (\text{A.30})$$

Now we enforce the requirement that there are no Israel layers. At a static interface $r = R$, the Israel junction conditions in Eq. (3.12) and Eq. (3.10) require:²⁹

$$K^\theta_\theta = \frac{\sqrt{j}}{R}, \quad K^t_t = \frac{\sqrt{j}}{2} \frac{f'}{f}. \quad (\text{A.32})$$

Here we let $\epsilon = 1$ without loss of generality. But since $f(r) = Ar^2$, the K^t_t and K^θ_θ components of the extrinsic curvature are equal throughout the ocean:

$$K^t_t = \frac{\sqrt{j}}{R} = K^\theta_\theta. \quad (\text{A.33})$$

Then we require continuity of $j(r)$, equivalently continuity of $m(r)$, at the two interfaces: $\widehat{m}(r_{\text{in}}) = m$, and $\widehat{m}(r_{\text{out}}) = M$. The exterior of the ocean region must be Schwarzschild by Birkhoff's theorem; the extrinsic curvature at the exterior edge reads:

$$K^\theta_\theta = \frac{\sqrt{1 - 2M/R}}{R}, \quad K^t_t = \frac{M}{R^2 \sqrt{1 - 2M/R}}. \quad (\text{A.34})$$

Within the ocean the extrinsic curvatures are equal; since there is no Israel layer, we must have $K^t_t = K^\theta_\theta$ on the Schwarzschild side as well, which gives:

$$R = 3M. \quad (\text{A.35})$$

Then we have:

$$j(r) = 1 - \frac{2\widehat{m}(r)}{r} \implies \widehat{m}(r) = \frac{r}{3}. \quad (\text{A.36})$$

Then:

$$4\pi r^2 P_r = 1 - \frac{3\widehat{m}}{r} \implies P_r = 0. \quad (\text{A.37})$$

This completes the argument, since we have already seen that $P_r = 0$ with $rf'/2f = 1$ uniquely determines the HBH.

²⁹We note in passing that the useful relations, equivalent to Eq. (3.5), follow from Eq. (A.32):

$$8\pi\sigma = -\frac{2}{R} \left[\sqrt{j} \right]_R, \quad 8\pi(\sigma + p) = \frac{1}{R} \left[\sqrt{j} \left(\frac{rf'}{2f} - 1 \right) \right]_R. \quad (\text{A.31})$$

The notion of ‘‘alignment’’ in the main text can be understood as following from the thought experiment in Fig. 1 ($\sigma = np$ for $n = 2$), or, equivalently, from the fact that $rf'/2f = 1$ at the interface for the HBH.

B The Euclidean Action and Thermodynamics

Euclidean Action from Shells

Here we perform a consistency check. Consider the Euclidean action:

$$I_E = -\frac{1}{16\pi G} \int_{\mathcal{M}} \sqrt{g} R - \frac{1}{8\pi G} \int_{\partial\mathcal{M}} \sqrt{\gamma} K. \quad (\text{B.1})$$

Decompose the Euclidean geometry into N vacuum annuli separated by Israel shells at radii $R_1 < \dots < R_N$, with Schwarzschild masses $m_0 < m_1 < \dots < m_N = M$. Between shells the bulk is vacuum, so $R = 0$ and the Einstein-Hilbert term vanishes. The full action reduces to a sum of GHY boundary terms.

Using K , see Eq. (3.13), the integrated GHY contribution on a constant r surface is:

$$-\frac{1}{8\pi G} \int \sqrt{\gamma} K d^3x = -\frac{\beta r f}{2} \left(\frac{r f'}{2f} + 2 \right). \quad (\text{B.2})$$

At each interface R_k , the inner annulus (mass m_{k-1} , period β_{k-1}) contributes an outward facing GHY term. The outer annulus (mass m_k , period β_k) contributes an inward-facing GHY term. Their mismatch is:

$$\Delta_k = -\frac{R_k}{2G} \left[\beta_{k-1} f_- \left(\frac{R_k f'_-}{2f_-} + 2 \right) - \beta_k f_+ \left(\frac{R_k f'_+}{2f_+} + 2 \right) \right]. \quad (\text{B.3})$$

The induced metric on the shell must be continuous, so the proper circumference of the Euclidean time-circle matches across the interface:³⁰

$$\beta_{k-1} \sqrt{f_-} = \beta_k \sqrt{f_+} \equiv \beta_*. \quad (\text{B.6})$$

Then:

$$\Delta_k = -\frac{R_k \beta_*}{2G} \left[\sqrt{f_-} \left(\frac{R_k f'_-}{2f_-} + 2 \right) - \sqrt{f_+} \left(\frac{R_k f'_+}{2f_+} + 2 \right) \right] \quad (\text{B.7})$$

The static extrinsic curvature components are $K_\theta^\theta = \sqrt{f}/R$ and $K_\tau^\tau = f'/(2\sqrt{f})$, so:

$$K = K_\tau^\tau + 2K_\theta^\theta = \frac{\sqrt{f}}{R} \left(\frac{R f'}{2f} + 2 \right). \quad (\text{B.8})$$

The GHY mismatch at the interface is:

$$\Delta_k = \frac{\beta_* R_k^2}{2G} [K]. \quad (\text{B.9})$$

³⁰For a static shell, with $\dot{t} = dt/d\tau$:

$$\dot{t}^2 = \frac{j(R) + \dot{R}^2}{f(R)j(R)} = \frac{1}{f(R)} \quad d\tau = dt_- \sqrt{f_-(R)} = dt_+ \sqrt{f_+(R)}. \quad (\text{B.4})$$

The induced metric on the shell must match on both sides of the shell, so the proper circumference of the time-circle must agree. This recovers:

$$\beta_- \sqrt{f_-(R)} = \beta_+ \sqrt{f_+(R)} \implies \frac{T_+}{T_-} = \sqrt{\frac{f_+(R)}{f_-(R)}}. \quad (\text{B.5})$$

But by the Israel junction condition:

$$[K] = \frac{8\pi G}{n} T_a^a, \quad (\text{B.10})$$

where $T_a^a = -\sigma + np$ is the trace of the shell stress-energy. This gives:

$$\Delta_k = \frac{4\pi\beta_* R_k^2}{n} T_a^a = \frac{4\pi\beta_* R_k^2}{n} (-\sigma_k + np_k). \quad (\text{B.11})$$

The shell surface densities become the bulk densities in the continuum limit; that is, $\sigma_k \equiv \rho\delta R_k/\sqrt{j}$, $p_k \equiv P_\perp\delta R_k/\sqrt{j}$. Note also that $\beta_* \equiv \beta(R_k)\sqrt{f(R_k)}$.

The volume element takes the form:

$$\sqrt{g}d^{n+2}x = \frac{\sqrt{f}}{\sqrt{j}} r^n d\tau dr d\Omega_n, \quad (\text{B.12})$$

so the shell stress-tensor's trace is:

$$\frac{1}{2} \int T^\mu{}_\mu \sqrt{g}d^{n+2}x = \frac{\beta\Omega_n}{2} \int \frac{\sqrt{f}}{\sqrt{j}} r^n (-\rho + nP_\perp) dr. \quad (\text{B.13})$$

Then, to sum up, we have:

$$\lim_{k \rightarrow \infty} \sum_k \Delta_k = \frac{4\pi}{n} \int \beta \sqrt{f} \frac{r^2}{\sqrt{j}} (-\rho + nP_\perp) dr = \frac{1}{2} \int T^\mu{}_\mu \sqrt{g}d^4x = -\frac{1}{16\pi G} \int R \sqrt{g}d^4x, \quad (\text{B.14})$$

which is the Einstein-Hilbert action for $n = 2$. This calculation most likely exists in the literature in some form, because it is a straight-forward application of the IJC. Nonetheless, it can be used to see the vanishing matter action in [13], because $\sigma_k = np_k$ for the HBH.

Energy Fluctuations Near the Spinodal Point

For a black hole in thermal equilibrium with a cavity wall, the root-mean-square energy fluctuations ΔE have been shown to diverge when the cavity wall coincides with the photon sphere [8]. Here we show these fluctuations do not destabilize the HBH.

Briefly, the following calculation shows that the divergent fluctuations signal that the saddle-point approximation breaks down near the spinodal temperature. Nonetheless, these small fluctuations can be estimated near where the saddles merge at third order in $F(E)$. To see this, first expand $F(E)$ to second order in E :

$$F(E) = F(E_0) + F'(E_0)(E - E_0) + \frac{1}{2}F''(E_0)(E - E_0)^2 + \dots \quad (\text{B.15})$$

Near the saddle $F'(E) = 1 - TS'(E) = 0$, which gives $S'(E) = 1/T$. Then the quadratic term in the expansion satisfies $F'' = -TS'' = T^{-1}(dT/dE) = (TC_R)^{-1}$, where $C_R \equiv dE/dT$ is the heat capacity. In asymptotically flat spacetime, C_R^{-1} vanishes when the cavity wall coincides with the photon sphere of the black hole. As reviewed in the introduction, see Fig. 3, this occurs when the branches merge at the minimum temperature T_c :

$$M_c = \frac{r}{3}, \quad T_c = \frac{3\sqrt{3}}{8\pi r}, \quad E_c = r \left(1 - \frac{1}{\sqrt{3}}\right), \quad F_c = r \left(1 - \frac{\sqrt{3}}{2}\right). \quad (\text{B.16})$$

Define $\delta E \equiv E - E_c$ and $\epsilon \equiv (T - T_c)/T_c$. Expanding to third order in δE near T_c :

$$F(E) = F(E_0) + \frac{1}{6}F'''(E_0) \delta E^3, \quad M^2 = \frac{r^2}{9} + \frac{2r}{3\sqrt{3}}\delta E - \frac{1}{\sqrt{3}r}\delta E^3. \quad (\text{B.17})$$

Since $M(E) = E - \frac{E^2}{2r}$, the free energy $F(E)$ near the minimum temperature is given by:

$$F = F_c - \frac{\sqrt{3}r}{6}\epsilon - \epsilon \delta E + \frac{3}{2r^2} \delta E^3. \quad (\text{B.18})$$

The partition function Z can then be written as:

$$Z \equiv \int dE e^{-\beta F(E,T)} \simeq \int d(\delta E) e^{-\beta \left(F_c - \frac{\sqrt{3}r}{6}\epsilon \right)} e^{-\beta \left(-\epsilon \delta E + \frac{3}{2r^2} \delta E^3 \right)}. \quad (\text{B.19})$$

It is convenient to define an integration coordinate x and auxiliary variable ξ , where:

$$\delta E \equiv \left(\frac{2r^2}{3\beta} \right)^{1/3} x, \quad \xi \equiv \beta \epsilon \left(\frac{2r^2}{3\beta} \right)^{1/3}. \quad (\text{B.20})$$

Near the minimum temperature we have $0 < \xi \ll 1$. Then:

$$Z \simeq e^{-\beta \left(F_c - \frac{\sqrt{3}r}{6}\epsilon \right)} \left(\frac{2r^2}{3\beta} \right)^{\frac{1}{3}} \int dx e^{\xi x - x^3}. \quad (\text{B.21})$$

$$\log Z \simeq -\beta F_c + \beta \frac{\sqrt{3}r}{6}\epsilon + \frac{1}{3} \log \left(\frac{2r^2}{3\beta} \right) + O(1) \quad (\text{B.22})$$

Note that $\beta\epsilon = \beta_c - \beta$. Then applying $S = (1 - \beta\partial_\beta) \log Z$ gives:

$$(1 - \beta\partial_\beta) \left[\frac{\sqrt{3}r}{6}\beta_c - \beta \left(F_c + \frac{\sqrt{3}r}{6} \right) \right] = \frac{\sqrt{3}r}{6}\beta_c = 4\pi M_c^2. \quad (\text{B.23})$$

$$(1 - \beta\partial_\beta) \frac{1}{3} \log \left(\frac{2r^2}{3\beta} \right) = \frac{1}{3} \log \left(\frac{2r^2}{3\beta} \right) + \frac{1}{3}. \quad (\text{B.24})$$

In other words:

$$S(E_c) = 4\pi M_c^2 + \frac{1}{6} \log(A_{PS}) + O(1). \quad (\text{B.25})$$

More importantly, the energy fluctuations follow from the partition function:

$$\langle (\Delta E)^2 \rangle = \langle (\delta E)^2 \rangle - \langle (\delta E) \rangle^2, \quad \frac{d^n Z}{d\xi^n} \propto \int dx x^n e^{\xi x - x^3} \quad (\text{B.26})$$

$$\langle (\delta E^n) \rangle = \left(\frac{\int dx \exp(\xi x - x^3) x^n}{\int dx \exp(\xi x - x^3)} \right) \left(\frac{2r^2}{3\beta} \right)^{n/3}. \quad (\text{B.27})$$

The stable black hole branch lies on the $E > E_c$ side of the spinodal transition, so we restrict to $\delta E \geq 0$, hence $x \geq 0$. These integrals can be expanded as $e^{\xi x} = \sum_{n=0}^{\infty} \frac{(\xi x)^n}{n!}$:

$$\int_0^{\infty} dx x^m e^{\xi x - x^3} = \sum_{n=0}^{\infty} \frac{\xi^n}{n!} \int_0^{\infty} dx x^{m+n} e^{-x^3} = \frac{1}{3} \sum_{n=0}^{\infty} \frac{\xi^n}{n!} \Gamma \left(\frac{m+n+1}{3} \right). \quad (\text{B.28})$$

Only the scaling is important, because the integral is simply an $\mathcal{O}(1)$ number. Since $\beta \sim r$ and $E_c \sim r$, the energy fluctuations are suppressed as the system becomes large:

$$\Delta E \equiv \sqrt{(\Delta E)^2} \sim r^{1/3} \implies \frac{\Delta E}{E_c} \sim A^{-1/3}. \quad (\text{B.29})$$

The key point here is that $\Delta E/E_c$ is suppressed at large A . In any case, it does not diverge.

Bogoliubov Coefficients in 1+1 Dimensions for the HBH

This consistency check has been included to determine the normalization for the temperature in Sec. 5.5; it should not be surprising because, as is well-known, the Hawking temperature is set by the surface gravity κ at the horizon.

And so, we review the Hawking effect and verify that in the usual 1+1 dimensional s -wave approximation, the HBH has the same Hawking spectrum as a Schwarzschild black hole of mass M ; this holds for any interior mass m .

Starting with the general metric $ds^2 = -f(r)dt^2 + j(r)^{-1}dr^2$, the surface gravity at the horizon takes the form:

$$\kappa = \frac{1}{2} \sqrt{f'(r_+) j'(r_+)} \Big|_{r=2m}. \quad (\text{B.30})$$

To determine the modes we expand in plane waves $e^{-i\omega t + ikr_*}$, where ∂_t is the future-directed timelike Killing vector that defines positive frequency. The tortoise coordinate r_* tracking the phase of this wave satisfies $dr_*/dr = 1/\sqrt{f(r)j(r)}$; its light-cone coordinates are $u = t - r_*$ and $v = t + r_*$. The (u, v) coordinates that describe these waves for asymptotic observers at infinity break down at the horizon; however, the horizon is regular in the local coordinate system of an infalling observer that we now consider.

Expanding near that horizon, the local metric takes the form:

$$ds^2 \approx -f'(r_+) (r - r_+) dt^2 + \frac{dr^2}{j'(r_+) (r - r_+)}. \quad (\text{B.31})$$

The finite proper distance from the horizon is:

$$\rho = \int_{r_+}^r \frac{dr'}{\sqrt{j'(r_+) (r' - r_+)}} = \frac{2\sqrt{r - r_+}}{\sqrt{j'(r_+)}}. \quad (\text{B.32})$$

That gives Rindler coordinates:

$$ds^2 = \frac{-f'(r_+) j'(r_+) \rho^2}{4} dt^2 + d\rho^2 = -\kappa^2 \rho^2 dt^2 + d\rho^2. \quad (\text{B.33})$$

It is well-known that Minkowski coordinates are exponentially related to Rindler:

$$T = \rho \sinh(\kappa t), \quad X = \rho \cosh(\kappa t). \quad (\text{B.34})$$

The local Minkowski light-cone coordinates for an infalling Rindler observer are essentially the usual Kruskal coordinates:

$$V \equiv \frac{\sqrt{j'(r_+)}}{2} (T + X) = e^{+\kappa v}, \quad U \equiv \frac{\sqrt{j'(r_+)}}{2} (T - X) = -e^{-\kappa u}. \quad (\text{B.35})$$

The reason for the Hawking effect is that Minkowski time is exponentially related to asymptotic time. This is closely related to the fact that the horizon is regular in the (U, V) coordinates of an infalling observer, but not in the asymptotic coordinates:

$$ds^2|_{r=r_+} = -dT^2 + dX^2 = -\frac{2}{\kappa} \sqrt{\frac{f'(r_+)}{j'(r_+)}} dU dV. \quad (\text{B.36})$$

To find the modes we quantize, e.g., the Klein-Gordon equation for a scalar field ψ ; in 1+1 this gives $\partial_u \partial_v \psi = \partial_U \partial_V \psi = 0$. Only the right-moving (outgoing) modes at the horizon head to asymptotic infinity. Infalling observers expand in a -modes with positive frequency ν in U ; asymptotic observers use b -modes with positive frequency ω in u :

$$\psi_R = \int_0^\infty \frac{d\nu}{2\pi(2\nu)^{1/2}} (a_\nu e^{-i\nu U} + a_\nu^\dagger e^{+i\nu U}) = \int_0^\infty \frac{d\omega}{2\pi(2\omega)^{1/2}} (b_\omega e^{-i\omega u} + b_\omega^\dagger e^{+i\omega u}). \quad (\text{B.37})$$

The goal is to compute the expectation value of the number operator $b_\omega^\dagger b_\omega$ in the a -vacuum $|\psi\rangle$ where the horizon is regular, so we find the annihilation operator b_ω for the asymptotic observer using textbook Fourier analysis:

$$b_\omega = \sqrt{2\omega} \int_{-\infty}^\infty \frac{du}{2\pi} e^{i\omega u} \psi_R = \int_0^\infty \frac{d\nu}{2\pi} \left[\sqrt{\frac{\omega}{\nu}} \int_{-\infty}^\infty \frac{du}{2\pi} e^{i\omega u} e^{-i\nu U} a_\nu + \sqrt{\frac{\omega}{\nu}} \int_{-\infty}^\infty \frac{du}{2\pi} e^{i\omega u} e^{+i\nu U} a_\nu^\dagger \right] \quad (\text{B.38})$$

The prefactors for a_ν and a_ν^\dagger are the well-known Bogoliubov coefficients. The exponential map $U(u)$ converts plane waves into power laws, which do not have definite frequencies; the Mellin transform then leads to the phase difference responsible for the Hawking spectrum:

$$\alpha_{\omega\nu} \equiv \sqrt{\frac{\omega}{\nu}} \int_{-\infty}^\infty \frac{du}{2\pi} e^{i\omega u} e^{-i\nu U(u)} = \frac{1}{2\pi\kappa} \sqrt{\frac{\omega}{\nu}} \nu^{i\omega/\kappa} e^{-\pi\omega/2\kappa} \Gamma\left(\frac{-i\omega}{\kappa}\right), \quad (\text{B.39})$$

$$\beta_{\omega\nu} \equiv \sqrt{\frac{\omega}{\nu}} \int_{-\infty}^\infty \frac{du}{2\pi} e^{i\omega u} e^{+i\nu U(u)} = \frac{1}{2\pi\kappa} \sqrt{\frac{\omega}{\nu}} \nu^{i\omega/\kappa} e^{+\pi\omega/2\kappa} \Gamma\left(\frac{-i\omega}{\kappa}\right). \quad (\text{B.40})$$

The number operator for the asymptotic observer is:

$$b_\omega^\dagger b_\omega = \int_0^\infty \frac{d\nu}{2\pi} \frac{d\nu'}{2\pi} (\alpha_{\omega\nu}^* a_\nu^\dagger + \beta_{\omega\nu}^* a_\nu) (\alpha_{\omega'\nu'} a_{\nu'} + \beta_{\omega'\nu'} a_{\nu'}^\dagger). \quad (\text{B.41})$$

This integral sums over ν -frequencies of outgoing a -modes, in the local Minkowski frame of an infalling observer. This notion of time is exponentially related to asymptotic time. In any case, these modes contribute to a single outgoing mode of frequency ω .

By the adiabatic principle [72] these infalling modes annihilate the a -vacuum: $a_\nu|\psi\rangle = 0$. Then since $\langle\psi|a_{\nu'} a_{\nu'}^\dagger|\psi\rangle = 2\pi\delta(\nu - \nu')$, the expectation value of the number operator is:

$$\langle\psi|b_\omega^\dagger b_\omega|\psi\rangle = \int_0^\infty \frac{d\nu}{2\pi} \frac{d\nu'}{2\pi} \beta_{\omega\nu}^* \beta_{\omega'\nu'} \langle\psi|a_\nu a_{\nu'}^\dagger|\psi\rangle = \int_0^\infty \frac{d\nu}{2\pi} \beta_{\omega\nu}^* \beta_{\omega\nu} = \frac{2\pi\delta(\omega - \omega')}{e^{2\pi\omega/\kappa} - 1}. \quad (\text{B.42})$$

The Hawking spectrum is determined from the surface gravity κ , which scales the exponential map between the local notions of future-directed time for near-horizon and asymptotic observers. For the HBH we have $\kappa = 1/(4M)$, the same as for a Schwarzschild black hole

of mass M . This is due to the redshift of the near-horizon geometry, which is the same as that of an ordinary Schwarzschild black hole of mass m :

$$ds^2 = -\frac{2}{\kappa} \sqrt{\frac{f'(r_+)}{j'(r_+)}} dU dV = -8m dU dV. \quad (\text{B.43})$$

The main point is that this reproduces, by a partially independent route, the asymptotic temperature $T_\infty = 1/8\pi M$ obtained from shells in Eq. (5.88); since both share the redshift factor $f(r)$, the local temperatures $T(r) = T_\infty/\sqrt{f(r)}$ match, both within the ocean and at asymptotic infinity. The greybody factors in the full 3 + 1 dimensional calculation, which are sensitive to the potential barrier at the photon sphere, may be different. In any case, this is only a necessary condition for thermal equilibrium.

As usual, this calculation says nothing about where Hawking radiation originates. If a significant fraction is emitted at or near the photon sphere, it would clarify the physical meaning of our results. This seems reasonable in the eikonal limit, where modes near the critical impact parameter in the spherical harmonics will be amplified.

C Braneworld Cosmology

It is interesting to consider the influence of the photon sphere on the cosmological solutions. Branes move toward and away from photon spheres in analogy to ordinary particles.³¹

This methodology follows Per Kraus [43], but similar methods have also appeared elsewhere in the literature. We begin with the usual Randall-Sundrum ansatz:

$$ds^2 = dy^2 + e^{-2A(y)} \bar{\gamma}_{ab}(x) dx^a dx^b. \quad (\text{C.1})$$

It was shown in Sec. 3 that only pure tension branes are static. The induced metric is a warped product: $\gamma_{ab}(y, x) = e^{-2A(y)} \bar{\gamma}_{ab}(x)$; then:

$$K_{ab} = \frac{1}{2} \partial_y \gamma_{ab} = -A'(y) \gamma_{ab} \implies [K^\tau{}_\tau] = [K^\theta{}_\theta]. \quad (\text{C.2})$$

Then for a static brane, it follows from Eq. (3.5) that:

$$\frac{p}{\sigma} = -\frac{n-1}{n} - \frac{1}{n} \frac{[K^\tau{}_\tau]}{[K^\theta{}_\theta]} = -1 \implies p = -\sigma. \quad (\text{C.3})$$

The stress-energy tensor for moving branes is not pure tension.

For the pure tension case we can straightforwardly recover the RS solution. Note that:

$$K^a{}_b = -A'(y) \delta^a{}_b \implies K^\tau{}_\tau = K^\theta{}_\theta = -A'(y). \quad (\text{C.4})$$

Then from Eq. (3.3) and $[K^\theta{}_\theta] = -[A']$:

$$[A'] = (8\pi G_D) \frac{\sigma}{n}. \quad (\text{C.5})$$

³¹From a braneworld cosmology perspective, an expanding universe is similar to a particle escaping from the photon sphere of a black hole. Similar comments apply in other cases.

The relevant bulk Einstein equations are:

$$G_{yy} = 6 (A'(y))^2, \quad G_{rr} = 3e^{-2A(y)} \left(2 (A'(y))^2 - A''(y) \right). \quad (\text{C.6})$$

Then assuming the bulk is AdS₅, we have $G_{MN} = -\Lambda_5 g_{MN}$, and the yy equation gives:

$$6 (A')^2 = -\Lambda_5 \implies (A'(y))^2 = k^2. \quad (\text{C.7})$$

The rr equation can be written as $6 (A')^2 - 3A'' = -\Lambda_5$.

It follows immediately that $A''(y) = 0$. Then in each bulk region:

$$A'(y) = \pm k \implies A(y) = \pm ky + A_0. \quad (\text{C.8})$$

Imposing Z_2 symmetry around a brane at $y = 0$ gives the standard RS solution. The critical energy density for Randall-Sundrum follows from the Z_2 symmetry.

$$A(y) = k|y| + A_0, \quad 2k = \frac{8\pi G_5}{3} \sigma \Rightarrow \sigma = \frac{3k}{4\pi G_5}. \quad (\text{C.9})$$

For Z_2 symmetric thin shells, the angular junction condition can be written as:

$$\dot{R}^2 = \left(\frac{4\pi G_5}{3} \sigma R \right)^2 - j(R). \quad (\text{C.10})$$

Defining $H \equiv \dot{R}/R$ gives the Friedmann equation on the brane:

$$H^2 = \left(\frac{4\pi G_5}{3} \sigma \right)^2 - \frac{j(R)}{R^2}. \quad (\text{C.11})$$

The time-dependence of this brane is given by:

$$\ddot{R} + \frac{f'(R)}{2f(R)} (j(R) + \dot{R}^2) - \frac{j'(R)}{2j(R)} \dot{R}^2 = -\frac{4\pi G_5}{3} \sigma R \left[4\pi G_5 \left(\frac{2}{3} \sigma + p \right) \right]. \quad (\text{C.12})$$

These expressions depend on the metric functions $j(r)$ and $f(r)$. If we assume empty AdS₅, as in the RS case, then we have $f(r) = j(r) = k_s + \frac{r^2}{\ell^2}$, which gives:

$$H^2 = \left(\frac{4\pi G_5}{3} \sigma \right)^2 - \frac{1}{\ell^2} - \frac{k_s}{R^2}. \quad (\text{C.13})$$

Here we have $k_s = (-1, 0, 1)$, with $k_s = 0$ for planar slicing. This is static for $k_s = 0$ when $\sigma = \sigma_0 \equiv \frac{3k}{4\pi G_5}$. As usual $k = 1/\ell$; this gives the same critical RS tension that was determined earlier Eq. (C.9).

In fact, consistent with previous sections, the static brane for $k = 1$ sits at the photon sphere at the boundary of AdS₅. For this case, Eq. (C.10) gives:

$$1 + \frac{R^2}{\ell^2} = \left(\frac{4\pi G_5}{3} \sigma R \right)^2 \Rightarrow 1 = R^2 \left[\left(\frac{4\pi G_5}{3} \sigma \right)^2 - \frac{1}{\ell^2} \right]. \quad (\text{C.14})$$

For the RS critical tension, the bracket vanishes and the only way to satisfy the equation is $R \rightarrow \infty$. There is a ‘‘photon sphere’’ at this position, since:

$$\frac{Rf'(R)}{2f(R)} = \frac{R(2R/\ell^2)}{2(1 + R^2/\ell^2)} = \frac{R^2/\ell^2}{1 + R^2/\ell^2} \xrightarrow{R \rightarrow \infty} 1. \quad (\text{C.15})$$

This brane sits at the AdS boundary. The $k = 0$ and $k = 1$ cases are different foliations; the $k = 0$ coordinates cover the Poincare patch.

The critical brane tension σ_0 makes the brane static. For $k = 0$ the same condition applies at all R ; for $k \neq 1$ the pure tension brane can only be static at the photon sphere, where $rf'(r)/2f(r) = 1$.

It is useful to rewrite these equations in terms of σ_0 . Let $\rho(\tau)$ be the energy density of matter on the brane, and let $p_m(\tau)$ be the pressure of matter on the brane. Then $\sigma_{\text{tot}} = \sigma_0 + \rho$ and $p_{\text{tot}} = -\sigma_0 + p_m$. The stress-energy tensor is:

$$T_{ab} = -\sigma_0 h_{ab} + T_{ab}^{(m)}, \quad T_{ab}^{(m)} = (\rho + p_m)u_a u_b + p_m h_{ab} \quad (\text{C.16})$$

Here $T_{ab}^{(m)}$ is the stress tensor for the matter on the brane, which is conserved by the Bianchi identities. The conservation law $\dot{\rho} + 3H(\rho + p_m) = 0$ gives the familiar expression:

$$\frac{d \ln \rho}{d \ln R} = -3 \left(1 + \frac{p_m}{\rho} \right). \quad (\text{C.17})$$

If we assume constant coefficients $p_m = w\rho$, brane energy conservation gives:

$$\frac{d \ln \rho}{d \ln R} = -3(1 + w) \implies \rho(R) = \rho_0 R^{-3(1+w)}. \quad (\text{C.18})$$

For $1 + w < 0$, the energy density on the brane grows as the universe expands. If $\rho = 0$, then $\sigma_{\text{tot}} = \sigma_0$ and $p_{\text{tot}} = -\sigma_0$, which is a critical tension brane. It is static only at the photon sphere; for $k = 0$ it is static for any R .

In this notation, the Friedmann equation becomes:

$$H^2 = \left(\frac{4\pi G_5}{3} \right)^2 (2\sigma_0 \rho + \rho^2) - \frac{k_s}{R^2}. \quad (\text{C.19})$$

The usual Friedmann equation is recovered when $\rho \ll \sigma_0$. This defines G_4 as:

$$\frac{8\pi G_4}{3} \rho \equiv \left(\frac{4\pi G_5}{3} \right)^2 (2\sigma_0 \rho), \quad H^2 = \frac{8\pi G_4}{3} \rho \left(1 + \frac{\rho}{2\sigma_0} \right) - \frac{k_s}{R^2}. \quad (\text{C.20})$$

Although $\sigma_0 = \frac{3}{4\pi G_5 \ell}$ in RS, it has a slightly different value for other metrics:

$$\sigma_0 = \frac{3}{4\pi G_5} \frac{\sqrt{j(R)}}{R}, \quad G_4 = \frac{G_5}{\ell} = G_5 k. \quad (\text{C.21})$$

This is fully consistent with the well-known expression [20, 21] in the limit $r_c \rightarrow \infty$:

$$M_{Pl}^2 = M^3 r_c \int_{-\pi}^{\pi} d\phi e^{-2kr_c|\phi|} = \frac{M^3}{k} \left[1 - e^{-2kr_c\pi} \right]. \quad (\text{C.22})$$

If we include a black hole in the bulk AdS₅, the argument goes through mostly unchanged. The Friedmann equation Eq. (C.11) for $f_{\pm}(r) = j_{\pm}(r) = k_s + \frac{r^2}{\ell^2} - \frac{\mu_{\pm}}{r^2}$ becomes:

$$H^2 = \frac{8\pi G_4}{3} \rho \left(1 + \frac{\rho}{2\sigma_0} \right) + \frac{\mu}{R^4} - \frac{k_s}{R^2}. \quad (\text{C.23})$$

The only difference is that a radiation term μ/R^4 has been added to the equation.

It is convenient to write:

$$H^2 = \left(\frac{4\pi G_5}{3}\right)^2 (2\sigma_0\rho + \rho^2) + \frac{\mu}{R^4} - \frac{k_s}{R^2}. \quad (\text{C.24})$$

Taking the derivative with respect to τ , using $\dot{\rho} + 3H(\rho + p_m) = 0$ and $\dot{R} = HR$ gives:

$$\dot{H} = -3\left(\frac{4\pi G_5}{3}\right)^2 (\sigma_0 + \rho)(\rho + p_m) - \frac{2\mu}{R^4} + \frac{k_s}{R^2} \quad (\text{C.25})$$

The curvature term k_s/R^2 can give $\dot{H} > 0$ without violating NEC.

More generally this can be written as a radius dependent curvature term:

$$\dot{H} = -3\left(\frac{4\pi G_5}{3}\right)^2 (\sigma_0 + \rho)(\rho + p_m) + \frac{j(R)}{R^2} \left(1 - \frac{Rj'(R)}{2j(R)}\right). \quad (\text{C.26})$$

The curvature changes at the photon sphere: negative inside, positive outside. The curvature vanishes for $k = 0$ slicing, causing R dependence to drop out. Since $p_m = \rho w$:

$$\dot{H}(R_{\text{ps}}) = -3\left(\frac{4\pi G_5}{3}\right)^2 (\sigma_0 + \rho)\rho(1 + w). \quad (\text{C.27})$$

The usual FRW equation holds at low energy $(\sigma_0 + \rho) \approx \sigma_0$, since $\frac{8\pi G_4}{3}\rho \equiv \left(\frac{4\pi G_5}{3}\right)^2 (2\sigma_0\rho)$.

Matter with $w < -1$ and $\rho > 0$ gives $\dot{H} > 0$, but only by violating NEC. For braneworlds, the geometric term in \dot{H} vanishes at the higher-dimensional photon sphere. This is only a different interpretation of the usual circumstance. In any case, this geometric contribution can drive $\dot{H} > 0$ even for brane matter satisfying $w \geq -1$.

References

- [1] J.D. Bekenstein, *Black holes and the second law*, *Lett. Nuovo Cim.* **4** (1972) 737.
- [2] J.D. Bekenstein, *Black holes and entropy*, *Phys. Rev. D* **7** (1973) 2333.
- [3] J.D. Bekenstein, *Generalized second law of thermodynamics in black hole physics*, *Phys. Rev. D* **9** (1974) 3292.
- [4] S.W. Hawking, *Black hole explosions*, *Nature* **248** (1974) 30.
- [5] S.W. Hawking, *Particle Creation by Black Holes*, *Commun. Math. Phys.* **43** (1975) 199.
- [6] S.W. Hawking, *Black Holes and Thermodynamics*, *Phys. Rev. D* **13** (1976) 191.
- [7] D.J. Gross, M.J. Perry and L.G. Yaffe, *Instability of flat space at finite temperature*, *Phys. Rev. D* **25** (1982) 330.
- [8] J.W. York, Jr., *Black hole thermodynamics and the Euclidean Einstein action*, *Phys. Rev. D* **33** (1986) 2092.
- [9] W. Israel, *Singular hypersurfaces and thin shells in general relativity*, *Nuovo Cim. B* **44S10** (1966) 1.
- [10] J. Frauendiener, C. Hoenselaers and W. Konrad, *A shell around a black hole*, *Classical and Quantum Gravity* **7** (1990) 585.

- [11] P.R. Brady, J. Louko and E. Poisson, *Stability of a shell around a black hole*, *Phys. Rev. D* **44** (1991) 1891.
- [12] M. Riojas and M.J. Strassler, “On black holes surrounded by radiation: Classical considerations.” 2026.
- [13] M. Riojas and M.J. Strassler, “On black holes surrounded by radiation: Thermodynamics.” 2026.
- [14] V. Cardoso and P. Pani, *Testing the nature of dark compact objects: a status report*, *Living Rev. Rel.* **22** (2019) 4 [[1904.05363](#)].
- [15] C. Bambi et al., *Black hole mimickers: from theory to observation*, 5, 2025 [[2505.09014](#)].
- [16] J.M. Bardeen, W.H. Press and S.A. Teukolsky, *Rotating black holes: Locally nonrotating frames, energy extraction, and scalar synchrotron radiation*, *Astrophys. J.* **178** (1972) 347.
- [17] R.D. Sorkin, R.M. Wald and Z.J. Zhang, *Entropy of selfgravitating radiation*, *Gen. Rel. Grav.* **13** (1981) 1127.
- [18] R.C. Tolman, *Static solutions of Einstein’s field equations for spheres of fluid*, *Phys. Rev.* **55** (1939) 364.
- [19] J.R. Oppenheimer and G.M. Volkoff, *On massive neutron cores*, *Phys. Rev.* **55** (1939) 374.
- [20] L. Randall and R. Sundrum, *A Large mass hierarchy from a small extra dimension*, *Phys. Rev. Lett.* **83** (1999) 3370 [[hep-ph/9905221](#)].
- [21] L. Randall and R. Sundrum, *An Alternative to compactification*, *Phys. Rev. Lett.* **83** (1999) 4690 [[hep-th/9906064](#)].
- [22] R.L. Bowers and E.P.T. Liang, *Anisotropic Spheres in General Relativity*, *Astrophys. J.* **188** (1974) 657.
- [23] H.-C. Kim and Y. Lee, *Entropy of self-gravitating anisotropic matter*, *Eur. Phys. J. C* **79** (2019) 679 [[1901.03148](#)].
- [24] R. Brustein and A.J.M. Medved, *Resisting collapse: How matter inside a black hole can withstand gravity*, *Phys. Rev. D* **99** (2019) 064019 [[1805.11667](#)].
- [25] R. Brustein, A.J.M. Medved and T. Simhon, *Black holes as frozen stars*, *Phys. Rev. D* **105** (2022) 024019 [[2109.10017](#)].
- [26] R. Brustein, A.J.M. Medved and T. Simhon, *Thermodynamics of frozen stars*, *Phys. Rev. D* **110** (2024) 024066 [[2310.11572](#)].
- [27] T. Banks, W. Fischler, A. Kashani-Poor, R. McNees and S. Paban, *Entropy of the stiffest stars*, *Class. Quant. Grav.* **19** (2002) 4717 [[hep-th/0206096](#)].
- [28] V. Cardoso, K. Destounis, F. Duque, R.P. Macedo and A. Maselli, *Black holes in galaxies: Environmental impact on gravitational-wave generation and propagation*, *Phys. Rev. D* **105** (2022) L061501 [[2109.00005](#)].
- [29] K. Jusufi, *Black holes surrounded by Einstein clusters as models of dark matter fluid*, *Eur. Phys. J. C* **83** (2023) 103 [[2202.00010](#)].
- [30] K.-i. Maeda, V. Cardoso and A. Wang, *Einstein cluster as central spiky distribution of galactic dark matter*, *Phys. Rev. D* **111** (2025) 044060 [[2410.04175](#)].
- [31] G.W. Gibbons and S.W. Hawking, *Action Integrals and Partition Functions in Quantum Gravity*, *Phys. Rev. D* **15** (1977) 2752.

- [32] R.C. Tolman, *On the Weight of Heat and Thermal Equilibrium in General Relativity*, *Phys. Rev.* **35** (1930) 904.
- [33] J.D. Brown and J.W. York, Jr., *Quasilocal energy and conserved charges derived from the gravitational action*, *Phys. Rev. D* **47** (1993) 1407 [[gr-qc/9209012](#)].
- [34] S.W. Hawking and D.N. Page, *Thermodynamics of Black Holes in anti-De Sitter Space*, *Commun. Math. Phys.* **87** (1983) 577.
- [35] E. Witten, *Anti-de Sitter space, thermal phase transition, and confinement in gauge theories*, *Adv. Theor. Math. Phys.* **2** (1998) 505 [[hep-th/9803131](#)].
- [36] E. Witten, *Introduction to black hole thermodynamics*, *Eur. Phys. J. Plus* **140** (2025) 430 [[2412.16795](#)].
- [37] G.W. Gibbons, *On Lowering a Rope into a Black Hole*, *Nature Physical Science* **240** (1972) 77.
- [38] A.R. Brown, *Tensile Strength and the Mining of Black Holes*, *Phys. Rev. Lett.* **111** (2013) 211301 [[1207.3342](#)].
- [39] A. Almheiri, D. Marolf, J. Polchinski and J. Sully, *Black Holes: Complementarity or Firewalls?*, *JHEP* **02** (2013) 062 [[1207.3123](#)].
- [40] H. Poincare, *On the irregular integrals of linear equations*, *Acta Math.* **8** (1886) 295.
- [41] R. Sorkin, *A Criterion for the onset of instability at a turning point*, *Astrophys. J.* **249** (1981) 254.
- [42] S.R. Green, J.S. Schiffrin and R.M. Wald, *Dynamic and Thermodynamic Stability of Relativistic, Perfect Fluid Stars*, *Class. Quant. Grav.* **31** (2014) 035023 [[1309.0177](#)].
- [43] P. Kraus, *Dynamics of anti-de Sitter domain walls*, *JHEP* **12** (1999) 011 [[hep-th/9910149](#)].
- [44] A. Karch and L. Randall, *Locally localized gravity*, *JHEP* **05** (2001) 008 [[hep-th/0011156](#)].
- [45] R. André and J.P.S. Lemos, *Thermodynamics of d-dimensional Schwarzschild black holes in the canonical ensemble*, *Phys. Rev. D* **103** (2021) 064069 [[2101.11010](#)].
- [46] A. Einstein, *On a stationary system with spherical symmetry consisting of many gravitating masses*, *Annals Math.* **40** (1939) 922.
- [47] C.G. Boehmer and T. Harko, *On Einstein clusters as galactic dark matter halos*, *Mon. Not. Roy. Astron. Soc.* **379** (2007) 393 [[0705.1756](#)].
- [48] L. Herrera and N.O. Santos, *Local anisotropy in self-gravitating systems*, *Phys. Rept.* **286** (1997) 53.
- [49] P.S. Florides, *A New Interior Schwarzschild Solution*, *Proceedings of the Royal Society of London Series A* **337** (1974) 529.
- [50] H. Andréasson, *Existence of Steady States of the Massless Einstein–Vlasov System Surrounding a Schwarzschild Black Hole*, *Annales Henri Poincaré* **22** (2021) 4271 [[2102.08170](#)].
- [51] H. Andréasson, *Sharp bounds on $2m/r$ of general spherically symmetric static objects*, *J. Diff. Eq.* **245** (2008) 2243 [[gr-qc/0702137](#)].
- [52] V. Cardoso, A.S. Miranda, E. Berti, H. Witek and V.T. Zanchin, *Geodesic stability, Lyapunov exponents and quasinormal modes*, *Phys. Rev. D* **79** (2009) 064016 [[0812.1806](#)].

- [53] M. Riojas and M.J. Strassler, “In preparation.” 2026.
- [54] E.A. Martinez, *Fundamental thermodynamical equation of a selfgravitating system*, *Phys. Rev. D* **53** (1996) 7062 [[gr-qc/9601037](#)].
- [55] R. André, J.P.S. Lemos and G.M. Quinta, *Thermodynamics and entropy of self-gravitating matter shells and black holes in d dimensions*, *Phys. Rev. D* **99** (2019) 125013 [[1905.05239](#)].
- [56] J.P.S. Lemos and O.B. Zaslavskii, *Black holes and hot shells in the Euclidean path integral approach to quantum gravity*, *Class. Quant. Grav.* **40** (2023) 235012 [[2304.06740](#)].
- [57] J.M. Maldacena, *The Large N limit of superconformal field theories and supergravity*, *Adv. Theor. Math. Phys.* **2** (1998) 231 [[hep-th/9711200](#)].
- [58] S. Hod, *On the number of light rings in curved spacetimes of ultra-compact objects*, *Phys. Lett. B* **776** (2018) 1 [[1710.00836](#)].
- [59] M. Headrick, “diffgeo.m: A package for doing GR-type tensor algebra and calculus.” <https://sites.google.com/view/matthew-headrick/mathematica>.
- [60] B. Shoshany, *OGRe: An Object-Oriented General Relativity Package for Mathematica*, *J. Open Source Softw.* **6** (2021) 3416 [[2109.04193](#)].
- [61] J. Keir, *Slowly decaying waves on spherically symmetric spacetimes and ultracompact neutron stars*, *Class. Quant. Grav.* **33** (2016) 135009 [[1404.7036](#)].
- [62] V. Cardoso, L.C.B. Crispino, C.F.B. Macedo, H. Okawa and P. Pani, *Light rings as observational evidence for event horizons: long-lived modes, ergoregions and nonlinear instabilities of ultracompact objects*, *Phys. Rev. D* **90** (2014) 044069 [[1406.5510](#)].
- [63] V. Cardoso, S. Hopper, C.F.B. Macedo, C. Palenzuela and P. Pani, *Gravitational-wave signatures of exotic compact objects and of quantum corrections at the horizon scale*, *Phys. Rev. D* **94** (2016) 084031 [[1608.08637](#)].
- [64] P.V.P. Cunha, E. Berti and C.A.R. Herdeiro, *Light-Ring Stability for Ultracompact Objects*, *Phys. Rev. Lett.* **119** (2017) 251102 [[1708.04211](#)].
- [65] P.V.P. Cunha, C. Herdeiro, E. Radu and N. Sanchis-Gual, *Exotic Compact Objects and the Fate of the Light-Ring Instability*, *Phys. Rev. Lett.* **130** (2023) 061401 [[2207.13713](#)].
- [66] Z. Mark, A. Zimmerman, S.M. Du and Y. Chen, *A recipe for echoes from exotic compact objects*, *Phys. Rev. D* **96** (2017) 084002 [[1706.06155](#)].
- [67] S. Chandrasekhar and S.L. Detweiler, *The quasi-normal modes of the Schwarzschild black hole*, *Proc. Roy. Soc. Lond. A* **344** (1975) 441.
- [68] K.D. Kokkotas and B.G. Schmidt, *Quasinormal modes of stars and black holes*, *Living Rev. Rel.* **2** (1999) 2 [[gr-qc/9909058](#)].
- [69] V. Ferrari, *Gravitational waves from perturbed stars*, *Bull. Astron. Soc. India* **39** (2011) 203 [[1105.1678](#)].
- [70] P. Boonserm, T. Ngampitipan and M. Visser, *Regge-Wheeler equation, linear stability, and greybody factors for dirty black holes*, *Phys. Rev. D* **88** (2013) 041502 [[1305.1416](#)].
- [71] Y. Kojima, S. Yoshida and T. Futamase, *Nonradial pulsation of a boson star. 1: Formulation*, *Prog. Theor. Phys.* **86** (1991) 401.
- [72] J. Polchinski, *The black hole information problem.*, in *Theoretical Advanced Study Institute*

in Elementary Particle Physics: New Frontiers in Fields and Strings, pp. 353–397, 2017,
[DOI \[1609.04036\]](#).